CW RADAR-BASED NON-CONTACT VITAL SIGN MONITORING

HOANG THI YEN

A dissertation submitted for the degree of

Doctor of Engineering

DEPARTMENT OF MECHANICAL AND INTELLIGENT SYSTEMS ENGINEERING

GRADUATE SCHOOL OF INFORMATICS AND ENGINEERING

THE UNIVERSITY OF ELECTRO-COMMUNICATIONS

September 2023

CW RADAR-BASED NON-CONTACT VITAL SIGN MONITORING

APPROVED

Prof. Guanghao SUN, Chairman

Prof. Takuji KOIKE

Prof. Norihiro KOIZUMI

Prof. Yinlai JIANG

Prof. Takemi MATSUI

Date approved by Chairman: _____

This page intentionally left blank

My dissertation is dedicated to my supervisors, my whole family and friends, who have been a continuous source of encouragement and support during the difficulties of graduate school and life.

This page intentionally left blank

Acknowledgements

Firstly, I would like to extend my sincere gratitude to my supervisors, Prof. Guanghao SUN, Prof. Takuji KOIKE and Prof. Norihiro KOIZUMI, for their intense support and guidance throughout my PhD studies and research at the University of Electro-Communications. My academic goals would not have been achieved without their persistence, inspiration, and expertise.

I am grateful for the feedback and suggestions provided by all the committee members who reviewed my dissertation, including Prof. Sun, Prof. Koike, Prof. Koizumi and Prof. Jiang from the University of Electro-Communications, and Prof. Matsui from Tokyo Metropolitan University.

Besides my supervisors, I want to express my gratitude to every member of Sun-Lab at the University of Electro-Communications for their extensive support, constant companionship, valuable insights, and camaraderie during my stay thousands of miles away from my homeland. I am also thankful for the enjoyable experiences we shared over three years.

I would also like to thank The Ministry of Education, Culture, Sports, Science and Technology, Japan (MEXT) for providing me with the scholarship that allows me to pursue my PhD program at the University of Electro-Communications.

I am grateful to Le Quy Don Technical University for granting me the opportunity to work as a lecturer and researcher, which allowed me to gain valuable research experience.

Lastly, I express my sincere appreciation to my entire family in Vietnam, particularly my parents, husband, and little daughter, for their unwavering love, encouragement, and faith in me throughout my life.

This page intentionally left blank

This page intentionally left blank

論文概要

バイタルサインは臨床において重要な生体情報として，その測定は臨床現場では欠かせない．患者の身体へ負担を与えるような接触式生体計測法では，計測結果がその影響を受けることで真の情報が隠れてしまう恐れがある．このような問題を回避するため，近年，CWレーダーを用いた非侵襲，無拘束，非接触での生体計測法が注目を集めている．しかし，体動や環境ノイズの影響されやすく，計測安定・信頼性が低い問題がある．本研究では，同レーダーセンサーの計測安定性とバイタルサイン測定信頼性向上のために，生体レーダーに特化した信号処理法の開発が目的としている．

本研究は２４GHz帯CWレーダーを採用し，測定対象の呼吸運動に伴う体表面の約1.0 mmから5.0 mmの変位とその1/100程度の心拍由来の体表面振動を計測する．研究のアプローチとして，レーダーによる呼吸・心拍計測原理を数学的の導出を行い，体表面微小振動を再現できるアクチュエーターを用いて実験的に原理検証をした．それから計測原理に基づき，レーダーから観測した時系列生体信号から有効な特徴量を抽出でき，機械学習法を用いて信号質評価（signal quality index, SQI）をする．高品質SQI信号に対し，適応的にコンボリューションフィルタや特異値分解から呼吸・心拍信号分離を行い，分間呼吸数・心拍数のみではなく心拍変動までの複数のバイタルサインを抽出する．実験室での健康被験者と療養型病院で寝たきり患者を対象に，開発した信号処理法の有効性を検証した．本博士論文は５章から構成させている　（図１）．

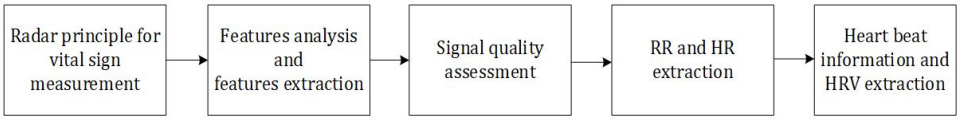

Figure 1: Summary of the research topic

第１章は，本研究の背景と目的を論じ，バイタルサインの生理学的な解釈から導入し，その接触と非接触的な計測法を紹介した．本研究のモチベーションと貢献について述べる．

第２章は，異なる生体レーダー方式の原理をまとめ，特にCWレーダー方式に関連する先行研究の調査結果から，本研究の問題点の提起する．

第３章は，CWレーダー方式のバイタルサイン計測法を数学的導出と実験的検証の両面アプローチから，本研究に使用する24GHzレーダーの特性を呼気と吸気フェイズに分けて理解する．I,Q信号をコンスタレーション表示し，信号のバランスとアンバランス現象を説明する．レーダーから観測した時系列生体信号から有効な特徴量（時間領域，周波数領域，Arctangent復調）を抽出でき，機械学習法を用いて信号質評価した．実験室で健康被験者と病院で患者を対象に，実地評価した．サポートベクターマシンを用いた方法では，実験室で健康被験者に対し99% の精度で信号質の評価が可能となる．

第４章は，前章で提案した信号質評価法から判定した信頼度の高い信号に対し，適応的にコンボリューショ ンフィルタや特異値分解から呼吸・心拍信号分離を行い，分間呼吸数・心拍数のみではなく，拍動間隔 (Inter-beat interval)から心拍変動指標（Heart ｒate variability）まで算出する．その有効性は実験室で健康被験者を対象に定量評価された．さらに臨床評価として，療養型病院で寝たきり患者を対象に，２４時間連続モニタリングを実現し，無呼吸やチェーンストーク呼吸の検出に成功した．

第５章は，開発した信号処理法を実装したリアルタイムアプリケーションを示し，本論文の結論と今後の発展性を示している

Abstract

Monitoring vital sign is a crucial task in health care setting. Traditional vital sign monitoring is difficult in cases of skin injury or long-term monitoring, because it requires placing multiple electrodes on the patient's skin surface. One solution to overcome these limitations is to use contactless sensors to monitor vital sign. Regarding non-contact sensor, camera or radar can be used. In particular, the radar was chosen for the reasons of simple installation and privacy issues. There are many types of radar that can be used for this purpose, Continuous Wave (CW) radar has the advantage of simple structure but still ensures the accuracy achieved for tracking vital sign of an individual. Therefore, in this study, 24 GHz CW radar is used as a sensor in a non-contact vital sign monitoring solution, in order to overcome the limitations of traditional methods. However, for radar, the disadvantage is that this sensor is very sensitive to noise, which reduces the accuracy of the vital sign detection and algorithms. Therefore, it is necessary to understand the working principle of radar in measuring the vital sign and the difficulties in measuring the vital sign, thereby finding solutions for measurement and signal preprocessing to improve the efficiency of vital sign detection algorithms. In this study, vital sign was detected on the basis of using 24 GHz CW radar and data processing algorithms, including breathing rate (BR), heart rate (HR) and heart rate variability (HRV).

Chapter 1 introduces the basis knowledge of vital sign and methods of vital sign measurement. This chapter will present the author's understanding of the vital sign and summarize the vital measuring method presented in published articles. Chapter 2 surveys the measurement principles of different types of radar, the vital sign detection methods that previous studies have performed on CW radar. In addition, this chapter highlights the advantages and disadvantages of the previous work. From there, the author will give

the solutions for CW radar, illustrated in chapters 3 and 4 to overcome the limitations of previous studies.

Chapter 3 will present the principle of CW radar in measuring vital sign, the problems encountered when using this radar, followed by solutions when measuring and preprocessing the data. Furthermore, this chapter presents the method of signal quality classification. For this chapter, the author published a conference paper [A.2.1] which is about the vital sign measurement principle of CW radar on the basis of giving mathematical formulas and proving by experiment. Addressing the imbalance problem for radar is presented in the conference paper [A.2.3]. The signal quality-based classification method is presented in the first half of the journal article [A.1.1].

Chapter 4 presents methods of vital sign detection. In which, on the basis of understanding the signal, the detected breathing rate is suitable for many postures. Heart rate is detected by machine learning algorithm with very clear pulse peaks. Finally, the heart rate variability is found on the mathematical basis, this research improves the method in previous work to reduce computation time and computational complexity while ensuring high accuracy. The solution to find RR and HR is presented in the conference paper [A.2.2, A.2.3] and the last half of the journal article [A.1.1]. The method to find out HRV is described in the journal article [A.1.2] which is under reviewed.

Chapter 5 discusses the applications of this research. This chapter shows the real-time performance of this study as presented in the conference paper [A.2.2]. In particular, this research has been applied to the signal measured from the actuator, a device with motion and input parameters can be set, the signal on the healthy subjects measured from the members of the Laboratory and clinical data measured from patients of Yokohama hospital, Japan. Those are the proofs to the trend and development potential of this research.

TABLE OF CONTENTS

LIST OF ABBREVIATIONS

ADC	Analog-to-digital converter
BBI	Beat-to-beat interval
BCG	Ballistocardiograph
BP	Blood pressure
BPF	Band-pass filter
bpm	Beat per minute
BT	Body temperature
CSR	Cheyne-Stokes respiration
CW	Continuous wave
DAQ	Data acquisition
ECG	Electrocardiogram
FFT	Fast Fourier transform
FIR	Finite impulse response
FMCW	Frequency modulated continuous wave
FPGA	Field-Programmable Gate Array
HF	High-frequency power
HR	Heart rate
HRV	Heart rate variability
I	In-phase
IBI	Inter-beat interval
ICA	Independent component analysis
IF	Intermediate frequency

LCD Liquid-crystal display

LF Low-frequency power

LPF Low-pass filter

LPNR Locally projective noise reduction

MRE Mean relative error

PC Personal Computer

PCA Principal component analysis

PCG Phonocardiogram

PPG Photoplethysmography

PW Pulse wave

Q Quadrature

RGB Red green blue

RMSE Root-mean-squared error

RMSSD Root mean square of successive differences

RR Respiration rate

RX Receive

SDNN Standard deviation of the NN (R-R) intervals

SMD Standard mean deviation

SVD Singular value decomposition

SVM Support vector machine

TX Transmit

UWB Ultra-wideband

LIST OF FIGURES

LIST OF TABLES

Chapter 1

INTRODUCTION

This chapter gives a brief summary of the two main methods that are used in vital signs measurement: contact method and con-contact method. Accordingly, the motivation of this thesis is explained, as are the contributions made by this dissertation. This chapter also describes the dissertation's layout.

1.1 Introduction Of Vital Signs

Basic body functions are assessed using vital signs, which provide valuable information about an individual's physical and psychological wellbeing [1,2]. Vital signs can indicate the presence of illnesses, as well as track progress in recovery. Normal vital sign ranges differ according to a person's age, weight, sex, and overall health. The four primary vital signs are body temperature, blood pressure, heart rate, and respiration rate. Body temperature (BT): A healthy person's body temperature usually falls within the range of 36.5 to 37.2 degrees Celsius or slightly above, despite the average body temperature being 36 degrees Celsius. Body temperature can be measured by inserting a thermometer into the mouth, anus, or under the armpit, as well as with a specialized thermometer in the ear canal. If a person's temperature exceeds the average body temperature, they are considered to have a fever. Conversely, if body temperature drops below 35 degrees Celsius, it is considered hypothermia [3,4]. Factors other than illness or infection can also cause fluctuations in body temperature. There are many factors can affect body

temperature. Previous research has shown that body temperature is a non-linear function of several variables including age, health status, gender, environmental temperature, duration of the diurnal cycle [5]. Blood pressure (BP): Blood pressure refers to the force or pressure of blood against artery walls, and is typically recorded as two numbers separated by a slash, such as 120/80 milli-meter of mercury (mm Hg). The first number, known as systolic pressure, measures the pressure in arteries when the heart pumps blood out to the body. The second number, diastolic pressure, measures the pressure in arteries when the heart is resting between beats [6]. A blood pressure reading of less than 120/80 mm Hg is considered healthy for a relaxed adult. However, a systolic pressure of 120-139 or diastolic pressure of 80-89 is classified as "prehypertension" and requires careful monitoring. A reading of 140/90 mm Hg or higher is indicative of hypertension, or high blood pressure. Prolonged high blood pressure can lead to health issues like atherosclerosis, heart failure, and stroke. Various factors, including stress, smoking, low temperatures, physical activity, eating, caffeine, and alcohol intake can influence blood pressure levels. Heart rate (HR) refers to the number of contractions of the ventricles (the heart's lower chambers) per minute, typically measured over a period of one minute [7]. The unit of measurement is beats per minute or bpm (beat per minute). Heart rate measurement is very important. Each person has only one heart, it was formed when we were still embryos. This organ helps to pump blood to the organs in the body to maintain life. Thus, measure heart rate to see if the heart is working properly, whether it is pumping enough blood, checking the general health and fitness. The heart has an electrical conduction system, or the heart is a specialized group of heart muscle cells where an electrical impulse is generated in the sinoatrial node or the heart's natural pacemaker, and it sends signals to the heart muscle that cause the heart muscle to contract and pump blood to the lungs and

body. The electrical activity of the heart can be detected by an electrocardiogram (ECG). When there is a problem with this system, a person may experience an arrhythmia. Symptoms may be like palpitations, dizziness, shortness of breath, loss of consciousness, light headedness [7,8]. Respiratory rate (RR): respiratory rate is the number of breaths taking in one minute. One breath is defined to include one inhalation and one exhalation. The observation and recording of breathing indicate a general physical assessment of respiration. Assessing and recording breathing should be accurate and an essential nursing skill. Evidence suggests that, among all vital signs, a change in breathing is an early sign of a patient's condition, and that failure to recognize such a change can lead to poor outcomes [9, 10]. When an adult is at rest, a normal respiration rate typically ranges from 12 to 20 breaths per minute (bpm), with a rate outside of this range considered abnormal [11]. Certain medical conditions such as asthma, anxiety, pneumonia, congestive heart failure, lung disease, as well as the use of narcotics or drug overdose can alter the typical respiratory rate.

1.2 Methods Of Vital Sign Measurement

There are many methods to measure the vital sign based on the principle of the device, or principle of measurement. Classification based on the principle that the device touches the person or does not touch the body, the measurement methods can be divided into two main groups: contact measurement and non-contact measurement. Contact measurement is a traditional form whereby medical devices are put on the skin, or to the body, and the device then records the measured parameter, via an in-device conversion can give parameter of vital sign. The contact methods of measuring vital sign can be described as below.

1.2.1 Contact method

Body temperature can be taken in some of the following ways. Temperatures can be taken orally with a classic glass thermometer or more modern digital thermometer that uses an electronic probe to measure body temperature. Temperatures taken rectally (using a glass or digital thermometer) tend to be slightly higher than that taken orally. The temperature can be taken under the arm with a glass or digital thermometer. Temperatures measured using this route tend to be lower than those measured orally. A special thermometer can quickly measure the temperature of the eardrum, which reflects the temperature of the internal organs.

To measure blood pressure, it is needed to have a sphygmomanometer, blood pressure cuffs and stethoscope. Ask the patient to loosen tight clothing or remove long sleeves to allow upper arm access. It should not use an arm with medical problems. Place the cuff around the upper arm and secure. Connect the cuff to the sphygmomanometer and secure. Place the patient's arm on a surface level with their arm. Place the stethoscope over the brachial artery at the bend of the elbow and listen for the pulse. Inflate the cuff slowly and listen to see when the pulse disappears. This is a sign to stop inflating the cuff. Begin to deflate the cuff very slowly while observing the mercury level in the sphygmomanometer. Note the sphygmomanometer, reaching the mercury level, when the pulse reappears: record this as the systolic blood pressure. Continue to deflate the cuff until the pulse disappears: record this reading as the diastolic pressure. Record these two measurements, first systolic and then diastolic (example 120/80).

To measure heart rate, the traditional method that doctors and nurses do, is to put the hand on the wrist of the person to count heartbeat, use a watch to calculate the period of one minute and count the number of times of recognizing the vibration in one minute.

Another way is to use a stethoscope, by holding the stethoscope to human bare chest, and listening, counting each heartbeat. The more advanced method is to use photocardiogram (PPG) and ECG.

The measuring principle using PPG is based on the light reflection of the human body's blood vessels. Blood vessels throughout the body are often classified as either arteries or veins, and there is a difference in how much blood flows through each type of blood vessel. The blood flow through the veins is little changed, while the blood flow through the arteries varies with the beat. Furthermore, one of the properties of oxidized hemoglobin in the blood flowing through the arteries is that it readily absorbs light from a particular wavelength. Due to these properties, when the skin is exposed to continuous light of a specific wavelength, the reflected light changes with the change of blood flow, and pulse waveforms can be obtained by measuring reflected light [12]. The impulse wave obtained here is called the volume pulse wave. The simplicity of PPG measurements has led to the application of PPG sensors as a tool for health monitoring [13, 14].

The principle of measuring heart rate by ECG is based on the electrical activity of the heart. The human heart has 4 chambers to store and pump blood, the upper 2 parts are called the atria, and the 2 larger lower parts are called the ventricles. Blood flows from the veins to the right atrium and from the lungs to the left atrium. Squeezing the left atrium pumps blood into the left ventricle, and the right atrium pumps blood into the right ventricle. The right ventricle then squeezes to pump blood through the arteries to the lungs, and the left ventricle squeezes to pump blood down the body. The heart is able to function at a regular and orderly pace thanks to a special system of conductive cells located in the heart muscle. In the right atrium, there is a sinus node composed

of cells capable of generating electrical impulses. This electrical impulse is transmitted to the surrounding muscles, causing the two atria to contract (creating a P wave on the electrocardiogram). Then, the current continues to pass along a special cell chain to the atrioventricular node located near the interventricular septum, and then along the Purkinje fiber cell chain, running along the interventricular septum and spreading into the surrounding muscles, causing the two ventricles contract (generating a series of QRS waves). Then, the electrical impulses decrease, the ventricles relax (creating a T wave) [15,16,17]. Overall, the mechanism of an electrocardiogram is as follows: cells in the chambers of the heart produce an electrical impulse when the heart is working, these electrical impulses travel through the heart according to a conduction system and are recorded by the electrocardiogram [18]. Some diseases such as arrhythmia, angina can be detected after conducting an electrocardiogram. Therefore, electrocardiogram plays a very important role and is regularly conducted in the hospital.

Respiration rate monitoring: Devices that monitor respiration rate generally rely on measuring one of several parameters, including respiratory sounds, airflow, chest or abdominal movements related to breathing, CO2 (carbon dioxide) output, and SpO2 (Saturation of Peripheral Oxygen) measured with an oximetry probe. It is also possible to determine respiration rate through analysis of the electrocardiogram (ECG) [19]. Respiratory sound can be measured with a microphone placed near the airway or on the throat to detect changes in sound. After that, frequency analysis and loudness estimation can be performed. The measurement of air flow can be achieved using the nose or the nasopharyngeal thermistor that detects the temperature change between inhaled and exhaled air [20]. Breathing-related chest or abdominal movements can be measured by using a breathing belt wrapped around the abdomen or chest to measure the rise and fall

of the body due to breathing activity. However, in many cases, due to patient discomfort, the doctor will not place many electrodes on the patient's body. To limit the number of devices in contact with the patient's body, the monitored breathing will be reduced, and breathing rate will be extracted from the ECG signal as shown in the Figure 1.1. The blue line is the ECG signal measured by the contact device, which is an ECG with electrodes attached to the human body. The brown curve is the respiration signal, measured from a breathing belt device wrapped around the chest to measure the pressure of the chest wall compressed against the belt each time of breathing. And the green line is the signal derived from the ECG, it can be seen that the green curve has the same frequency as the brown line.

1.2.2 Non-contact method

Non-contact measurement is a method in which the measuring device is placed at a fixed distance from the person being measured. Today, non-contact devices are of

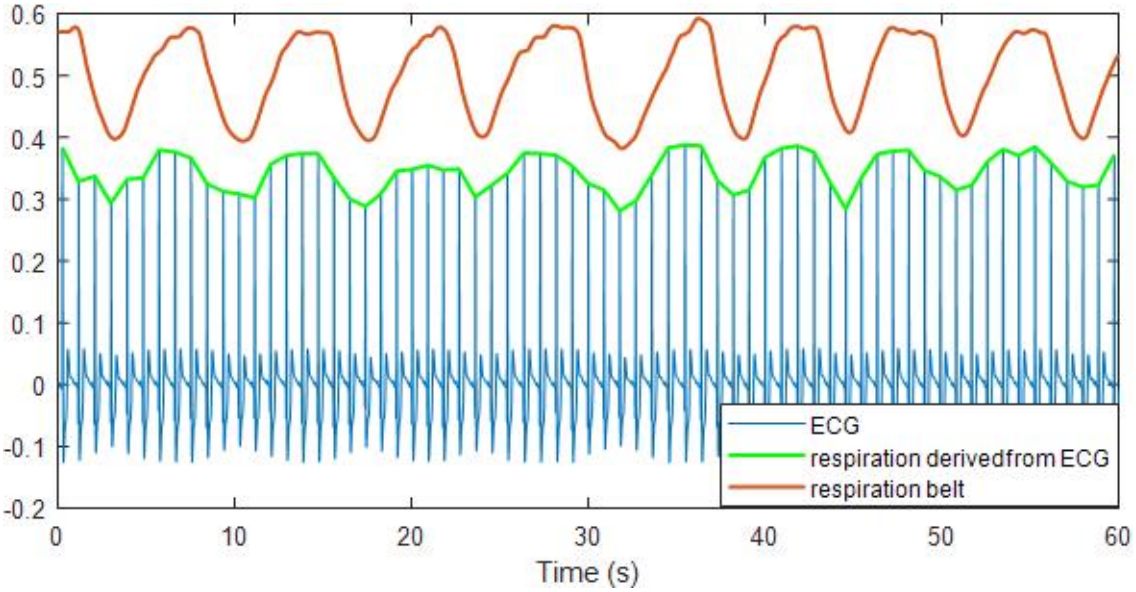

Figure 1.1: ECG signal, respiration signal derived from ECG and breathing signal of respiration belt

great interest, because of their advantages, including: no contact with the body, comfortable feeling, suitable for long-term measurement, especially suitable for the measurement context during the epidemic period because it does not require to contact with the patient. Several methods are applied to extract vital signs based on processing images and videos obtained from cameras [21-25]. Some studies use radar as vital sign receiver [26-34]. Some studies use Ballisto-cardiography (BCG) by recording body movements caused by ballistic forces (heart muscle contracting and ejecting blood, filling ventricles, accelerating and decelerating blood flow through large vessels); These minute movements are amplified and recorded on motion chart paper after being converted to potential by the receiver. BCG makes it easier to monitor heart (as well as breathing) activity. Usually focusing on external pressure or strain gauges, the BCG records vibrations caused by the mechanical action of the heart and lungs [35-37].

Heart rate can be measured with the RGB camera by capturing the change in hemoglobin absorption in the facial blood vessels because the facial skin is more sensitive to this change. In this way, a short video with a number of frames is recorded, then the algorithm extracts information about the change of the colour change parameters on the video frames to give the heart rate parameter [24,25]. Respiration rate and body temperature are measured using an infrared camera, because during exhalation, warm air from inside the lungs is released and increases the temperature in the nasal region, while inhaling, cool air from the lips. The external field is inhaled and reduces the temperature in the nasal area. Thus, using an infrared camera, it is possible to measure the temperature change in the nasal area, this period of change represents the breathing rate [25]. RR, HR and BP can be measured by radar. Radar measures the surface movement of the body wall due to breathing and heart rate, extracting the pattern of that movement giving us

Table 1.1: The main characteristics of the contact and non-contact methods

Some main points	**Contact method**	**Non-contact method**
Tradition	Traditional method	New method
Some device	For BT: Thermometer. For BP: Sphygmomanometer, blood pressure cuffs, stethoscope. For HR: PPG, ECG. For RR: Breathing belt, microphone, nasopharyngeal thermistor, ECG.	Camera Radar
Requirements	Put device contact with measured subjects.	Do not require to contact with subjects.
Advantage	High accuracy, high stability	Contactless, compact.
Disadvantage	Contact, cumbersome	Sensitive to noise. Low accuracy with body random movement

information about breathing and heart rate [31-34]. BP is calculated by detecting phase variations at two points on the body namely distal points (carotid artery in the neck) and proximal points (thoracic). The time interval between occurrences of peak phase values was calculated as the pulse propagation time, which was then used to predict systolic and diastolic blood pressure values using the calculated algorithm [38,39]. To summarize the two main methods of measuring vital signs, the Table 1.1 shows the main characteristics of the two methods briefly.

1.3 Motivation And Key Contribution

In the period when the epidemic is increasing, monitoring the vital sign by non-contact method is inevitable because of its advantages, it does not require contact with the measured person, which is very suitable for the requirement of keeping social dis-

tance. Furthermore, using the non-contact method is suitable for long-term monitoring [40,41,42]. There are many devices that can be used as non-contact medical ones, such as camera and radar. However, in some applications, the camera reflects the image; so the private issue may not be guaranteed, so using radar as a method can meet the both requirements.

However, current research focuses on building algorithms to extract the vital sign at different measurement positions. There are very few studies on the principle of measuring the vital sign of radar. While in order to use radar in raw signal measurement, to obtain a signal that carries vital sign information, to enhance the processing performance of vital sign extraction algorithms, it is important to understand the radar working principle in vital sign measurement. The principle is based on measuring the movement of the body wall due to the breathing activity causing the chest rise and fall and the heartbeat. This displacement is processed to get the required information. Understanding the characteristics of vital sign helps researchers enhance the performance to detect vital sign. In this thesis, the principle of measuring the vital sign of Continuous Wave (CW) radar is presented and related issues when measuring [43].

Being different from the contact method, the vital sign measurement using radar is very susceptible to noise. Even small random body movements can reduce the accuracy of vital sign detection methods [44]. Therefore, before detecting and separating vital sign, it is necessary to detect and classify signals with and without body random movements. In order to classify signals that contain random movement and signals do not contain random movement, an understanding of the signal features is required. The method of signal classification is machine learning algorithms, and then it is to extract vital sign from a set of signals that do not contain random body movements, which presented in the

author's published paper [33].

For the separation of vital sign signals, a method such as using bandpass filters can be used. However, because of the filter's characteristic, the output contains unwanted harmonics. In order to limit unwanted harmonics, the author in the study [32] used many band-pass filters with narrow frequency bands, then the output signal was selected through Wavelet algorithm and multiplexer. We can also use more complex classical algorithms including principal component analysis (PCA), independent component analysis (ICA) and the singular value decomposition (SVD). These methods have the advantage of showing very clear cardiac peaks. However, these methods are still essentially frequency separation of the vital sign. Therefore, to find the inter-beat-interval (IBI), more sophisticated methods are required, in order to find the peak of the beats without distorting its peak distance (without distorting the IBIs in time domain).

RR and HR are important in monitoring health status, however, heart rate variability (HRV) can bring more heart information, as it shows the changing in heart rate. Because heart rate is not a fixed parameter over time, but it changes with each inhalation and exhalation. Our heart rate increases when we inhale, and decreases when we exhale. And over time, a gradual increase or decrease in heart rate when we are relaxed is a sign of abnormality of health, and have to be monitored. To monitor HRV, it is necessary to implement a more complex algorithm [34]. Because this task requires precision about the interval of the beats. This dissertation has the following main contributions:

1. Explain the principle of transmitting and receiving signal of radar when measuring vital sign. On that basis, the dissertation analyses the related problems and encountered difficulties when measuring signals. After that the study offers the solutions to overcome those difficulties.

2. After receiving the signal, the thesis analyses the features characteristic of the signal with random body movement and those of signal without body movement. Evaluate signal quality using machine learning algorithms.

3. The signal quality classification is performed in real time, toward to the practical applicability of the vital sign measurement system using radar.

4. The thesis offers a solution to extract respiration rate and heart rate. Using the method of separating the frequencies contained in the raw radar signal, this is firstly demonstrated by simulated signal, then applied to the measured signal from the human subject.

5. The thesis proposes a solution combining the locally projective noise reduction algorithm with convolution filter to find beat-to-beat intervals (BBIs). For the first time, the algorithm to find heart peaks with the largest slope in the radar signal is applied to correspond to R peaks in ECG, this is based on the physiological mechanism of heart rate. Combining these, BBIs are found with high accuracy.

To describe the main contributions of the author in this research topic, a summary block diagram is visually presented as the Figure 1.2.

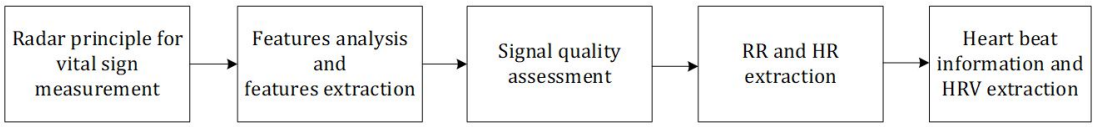

Figure 1.2: Summary of the research topic

1.4 The Layout Of Dissertation

The dissertation is structured into five chapters, and the rest of the thesis is arranged in the following manner.

- **Chapter 2** offers an overview of previous research on monitoring vital signs using radar and focuses on studies using 24 GHz CW radar. The relationship between previous studies and the content in the dissertation.

- **Chapter 3** presents the radar principle for vital sign measurement, the obstacles and problems related to measuring the vital sign, and signal quality classification. In addition, the solution is figured out when measuring to get the raw signal carrying more information of the vital sign.

- **Chapter 4** provides the method to detect three parameters of vital sign, including RR, HR and HRV. This chapter presents a method for frequency separation to find the respiration rate and heart rate, implementation steps and frequency components selection steps of RR and HR. Next, this chapter also gives the method to find out the peak of the radar signal corresponding to the R peak of the ECG signal, in order to obtain IBI and HRV with high accuracy.

- **Chapter 5** discusses related issues and practical applications that have done in this study. After that, the dissertation summarises the achieved and the limitation, figure out the future plan of the research.

Chapter 2

LITERATURE REVIEW ON RADAR BASED-VITAL SIGN MONITORING

Based on the reason of simple structure, low power consumption, aim to measure vital sign of single subject and frequency allowance in Japan, 24 GHz CW radar was selected in this study. This chapter aims to survey the research related to the field of vital sign detection using radar, focus on 24 GHz CW radar. The first section will survey some type of radars which used in vital sign measurement and present the overview of radar principle in measuring the vital sign. The second section surveys the studies and methods related to detecting vital sign including respiration rate and heart rate. Accordingly, the advantages and disadvantages of the studies are considered and the problems still need to be solved. In addition, this section will survey the research of HRV detection, methods, advantages and disadvantages of previous studies. The relationship between the previous research methods and the method presented in this dissertation.

2.1 Radar Principle For Vital Sign Measurement

Radar is a type of non-contact sensor for monitoring human vital signs. The principle is based on signal modulation of the received radar signal when measuring the displacement of the chest wall and the shift of the transmitted signal before and after hitting the patient. Depending on the type of transmitted signal, the radar that researchers used to

measure vital signs can be divided into four categories: pulse wave radar (PW), continuous wave radar (CW), frequency modulated continuous wave radar (FMCW) and ultra-wideband band radar (UWB) [45]. CW radar systems [46], such as Doppler radar cannot measure distances and are susceptible to interference from the movement of surrounding targets, however, it has the advantage of relatively low power consumption and has a simple architecture [47], so it is preferred for vital sign monitoring, which can be extracted from displacement information without the requirement of distance information. Although it comes at a higher cost, UWB radar [48] outperforms other types of radar with regards to distance resolution and detection capability. On the other hand, FMCW has superior resolution and accuracy compared to the aforementioned methods [49,50]. It combines the strengths of CW and UWB radar while consuming low power, displaying high sensitivity, and offering accurate measurement of target characteristics. This enables FMCW to provide information on target distance, velocity, and angular information.

In principle of operation, the PW radar is a type of radar where the transmitted signal is transmitted in the form of pulse, then it will receive a reflected signal. From information about the time between transmission to receipt and velocity of light, the range information will be calculated.

For CW radar, the transmitted signal is a continuous wave, therefore, on the basis of the Doppler effect, radar can measure instantaneous rate-of-change in the target's range. The Doppler effect states that, as the object approaches the radar, the frequency is increasing and when the object moves away from the radar the frequency is decreasing. For the vital sign chest wall motion measurement, the chest moves according to the repetition of approaching and moving away from the radar. This periodic motion is detected by radar and based on the conversion formula between frequency variation and displacement, we

will calculate displacement as the movement of the chest wall.

A Doppler sensor transmits a microwave from TX (transmit) antenna and the part receives again what was reflected by the movable object with an RX (receive) antenna. At this time, the received frequency is slightly changed by Doppler effect with the velocity of a moving object. A sensor compares a transmitted wave with a received wave by a mixer, and takes out only the frequency of a difference (Doppler frequency: f_d)

In order to obtain f_d in a sensor output, the wave shape of at least one or more periods is necessary. To do this, the target object is required to move at least more than a half of transmitted frequency wavelength. This minimum distance, in the case of a 24GHz sensor is about 6.2 mm ($f_0 = 24.15GHz$, $\lambda = 12.4mm$, $\lambda/2 = 6.2mm$). The relationship between the Doppler frequency and a velocity is shown by the following formula on the above mentioned conditions.

$$f_d = 2f_0\frac{v}{c}\cos(\alpha) \tag{2.1}$$

f_0: transmitted frequency

f_d: Doppler frequency

v: velocity of moving object

c: speed of light

α: angle between target moving direction and the radial line that is centering on a sensor.

The principle of direction identification is based on I and Q output (in-phase: I channel and quadrature: Q channel). The basic operation of the mixer is shown in the Figure 2.1. Here, when the $f_1 = f_0$ and $f_2 = f_0 \pm f_d$, the output in case of the approaching and leaving is shown by the formula in Figure 2.2.

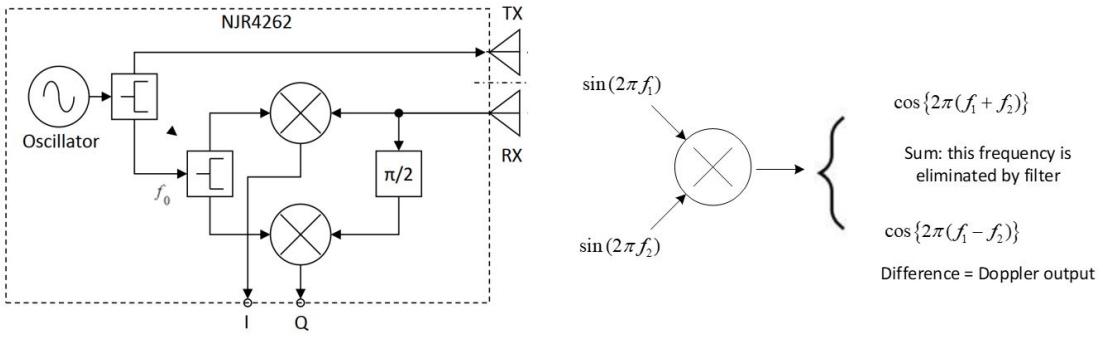

Figure 2.1: Structure of CW Doppler radar

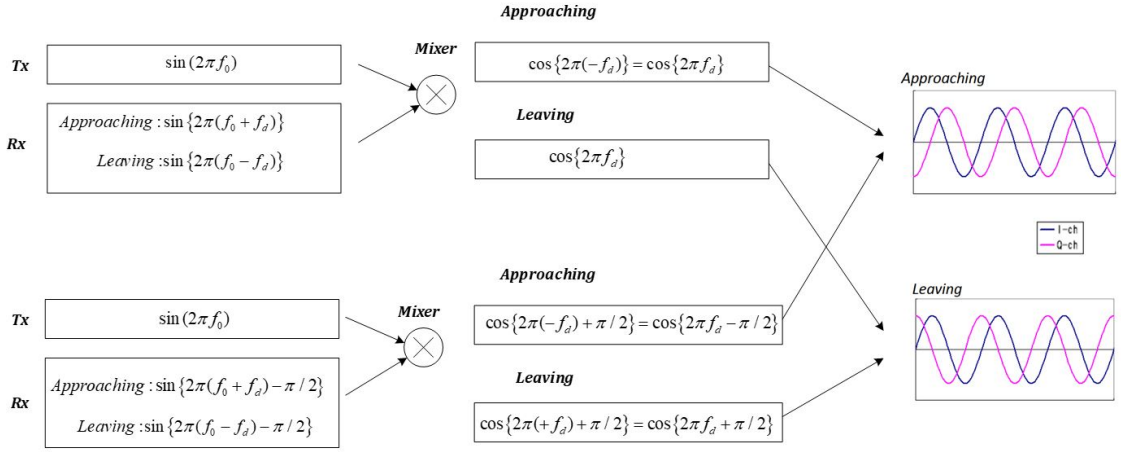

Figure 2.2: Doppler radar principle of receiving base-band signal

IQ output of the phase is changes depends on the moving direction of target as shown in below. In case of approaching, Q output is delayed 90 degrees from I. In case of leaving, the relation of I and Q becomes opposite. Because there is a phase difference when approaching and leaving, radar can be applied to detect movement of the chest wall, when people inhale, the chest moves closer to the radar, and when people exhale, the chest moves away from the radar. Monitoring the phase change on two signal I and Q channels, allowing us to monitor the movement of the chest wall during inhalation and exhalation, as well as the heartbeat caused at the surface of the body wall in the chest region.

Principle of FMCW is based on CW radar, however, the transmitted signal is the frequency modulated signal. Base on CW radar principle, FMCW can recognize the

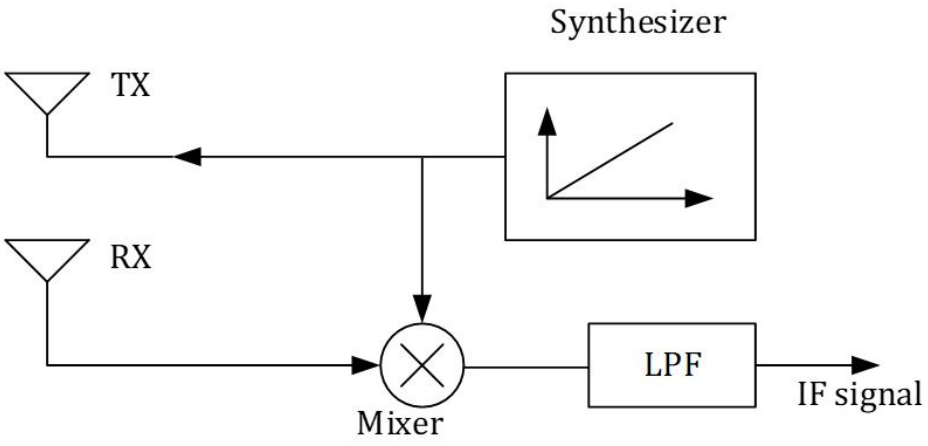

Figure 2.3: Structure of FMCW radar

velocity of object and by transmitting the modulated frequencies and receiving them, the range can be measured.

Principle of range detection is as follow. A signal generator produces a chirp waveform which is transmitted using a transmitting (TX) antenna. This chirp signal is then

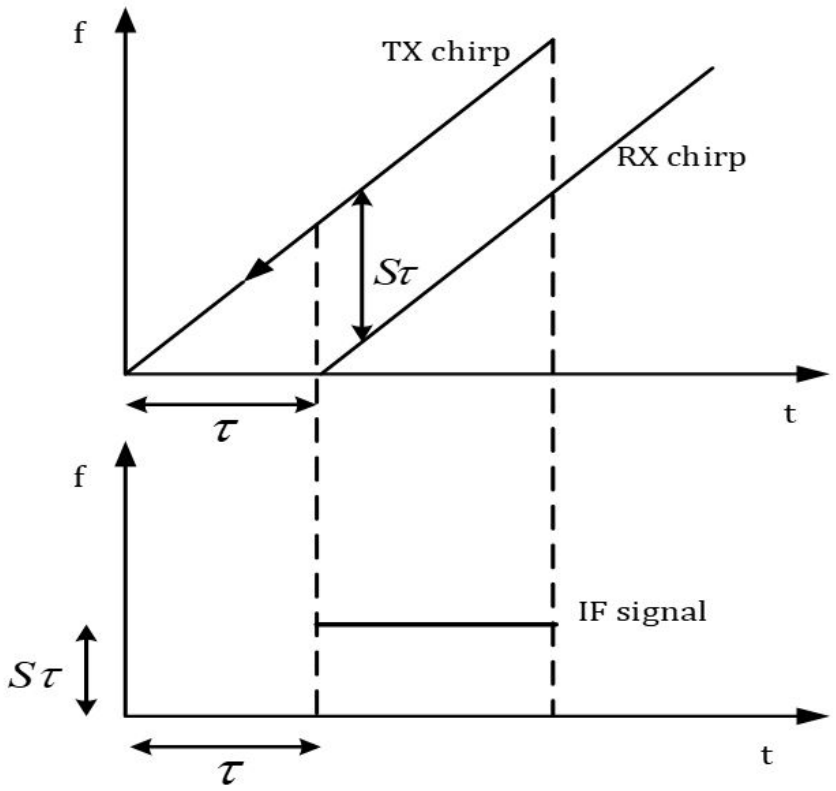

Figure 2.4: An IF signal of a constant frequency $S \times 2d/c$ is generated by the presence of a object within the radar's range

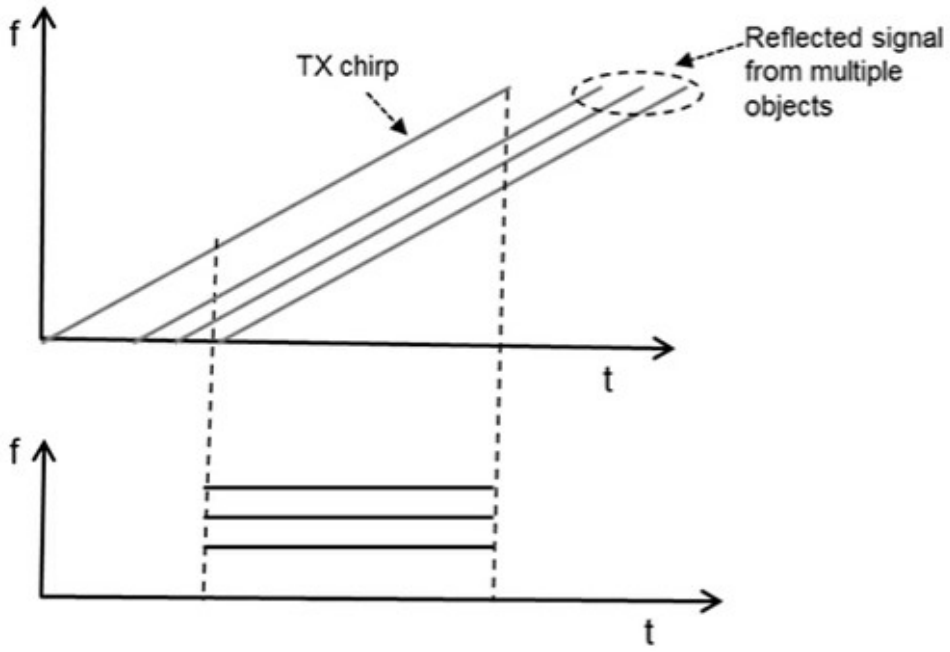

Figure 2.5: The IF signal contains multiple frequencies

reflected off an object and received by a receiving (RX) antenna in the form of a reflected chirp signal. RX and TX signal are multiplied by mixer and result signals is filtered by low-pass-filter to keep the frequency of subtracted frequency signal, call IF signal (intermediate frequency signal), as given in Figure 2.3.

In Figure 2.4, The received signal is a time-shifted replica of the transmitted signal.

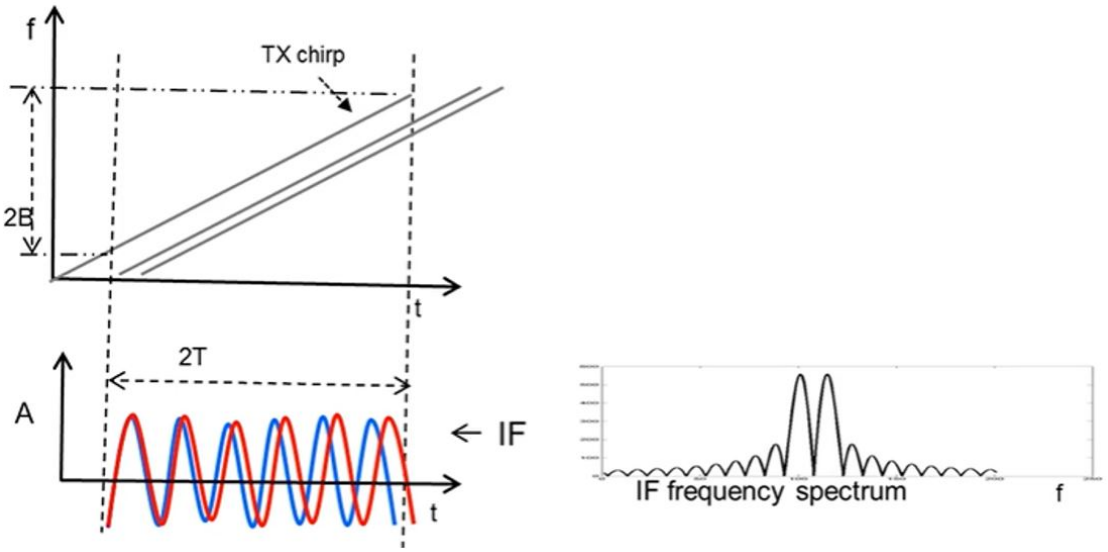

Figure 2.6: Demodulation of multiple tones in the IF signal using FMCW radar

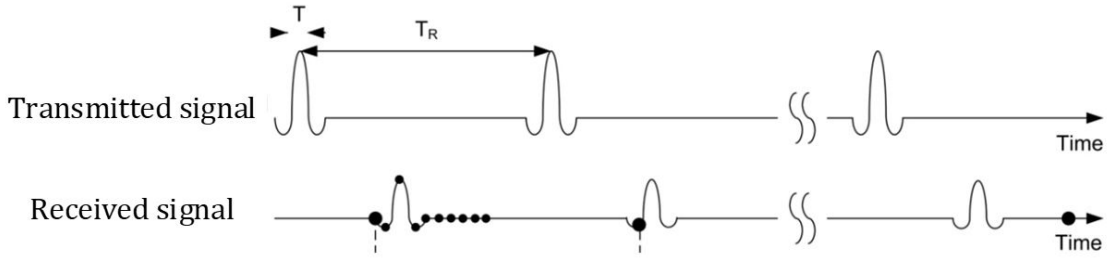

Figure 2.7: UWB radar signal in time domain

τ is the round-trip time between the radar and the object. The slope of the chirp is represented by $S\tau$. The frequency of the signal at the mixers output is the difference of the instantaneous frequency of the TX-chirp and RX-chirp. This is a straight line as Figure 2.4. So that, when the radar is facing a single object, an IF signal with a steady frequency is generated, and this frequency is identified as $S\tau = S \times 2d/c$ with $\tau = 2d/c$, d is the distance of the object and c is the light speed. In order to detect two objects moving with different frequencies, it is necessary to take a sufficiently long signal, and it is usually taken a signal length of 2T to make it be distinguishable, as shown in the Figure 2.5.

In Figure 2.6, assuming that we take the signal length to be $1T$, the two signal in blue and red, when analyzed on the frequency domain by FFT (fast Fourier transform) it will have the same frequency. However, if the signal length is $2T$, the frequencies can be distinguished as shown in the right part of Figure 2.6.

About principle of UWB radar, it uses wireless carrier communication technology. UWB radar systems use transmitter antennas to transmit input signals with very short-time pulse, mainly in nanoseconds, as shown in Figure 2.7. This input signal comes from the antenna of the input transmitter which transmits at the speed of light. A short pulse is transmitted, the transmitted signal hits the subject and is reflected back to the receiving antenna. By measuring the time took for the pulse to be transmitted and received, the

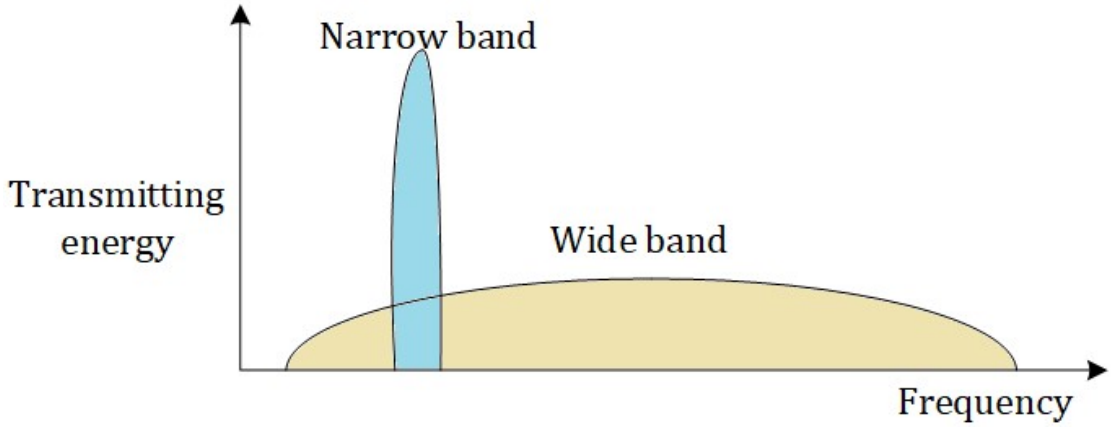

Figure 2.8: UWB radar signal and narrow band radar signal in frequency domain

distance between the radar and the subject can be calculated. This applies to the medical measurement of chest wall motion, consecutive distances can be measured, and therefore, the range of the chest wall can be calculated. An advantage of UWB radar is that it is energy efficient and the detectable frequency range is wide. By transmitting and receiving pulses under nanoseconds carrier-free or short-pulse modulation with carrier. Since the energy is calculated as power multiply to lifetime of the signal, so for the same transmit power, the UWB with the use of a pulsed signal, in which the exist pulse is shorter than that of the continuous signal as the two types of radar CW and FMCW, so it can be said that UWB is more energy efficient, as illustrated in Figure 2.8. Such systems have the ability to offer high data rates while maintaining low system complexity, low power consumption, and low cost [51,52].

2.2 Survey On Radar-based Vital Sign Detection And Aim Of The Dissertation

Measuring vital signs by non-contact methods are desirable both in hospital settings and ubiquitous on-site health monitoring such as mobile phones and computers equipped

with cameras that are connected to the internet. Recently, camera-based contactless vital sign monitoring has been shown to be feasible. However, monitoring vital signs using cameras poses difficulties for individual with dark skin complexion, in low light level or while a person is moving in front of the camera. In addition to that, camera-based in some cases is not suitable for private issue. So that, this thesis focuses on radar-based vital sign detection.

Breathing rate and heart rate are detected using peak estimation algorithms, which are performed by signal processing in the time domain [53,54,55]. On the basis of breathing and heart rate monitoring, influenza diagnostic systems are designed to support medical purposes [56]. In radar signal, using digital processing algorithms, the signal then still contains harmonics, accordingly, a system based on ultra-wideband radar (UWB) was researched and built to eliminate the harmonics and noise [57,58,59]. Recent studies also used neural networks to find out breathing and heart rate [54], [60]. Recently, the application of radar in detecting breathing and heart rate has been focused. However, these studies mainly focus on finding the vital sign from the radar received signal. There are few studies explaining details why the radar channel signal can carry information about the small movements of the human thorax relative to the heart and lung peaks [61], and the encountered problems when measuring to obtain the signal to carry the information of body movement due to vital sign. Therefore, this study will present the principle of signals acquisition on I and Q channels of 24 GHz Doppler radar, and explain why the received signal contains information about chest movement. In addition, by theoretical analysis, this study shows that motions greater than half of wavelength and less than half of wavelength will behave differently on the radar signal. For motion with displacement less than half of wavelength, the 24 GHz radar signal on the I and Q channels does not

require to demodulate, the center frequency of the signal will coincide with the breathing frequency. Previous studies have shown that the movement of the thoracic surface due to breathing activity is between 4 and 12 mm depending on the individual physiology [62], while the movement of the chest wall due to the heart beat action is 0.6 mm [63]. Meanwhile, experimentally, it has been shown that the movement of the chest wall from the front of the body can be greater than half the wavelength, and the movement of the chest wall from the back of the body, i.e. in the lying position, is less than half the wavelength.

In this study, in order to present more deeply the principle of 24 GHz radar in measuring vital sign, the experiment is designed with actuator movement. To find the doppler frequency, the displacement of movement must be greater than half of wavelength. It has to be said that with the 24 GHz doppler radar, the half of wavelength is approximately 6.2 mm (specifically $f_0 = 24.15\,\text{GHz}$, $\lambda = 12.4\,mm$, $\lambda/2 = 6.2\,mm$). Because the displacement of the actuator movement can be adjusted from the computer program, so the motion of a plate with a greater displacement of motion and less than half the wavelength is created. The radar signal in two cases is captured and analyzed. Next, after concluding for the signal of the plate movement and actuator, the experiment on the human body is performed. The individual being measured was breathing normally, and the signal is measured from the front and back of the body. The individual then performs deep inhalations to produce anterior chest wall movement greater than half a wavelength.

In another analysis, the study will show that, for motion with displacement greater than half of wavelength, no imbalance occurs, and doppler frequency are found. Conversely, for motion with displacement less than half of wavelength, an imbalance can occur, and the doppler frequency is not found. In the case of motion with displacement less than half a wavelength, in order to obtain a balanced signal, the distance from the

measured object to the radar needs to be established, this study will give a formula to calculate that distance.

The traditional method of measuring the vital sign requires to place multiple electrodes on the patient's body. This is difficult for people with skin lesions, or skin allergies to the gel of the electrode. Although with the development of technology, contact devices are also miniaturized and increased in convenience [64]. However, the devices still need to be in contact with the human skin, and for this reason, sometimes accuracy is not guaranteed when the patient has skin problems such as wet skin and burned skin. The solution of using contactless devices will solve the above difficulties. Contactless devices can capture images, video by camera, or time series signals by radar. In some situations, for privacy reasons, radar is the preferred chosen device. In 1985 Lee and Lin proposed a model using continuous-wave radar to measure the vital sign [65]. By using radar for clinic purposes as well as home healthcare monitoring, it will help patient comfort, increase efficiency, and reduce the effort of medical staff [66, 67].

However, the radar output signal is very sensitive to noise. Signal including a small body movement will lead to low accuracy of the algorithm to find RR and HR [68]. Previous studies focused on finding the vital sign based on the measurement of the radar signal, but there are few studies presented on the signal quality classification. The signal quality classification is the distinction between the signal containing noise and no noise i.e the signal that guarantees a certain quality to find the parameter of interest. [69] classified the noisy segments in the PCG (phonocardiogram) record by taking a segment that was not noisy. This segment was used as a reference to compare all other segments. If the correlation between them exceeds a certain threshold, the segment was defined as good or bad quality. Reference labeling was performed by a clinician. However, there was no

separate dataset for training and testing. The author optimized their method and threshold on the same data used for testing. As a result, the reported metric was invalid for unseen data, as performance can be significantly reduced for data the processing system has never seen. Moreover, PCG is still a contact measuring device, in this research my focus is on the non-contact solution. The study [70] classifies signal quality for heart sound signal, but the signal set is taken from open data source, that was signal received from smart phone application and digital stethoscope, the results were about 94.3 % accuracy in 10-fold validation. However, this dissertation focuses on signals measured on real people, towards practical applications. Study [71] used a dataset of measurements on real subjects from university hospital volunteers. The equipment used to measure was six-port interferometers radar, the mechanism of which allowed the relative distance to be calculated. The features were extracted and trained, then the training parameter was used for the test model. Labeling the signal segments was after the signal to noise result of the signal is below the threshold level of 3dB. The signal quality classification achieved an accuracy of 96.36%. However, the aim of the two studies [70, 71] was to classify the signal as good enough for detecting heart sound. Heart sound studies are helpful in diagnosing disease related to heart valve. In research [72], vital sign quality assessment was based on assessing the correlation between the signal in the noise-containing and noise-free groups and analyzing the signal spectrum. However, the sensor used was a type of UWB radar while no study has been found to present the signal quality classification for vital sign purposes using CW doppler radar as this research. For using doppler radar, when the signal belongs to the good quality signal, many studies have found the vital sign [66,67, 73, 74, 75]. Once the vital sign was detected, then applications were included for the diagnosis of diseases related to lung and heart [76, 77].

In this study, the signal quality of 24 GHz CW radar measured on human subjects was classified into 2 groups: signals containing noise due to random body movement and signals without random body movements. For the signal segments that are considered to be of good quality, that is, there is no noise caused by random body movements, the detected RR and HR algorithms are applied. After applying the algorithm, the peaks shown in the RR and HR signal curves no longer contain unwanted harmonic peaks as in conventional methods.

When using radar to detect vital signs, the first parameters researchers look for are RR and HR. In the one hand, the RR can be found using the arctangent demodulation algorithm from the phase of the I and Q channels. Another method is using the complex FFT when combining the I and Q channels into the complex digital domain. RR is also detected by using a single signal channel when displacement is less than half the wavelength and find the envelop. In the other hand, HR detecting algorithms are presented by the study using bandpass filter, PCA, ICA and SVD algorithms as in this study. As a next step, a parameter that requires more accuracy in terms of heartbeat peak time is HRV. While HR is the number of heartbeats in one minute, HRV is the change in the interval between the heartbeats. HRV represents a physiological activity, it is different from a machine, the beat is the same, the human heart rate has a variation of fast and slow, when human exhale, the heart rate is slower and therefore higher HRV curve. In contrast, when human breathe in, the heart rate is faster, so the interval between the heartbeats is shorter, so the HRV curve is lower. HRV is the curve connecting the inter-beat interval (IBI), due to the influence of the autonomic nervous system [78]. IBI shows the distance from one beat to the next, thus, in order to find the HRV, it is required that the algorithm find the signal peaks accurately in time. A normal, healthy heart ticks at the milliseconds

between heartbeats. HRV is the calculated variable between multiple R-R intervals. The respiratory rate can change the central blood volume and R-R interval, in other words, HRV changes based on the interaction of the sympathetic and parasympathetic nervous systems so that we can assess and recognize fatigue of the body and predict cardiovascular disease [79]. While cardiovascular diseases are getting more attention, the monitoring of heart indicators is absolutely necessary, HRV is more important parameter than other vital sign parameters in monitoring heart status [80,81], which is an important predictor of arrhythmic events after myocardial infarction [82,83].

With conventional methods, HRV has been inferred and evaluated based on ECG signal [84,85,86]. However, ECG is a contact measurement method. When measuring, it is necessary to put many electrodes on the measured body, the contact measurement method with difficulties as shown in chapter I is not suitable for long-term patient monitoring. Nowadays, monitoring the vital sign using the non-contact method is a trend and a need, because this method does not require contact with the skin or the patient's body, it can calibrate the disadvantages of the contact measurement method [87,88]. Many previous studies have also calculated HRV based on radar [89,90,91,92,93]. Based on abnormalities in HRV monitoring, cardiovascular disease can be diagnosed and warned [88,94]. However, in previous studies, there are some disadvantages that need to overcome to be applied in practice. Furthermore, these methods are still mainly based on fast Fourier transform (FFT) and band-pass filter (BPF), which may be more suitable for finding average heart rate than for finding HRV. Because HRV requires precise time of R peaks. Specifically, the above methods can be summarized as follows. Research [89,93] required the measured subject to sit in front of the radar so that the radar measured from the front of the body, this is not appropriate in the context of long-term health monitor-

ing for patients lying in bed. Research [90,91] uses many time-window for fast Fourier transform (FFT), then, based on the amplitude to find the peak with the largest amplitude in a heartbeat cycle. Research [92] used the band-pass filter (BPF) combine with integrated spectrum to find the R-peak. Research [93] takes the raw signal from the radar, and performs the summation of the two-channel signal. For 24 GHz radar, because the body wall movement is very small by vital sign, the signal imbalance occurs. Therefore, the sum of the two signal channels can be attenuated or enhanced. However, this sum contains the RR, HR and noise components. Next, the author used a BPF array designed in different narrow frequency bands. The selection of the output of a BPF is done by a chirp Z transform. However, the above methods all cause IBI distortion in the time domain, due to the inherent characteristics of FFT and BPF, thereby affecting the accuracy of the HRV results. To overcome this, research [95] used the locally projective noise reduction (LPNR) technique to its effect. However, the author has used LPNR for both RR detection, resulting in a large computational load. And the author has not given HRV parameter.

Finding HRV requires finding the peak corresponding to the R wave in the ECG and ensuring precise timing. Conventional algorithms such as bandpass filters, PCA, ICA and SVD is not suitable for obtaining HRV with high accuracy. Therefore, in this study, finding HRV was performed in the following order. First, one of the two signal channels from the radar is selected, the signal channel with the standard deviation for the larger heart rate component is selected. Next, the breath component is separated from the signal by a convolution filter. The signal after subtracting the breathing component will still contain the heartbeat component and noise. LPNR technique is applied to remove noise. The received signal is used to find the peak corresponding to the R wave. A five-point

stencil filter is used to find the peak with the greatest slope. Because of the physiological workings of the body and the measuring principle of the radar, the corresponding peak of the R wave will produce the wave with the greatest slope in the signal. The peak with the greatest slope was found corresponding to the R wave. The IBI interval was calculated and inferred for HRV.

Chapter 3

CW RADAR PRINCIPLE AND RADAR SIGNAL OF VITAL SIGN MEASUREMENT

3.1 Radar Principle For Vital Sign Measurement

An explanatory model for the principle of radar operation in the vital sign measurement is shown in Figure 3.1. Radar transmits a signal, called transmitted signal. This signal hits the body wall, the reflected signal returns to the radar, called received signal. The terms "transmitted" and "received" are standing on the radar side to describe. When the person inhales, the chest wall opens wider, like a red dashed line. When exhales, the chest wall collapses. Thus, when the person inhales, the chest wall is moving towards the radar, and when the person exhales, the chest wall is moving away from the radar.

3.1.1 Inhalation reflect on radar signal

Inhalation make chest wall approaching radar. This process of principle can be described as follow. Let d_0 refer to the range at time t_0 (time reference); then the range from the radar to the chest wall at any time is

$$R(t) = d_0 - \int_{t_0}^{t} v(t)\,dt \tag{3.1}$$

Let $V(t)$ be the primitive function of the velocity, so we have

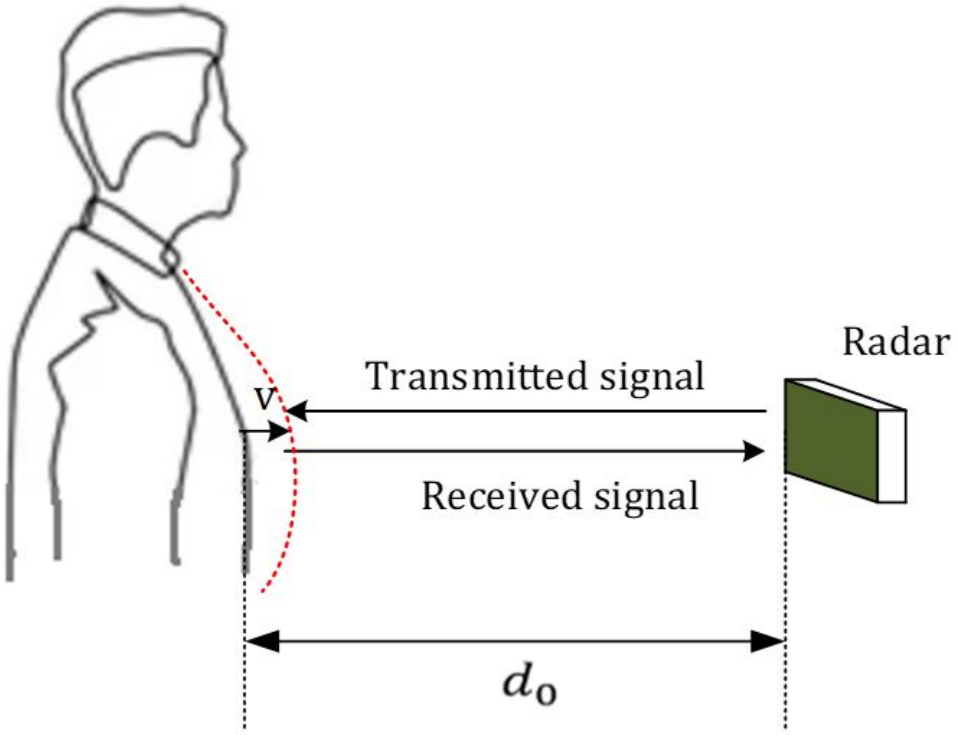

Figure 3.1: Principle of radar for vital signs measurement

$$R(t) = d_0 - V(t) + V(t_0) \tag{3.2}$$

The received signal is expressed by Equation (3.3)

$$x_r(t) = x(t - \psi(t)) \tag{3.3}$$

where $x(t)$ is the transmitted signal, and $\psi(t)$ is the time from signal transmitting to receiving, as

$$\psi(t) = \frac{2}{c}(d_0 - V(t) + V(t_0)) \tag{3.4}$$

Substituting Equation (3.4) into Equation (3.3), the received signal can be written as

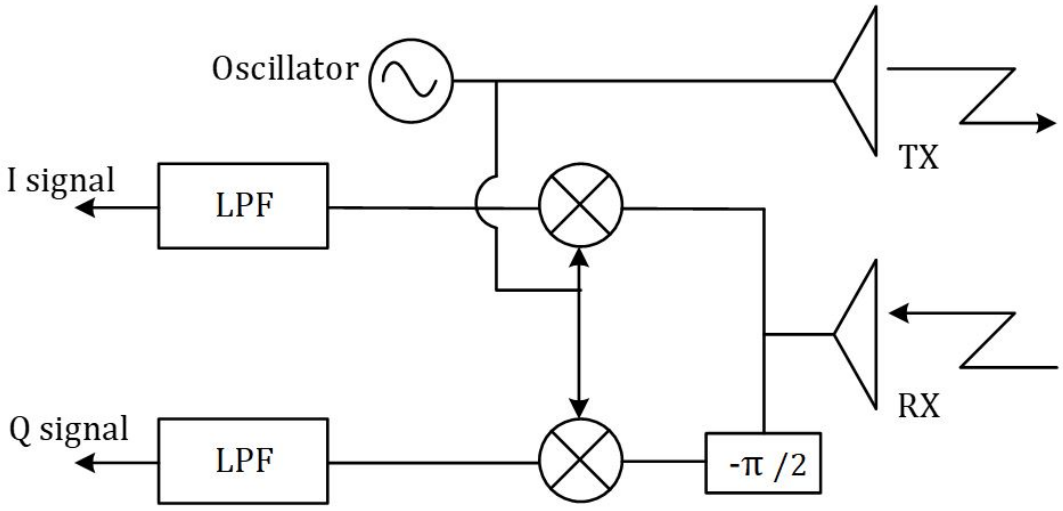

Figure 3.2: CW radar structure

$$\begin{aligned} x_r(t) &= x\left[t - \frac{2}{c}(d_0 - V(t) + V(t_0))\right] \\ &= x\left(t - \frac{2d_0}{c} + \frac{2V(t)}{c} - \frac{2V(t_0)}{c}\right) \end{aligned} \tag{3.5}$$

The above are general formulas of transmitted and received signals. A cosine signal can be used as a model for the transmitted signal as (3.6)

$$T(t) = A.cos(2\pi ft) \tag{3.6}$$

The reflected signal at Equation (3.5) can be re-written as Equation (3.7)

$$R(t) = A.cos\left(2\pi ft - \frac{4\pi fd_0}{c} + \frac{4\pi fV(t)}{c} - \frac{4\pi fV(t_0)}{c}\right) \tag{3.7}$$

Rewrite and transfer (3.7) to (3.8), then (3.9) and (3.10)

$$R(t) = A.cos\left(2\pi ft - \frac{4\pi d_0}{\lambda} + \frac{4\pi V(t)}{\lambda} - \frac{4\pi V(t_0)}{\lambda}\right) \tag{3.8}$$

$$R(t) = A.cos\left(2\pi ft - \frac{4\pi d_0}{\lambda} + \frac{4\pi s(t)}{\lambda} - \frac{4\pi s(t_0)}{\lambda}\right) \tag{3.9}$$

$$R(t) = A.cos\left(2\pi ft + \frac{4\pi s(t)}{\lambda} + \theta\right) \tag{3.10}$$

where $\theta = -\frac{4\pi d_0}{\lambda} - \frac{4\pi s(t_0)}{\lambda}$ and $s(t)$ is the function of movement due to vital sign.

Based on the structure of the CW doppler radar presented as Fig. 3.2, the received signal in Equation (3.10) will be combined with the signal from oscillator in Equation (3.6) by a multiplier.

$$T(t) * R(t) = A^2 cos(2\pi ft).cos\left(2\pi ft + \frac{4\pi s(t)}{\lambda} + \theta\right) \tag{3.11}$$

After that, a signal with high frequency at double the transmitted frequency and a baseband signal are acquired. The baseband signal is obtained by applying a low-pass filter (LPF). The I channel signal can then be obtained in the following

$$B_I(t) = A_r.cos\left(\frac{4\pi s(t)}{\lambda} + \theta\right) \tag{3.12}$$

where $A_r = \frac{A^2}{2}$. To obtain the Q-channel signal, the received signal is delayed by $\pi/2$ and then multiplied by the transmitted signal. After passing through a filter to acquire the baseband signal, the Q channel signal can be obtained according to equation (3.13)

$$B_Q(t) = A_r.cos\left(\frac{4\pi s(t)}{\lambda} + \theta - \frac{\pi}{2}\right) \tag{3.13}$$

3.1.2 Exhalation reflect on radar signal

Exhalation makes chest wall leaving radar. This process can be described as follow. The range from the radar to the chest wall at any time is

$$R(t) = d_0 + \int_{t_0}^{t} v(t)\,dt \tag{3.14}$$

Let V(t) be the primitive function of the velocity, so we have

$$R(t) = d_0 + V(t) - V(t_0) \tag{3.15}$$

The reflected signal is given by (3.16)

$$x_r(t) = x(t - \psi(t)) \tag{3.16}$$

where $x(t)$ is the transmitted signal, and $\psi(t)$ is the time from signal transmitting to receiving, as (3.17)

$$\psi(t) = \frac{2}{c}\left(d_0 + V(t) - V(t_0)\right) \tag{3.17}$$

Substituting Equation (3.17) into Equation (3.16), the received signal can be written as (3.18)

$$\begin{aligned} x_r(t) &= x\left[t - \frac{2}{c}\left(d_0 + V(t) - V(t_0)\right)\right] \\ &= x\left(t - \frac{2d_0}{c} - \frac{2V(t)}{c} + \frac{2V(t_0)}{c}\right) \end{aligned} \tag{3.18}$$

A cosine signal can be used as a model for the transmitted signal as

$$T(t) = A.cos(2\pi ft) \tag{3.19}$$

The reflected signal at Equation (3.18) can be re-written as Equation (3.20)

$$R(t) = A.cos\left(2\pi ft - \frac{4\pi fd_0}{c} - \frac{4\pi fV(t)}{c} + \frac{4\pi fV(t_0)}{c}\right) \tag{3.20}$$

Rewrite and transfer (3.20) to (3.21)

$$R(t) = A.cos\left(2\pi ft - \frac{4\pi s(t)}{\lambda} + \theta\right) \tag{3.21}$$

where $\theta = -\frac{4\pi d_0}{\lambda} + \frac{4\pi s(t_0)}{\lambda}$ and $s(t)$ is the function of movement due to vital sign.

Based on the structure of the CW doppler radar presented as Fig. 3.2, the received signal in Equation (3.21) will be combined with the signal from oscillator in Equation (3.19) by a multiplier.

$$T(t) * R(t) = A^2 cos(2\pi ft).cos\left(2\pi ft - \frac{4\pi s(t)}{\lambda} + \theta\right) \tag{3.22}$$

After that, a signal with high frequency at double the transmitted frequency and a baseband signal are acquired. The baseband signal is obtained by applying a low-pass filter (LPF). The I channel signal can then be obtained in the following

$$B_I(t) = A_r.cos\left(\frac{-4\pi s(t)}{\lambda} + \theta\right) \tag{3.23}$$

where $A_r = \frac{A^2}{2}$. To obtain the Q-channel signal, the received signal is delayed by $\pi/2$ and then multiplied by the transmitted signal. After passing through a filter to acquire the baseband signal, the Q channel signal can be obtained according to equation (3.24)

$$B_Q(t) = A_r.cos\left(\frac{-4\pi s(t)}{\lambda} + \theta - \frac{\pi}{2}\right) \tag{3.24}$$

3.1.3 I-channel and q-channel signal on unit circle

To understand more the I and Q channel signal, the relationship between I and Q signal can be described on the unit circle. Rewrite expression (3.13) as follows

$$B_Q(t) = A_r.sin\left(\frac{4\pi s(t)}{\lambda} + \theta\right) \tag{3.25}$$

Then divide the corresponding sides of (3.25) by (3.12), we can infer

$$\frac{4\pi s(t)}{\lambda} = arctan\left(\frac{B_Q(t)}{B_I(t)}\right) - \theta \tag{3.26}$$

So that, $s(t)$ has a linear relationship with $arctan\left(\frac{B_Q(t)}{B_I(t)}\right)$ when wavelength is constant.

Rewrite (3.26), $s(t)$ can be gotten as (3.27)

$$s(t) = \frac{\lambda}{4\pi}.arctan\left(\frac{B_Q(t)}{B_I(t)}\right) - \frac{\lambda}{4\pi}.\theta \tag{3.27}$$

For displacement:

$$|s(t_2) - s(t_1)| = d(t) \tag{3.28}$$

We define:

$$\alpha = arctan\left(\frac{B_Q(t)}{B_I(t)}\right) \tag{3.29}$$

So that displacement $d(t)$ can be written as (3.30)

$$d(t) = |s(t_2) - s(t_1)| = \frac{\lambda}{4\pi}.\alpha \tag{3.30}$$

When $\alpha = k.2\pi$, then

$$d(t) = k.\frac{\lambda}{4\pi}.2\pi = k.\frac{\lambda}{2} \tag{3.31}$$

From Equation (3.31), for k=1, means $\alpha = 2\pi$, then the displacement is $d(t) = \lambda/2$. This means that a displacement $\lambda/2$ corresponds to arctangent 2π (a circle). In addition, for simple, I and Q signal can be re-written as follows:

$$B_Q(t) = \frac{B_Q(t)}{A_r} = sin\left(\frac{4\pi s(t)}{\lambda} + \theta\right) \tag{3.32}$$

$$B_I(t) = \frac{B_I(t)}{A_r} = sin\left(\frac{4\pi s(t)}{\lambda} + \theta\right) \tag{3.33}$$

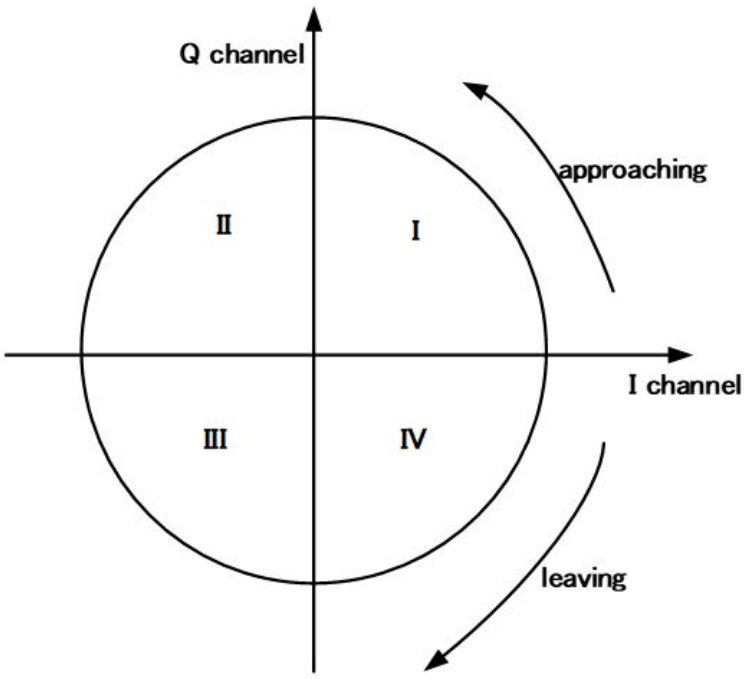

Figure 3.3: Radar signals including I and Q channel illustrated on the unit circle

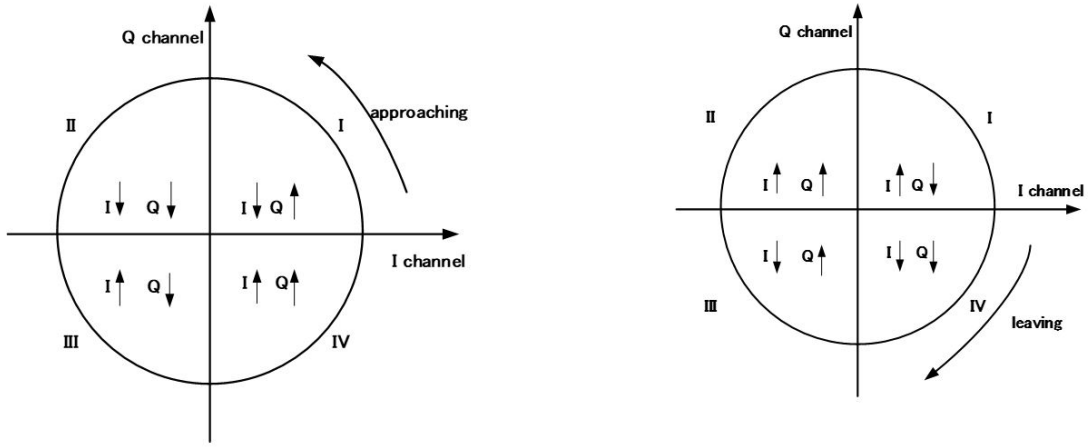

Figure 3.4: The description of I and Q channels direction when object approaching and leaving radar

So that we can point out B_I and B_Q on a circle as Figure 3.3

About increasing and decreasing analysis of I and Q signal when target moving. For approaching process, in quadrant I, II, III and IV on unit circle, I signal decreases and Q signal increases, I signal decreases and Q signal decreases, I signal increases and Q signal decreases, I signal increases and Q signal increases, respectively, as show in Figure 3.4 (a). And the increase and decrease of signal I, Q for leaving process is shown in Figure 3.4 (b).

Figure 3.5 analyzes an experiment with the plate moving a 10 mm displacement. The experiment arrangement is in Figure 3.6, the movement of the metal plate is repeated

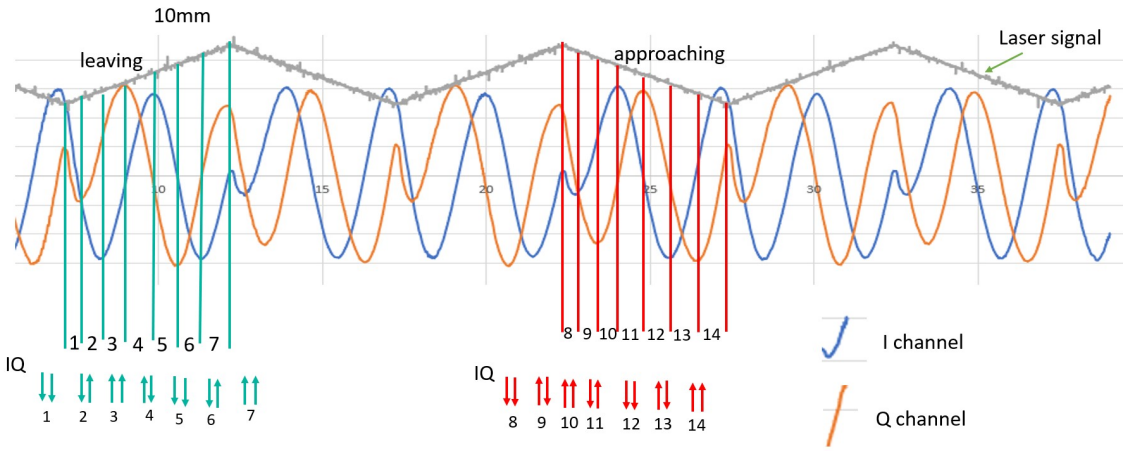

Figure 3.5: Analysis of I and Q signal by experiment output

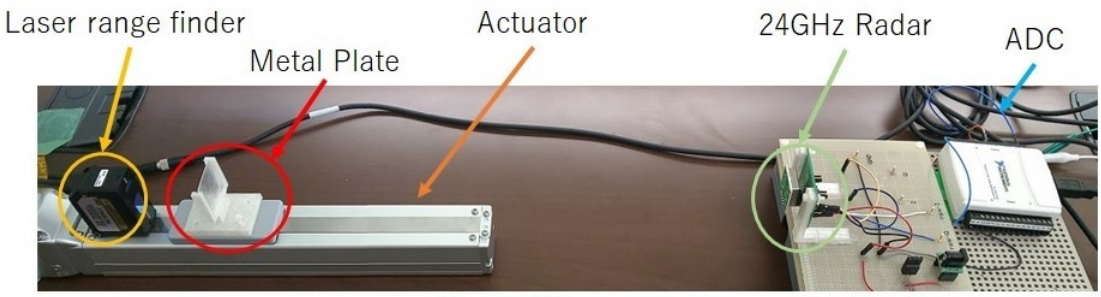

Figure 3.6: Arrangement of device for radar measurement

thanks to the actuator being precisely controlled from the computer. Radar is placed a distance from the plate to measure the signal when the plate moves. The laser is placed on the opposite side of the radar. As the plate approaches the radar, the voltage signal from the laser decreases and when the plate moves away from the radar, the voltage signal from the laser increases.

From the analysis of the increasing and decreasing trend of I, Q signal in Figure 3.5 by experiment and the trend described by theory in Figure 3.4, the direction moving of the object on the unit circle along with the I signal and Q channel can be marked as shown in Figure 3.3.

3.1.4 Some inferences

It can be seen from formulas (3.12), (3.13), (3.23) and (3.24) that, when object approaching radar, I channel is phased earlier than Q channel by an angle of $\lambda/2$, as in formulas (3.12) and (3.13). When leaving, Q channel is phased earlier than I channel by $\lambda/2$, as in formulas (3.23) and (3.24). This also completely coincides with the figure in Figure 3.5, plotting the signal by experiment.

When depict the I and Q signals on the unit circle, depending on the magnitude of the displacement, the point representing the motion of the object will pass through a different number of quadrants. Displacement equal to $\lambda/2$ corresponds to a unit circle.

For displacement less than $\lambda/2$, the object point does not go more than one unit circle, and therefore the doppler frequency is not seen. However, in this case, the number of peaks of the I or Q signal is exactly equal to the number of peaks of the baseband signal of the object.

For displacement greater than $\lambda/2$, the object point goes through more than one unit circle, and thus the doppler frequency is seen. In this case, the number of peaks of the I or Q signal is greater than the number of peaks of the baseband signal of the object. Therefore, in this case, to find out the frequency of the baseband motion, it is required to use the signals of both channels, to find the change in the phase relationship. From the phase relationship, the frequency of based-band motion is found.

These conclusions are drawn from theory and experiment with actuators, and are applied to measure vital sign. When measured from the front of the body, displacement can be greater or less than $\lambda/2$, but when measured from the back of the body, displacement is always less than $\lambda/2$. And so, depending on whether it is measured from the front or back of the body, the above conclusions applied accordingly.

3.2 The Problems With CW Radar- Based Vital Sign Measurement And Signal Quality Assessment

3.2.1 Imbalance between two channel signals

From Equation (3.31), for $k = 1$, means $\alpha = 2\pi$, then the displacement is $d(t) = \lambda/2$. This means that a displacement $\lambda/2$ corresponds to arctangent 2π (a circle). Therefore, for motions with displacement greater than or equal to $\lambda/2$, the two signal channels I and Q are always balanced for any distance from radar to object, because when projected

on the unit circle both channels shift from -1 to 1 on the unit circle as shown in Figure 3.7a. However, for motion with displacement less than $\lambda/2$ the balance will depend on the distance of the radar to the object. If the distance of the radar to the object causes the displacement oscillated around a point on the bisector of the quadrant, the signal is balanced. Conversely, if the distance from the radar to the object causes displacement oscillated not on the bisector, an imbalance will occur, as shown in Figure 3.7.

Figure 3.7a shows the movement with the displacement larger than $\lambda/2$, the amplitude of I and Q channel is equal to each other, the signals are balanced between the two channels, and the two signal channels carry the same information about the vital sign. For 3.7b, the movement with the displacement smaller than $\lambda/2$, the motion oscillates around point A which is not on the bisector of the quadrant. In this case, the Q channel has a larger amplitude and a larger standard deviation than channel I.

Regarding the balance and imbalance in amplitude, this study will show the experiment result with the plate. With the plate movement, the displacement magnitude, frequency and reference can be controlled exactly by PC (Personal Computer). Experimental arrangement as shown as the Figure 3.8.

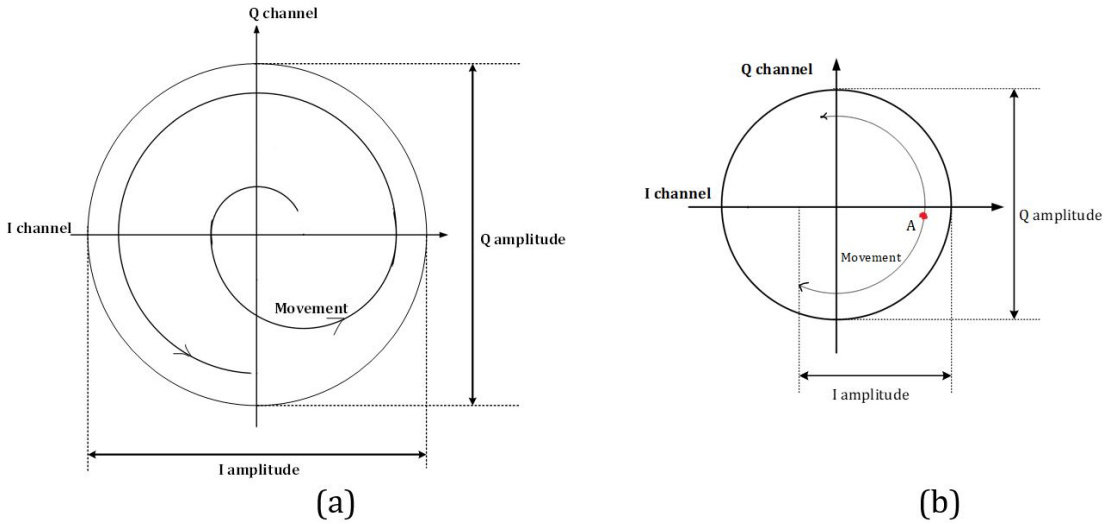

Figure 3.7: Displacement representation on the unit circle

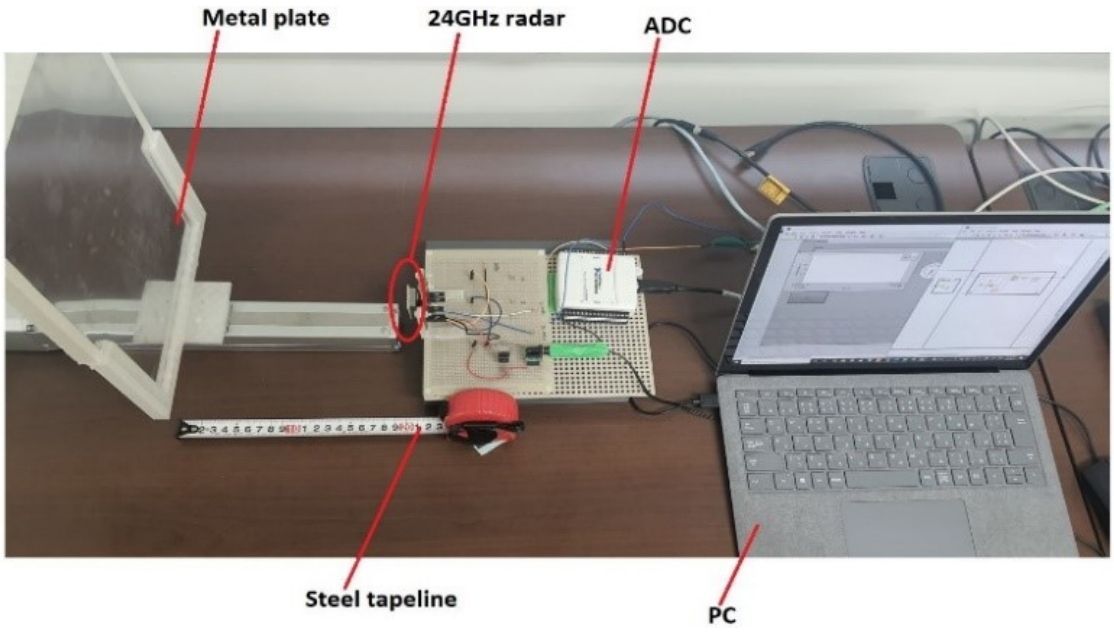

Figure 3.8: Arrangement of measuring radar signal with plate movement

This experiment is to measure motion with $s(t)$ bigger than half of radar wavelength, on the unit circle, the moving point moves larger than a circle 2π, so that the amplitude of both the I and Q signals is consistently balanced. Furthermore, with displacement of 8mm, 8mm is bigger than half of wavelength, so once approaching or once leaving of the plate (within green line) will produce more than 1 peak on radar signal. With displacement of 20mm, 20mm is more than 3 times the half wavelength, so a once approaching or once leaving of the plate will produce more than 3 peaks on the radar signal, as shown in the Figure 3.9.

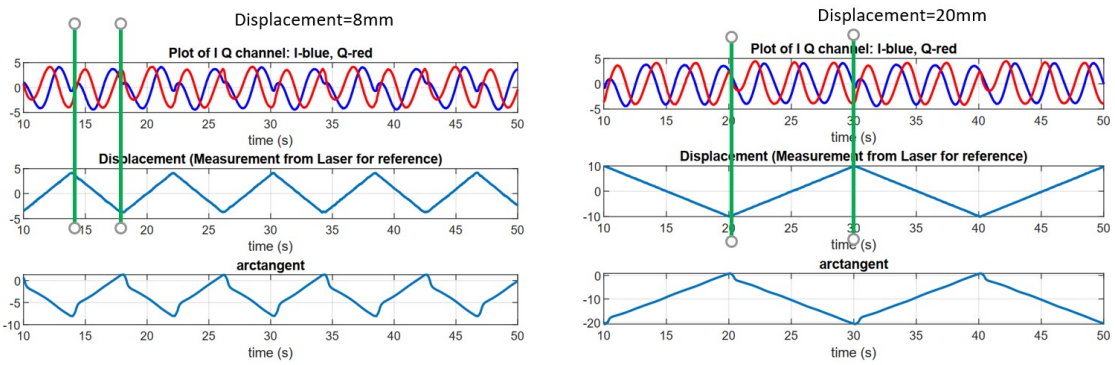

Figure 3.9: Radar signal analysis with reference signal

With the body wall due to vital signs, displacement is smaller than half wavelength, so the I and Q signals can be balanced or imbalanced in amplitude depending on the distance to the radar. This motion can be described by experimenting with a plate of displacement 1.5 mm, frequency 0.4Hz. Because the body wall motion due to vital signs measured from the back side will be smaller than 2 mm [43, 62], so the thesis chose this displacement with the plate experiment. The generated I, Q signals will be different, as shown in the Figure 3.10. We can see that the displacement in 4 figures is the same (laser signal for reference) but raw radar signals are different due to different distance.

In Figure 3.10, figure (a) and figure (c) represent signals I, Q with balanced amplitude. And if we represent the center point of the displacement on a circle, these two positions are separated by $\pi/4$ and these distances is separated by $\lambda/8$, as shown in the Figure 3.11.

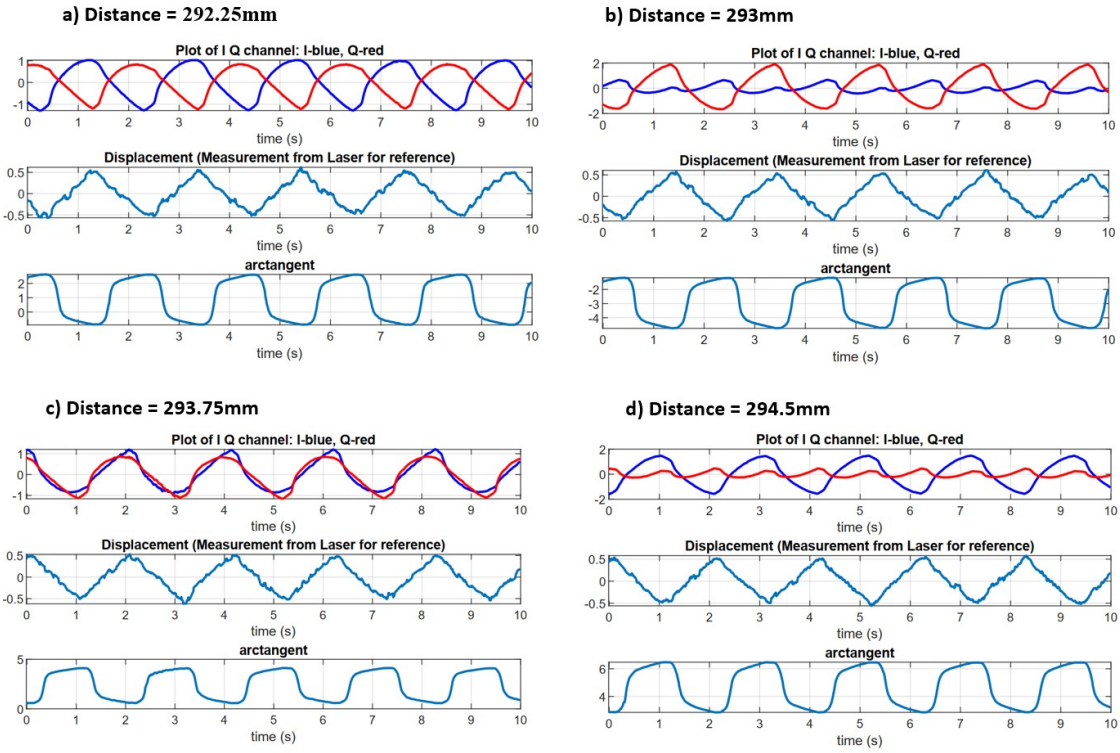

Figure 3.10: Radar signal analysis with imbalance and balance

Recall equation (3.31)

$$d(t) = k.\frac{\lambda}{4\pi}.2\pi = k.\frac{\lambda}{2} \tag{3.34}$$

For k=1, means $\alpha = 2\pi$, then the displacement is $d(t) = \lambda/2$. According to Equation (3.34), a displacement of $\lambda/2$ results in a circular pattern. If the object's displacement exceeds $\lambda/2$, the Doppler frequency is detectable in the signal, and the amplitudes of the I and Q channels remain balanced. However, the displacement of the body wall from the back side is typically less than 2mm [43, 62], whereas $\lambda/2 \simeq 6.2mm$. This can cause an imbalance in the signals. To achieve balanced signals between the I and Q channels, object-to-radar distances are chosen strictly. In this study, two 24 GHz channels were utilized, and the optimal distance from the radar to the object was determined to obtain amplitude balanced signals. Figure 3.11 displays that a balanced distance on the unit circle is situated on the bisectors of the four quadrants, which is expressed by Equation (3.35).

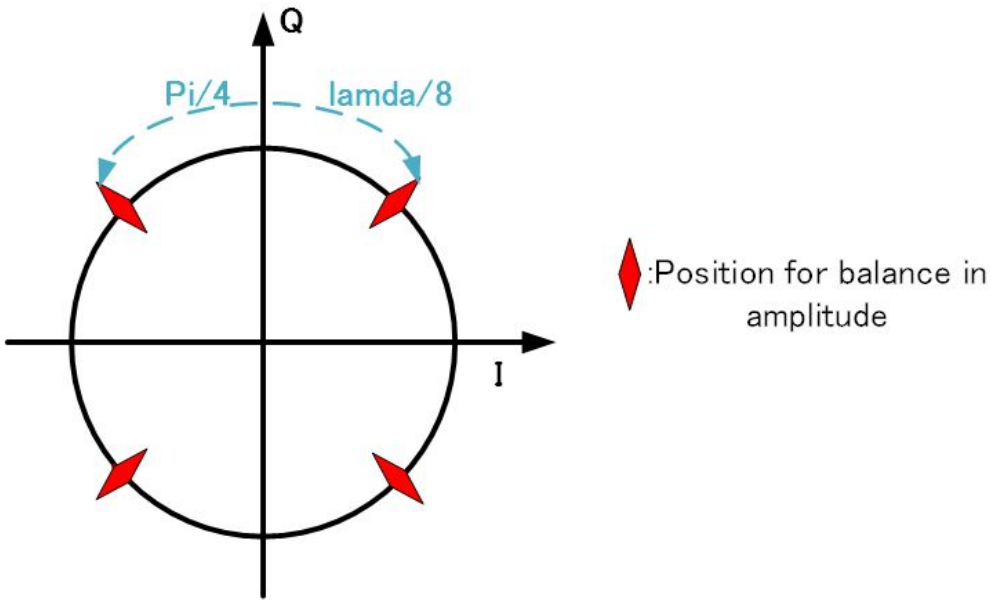

Figure 3.11: Position for balance of radar measurement

$$d_b = \frac{\lambda}{16} + k\frac{\lambda}{8} - \frac{\lambda}{4\pi}\alpha_0, k \in \mathbf{Z} \tag{3.35}$$

where α_0 is arctan $(I(t), Q(t))$ at distance $n.\lambda/2(n \in Z)$ with the easiest visualization at $n = 0$. Equation (3.35) includes $\lambda/16$ as a representation of the location of the first quadrant bisector, while $k.\lambda/8$ indicates that the signal is balanced when the distance increases or decreases by a multiple of $\lambda/8$, as demonstrated in Figure 3.11. Additionally, $\lambda.\alpha_0/4\pi$ is the phase angle of distance $n.\lambda/2(n \in Z)$. At multiples of distance $\lambda/4$, the phase angle demodulation of the two channels is repeated.

Some inferences

In the vital sign measurement using radar, with motion having displacement greater than or equal to half of the radar wavelength, the signals on the two channels are balanced for any distance from the radar to the object. For motion with a displacement of less than half of the radar wavelength, the signals on the two channels may be balanced or imbalanced. The signal is only balanced when the distance is as defined in Equation (3.35). When imbalanced phenomenon occurs, up to the purpose of the problem, both signal channels or one signal channel can be used. For imbalanced signals, the signal channel with a larger standard deviation carries more information about the vital sign.

3.2.2 Low quality signal and signal quality classification

The second problem of non-contact radar is that the signal quality is reduced by even very small random body movements. The vital signs detection algorithm may not be accurate in the presence of random body movement. In this subsection, the study performs a signal quality assessment of the measured plate movement, and the measured signal of 10 healthy subjects, using the support vector machine (SVM) model, then apply the

model for clinical data.

Support vector machine (SVM) is deterministic not probabilistic [96,97]. For a binary classification problem where two classes are linearly separable, there are infinitely many hyperplanes that distinguish the two classes, i.e. the interface. For each interface, we have a classifier. The closest distance from a data point to that interface is called the margin of that classifier. The points that help to determine the hyperplane are called support vectors. SVM is the problem of finding the interface so that the margin found is the largest, which means that the data points are safest compared to the interface. With the classification where the two classes are nonlinearly separable, we can choose the Kernel, which is the way that converts non-linear data to linear by generating additional data dimensions.

By using SVM, memory can be saved since only the support vectors need to be memorized. In this study, the samples were labeled as "1" for low-quality samples and "-1" for high-quality samples, with each sample being 10240 ms radar signal length. The samples with 8 features and label for each sample were used as input for training the SVM, and the weights of the SVM model were saved for the testing stage. The weights were then multiplied by the 8 features of each testing sample, and the class for the testing sample was determined based on the signs of the results, as shown in the Figure 3.12.

a. Feature extraction

Base on radar principle, 8 features are extracted, which can assess the signal if it is included random body movement. The Doppler effect is the basis of radar operation, where the first step involves reflecting the displacement of the body surface as measured by the radar output. For random body movements, usually, the motion amplitude is always greater than the body wall displacement due to vital signs. Thus, when the distance between the body and the radar remains constant, the body random movements always

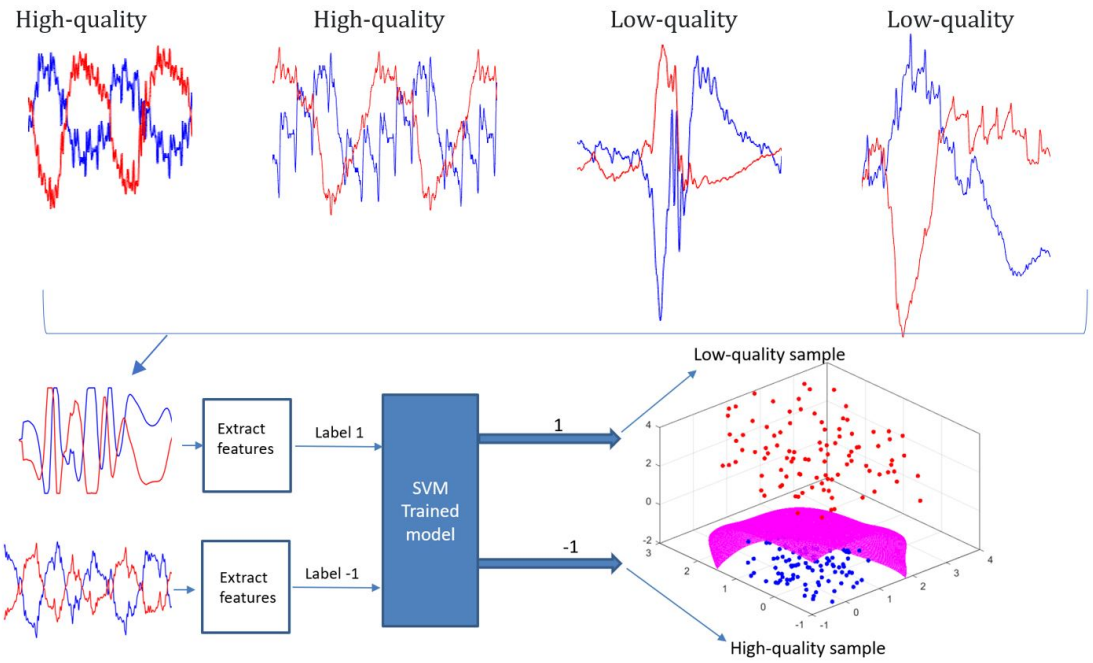

Figure 3.12: Overview of SVM training model

produce a larger amplitude in the radar signal, as reflected in Figure 3.13. Therefore, the author chooses the amplitude of the two signal channels I and Q as the extracted characteristic.

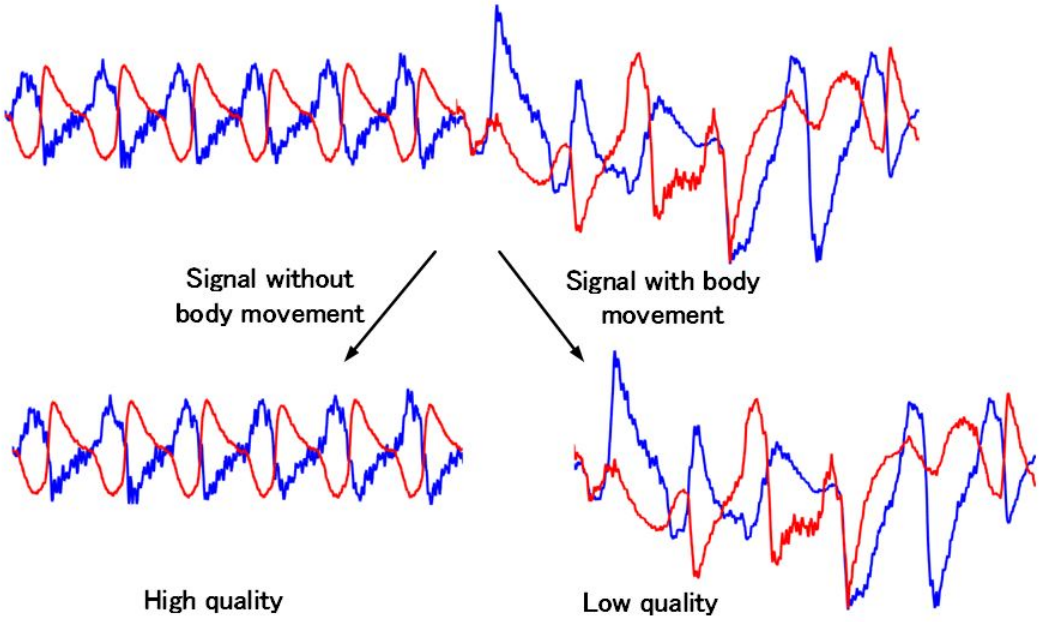

Figure 3.13: A segment of radar output signal when measuring human signals

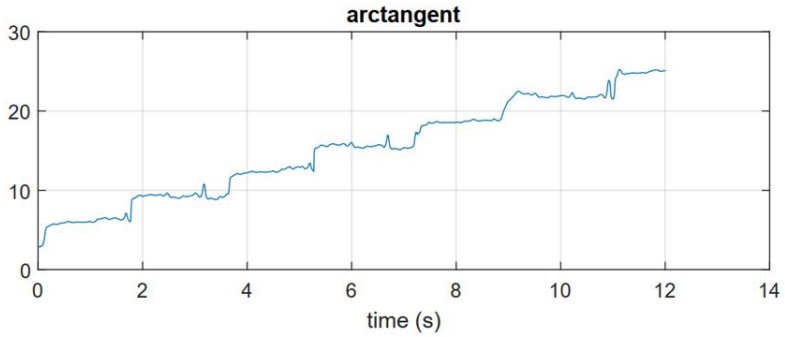

(a) Arctangent of high-quality sample

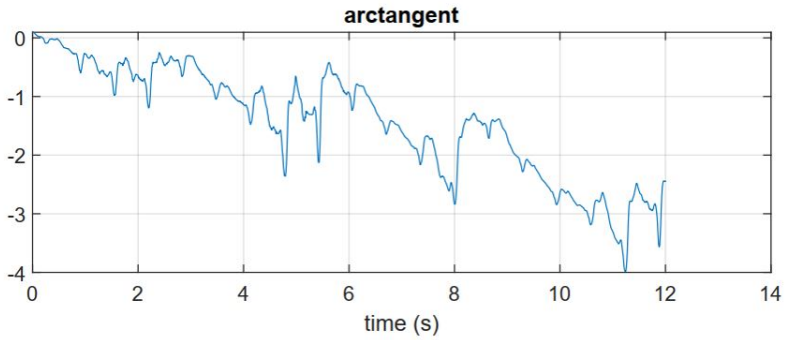

(b) Arctangent of low-quality sample

Figure 3.14: Analysis of arctangent of high-quality and low -quality sample

Secondly, since the vital sign-induced displacement when measured from the back is typically small, the output from the arctangent demodulation is uniformly variable. However, the displacement caused by random body movement is often greater than half of the wavelength, resulting in a fluctuation of the demodulated arctangent for a segment of the signal, as depicted in Figure 3.14. Therefore, the demodulated arctangent is featured extraction for this classification system.

Next, the thesis chooses the center frequency of the signal segment as a feature. In the absence of random body movement, the center frequency in a signal segment will typically be the breathing rate followed by the heart rate frequency, along with some low-power noise. However, when random body movement occurs, the movement frequency will dominate over time, and therefore, it will differ from the frequency of vital signs, as

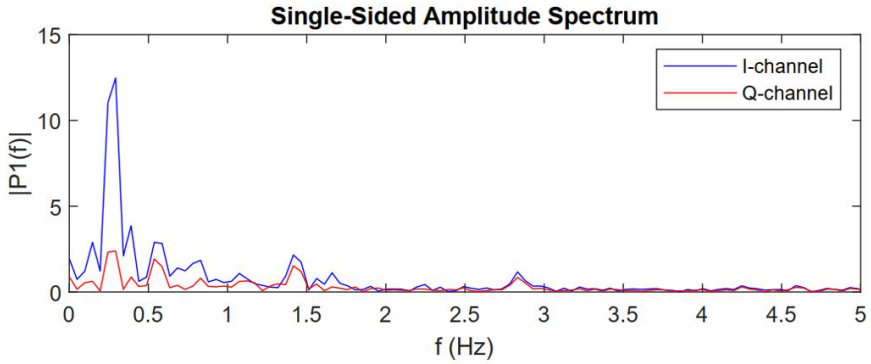

a) Frequency of high-quality sample

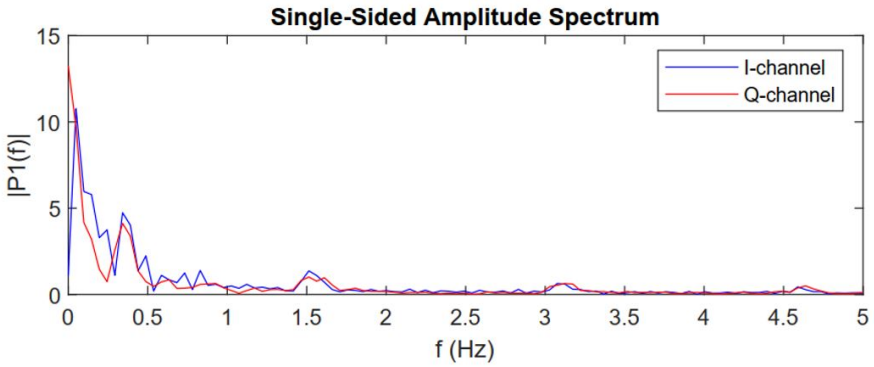

b) Frequency of low-quality sample

Figure 3.15: Analysis of frequency of high-quality and low -quality sample

illustrated in Figure 3.15. Finally, the features are summarized and listed as Table 3.1.

b. Signal quality classification of plate movement

The plate movement is controlled from the program on the PC, with a selected displacement of 1.5 mm and a frequency of 0.45 Hz. The distance from the plate to the radar is 230mm. By adding the movement of the hand in front of the plate, and changing the position of the plate by pulling away or pushing the radar closer to the plate, intervals of bad quality signal can be obtained. In contrast, when there is no external influence, the plate only moves under the control of the PC program, the received signal is a good quality signal.

Signals for 10 minutes of low-quality signals and 10 minutes of high-quality signals were measured and labeled. Each signal sample, which is 8 seconds long, was passed

Table 3.1: Input features for signal quality assessment

Feature number	Define	Base on
1	The maximum amplitude of I channel in the considered sample	Amplitude
2	The maximum amplitude of the Q channel in the considered sample	Amplitude
3	The larger of two values feature 1 and 2	Amplitude
4	The deviation from the starting point to the end point of the arctangent of the sample	Arctangent
5	The end point of the arctangent of the sample	Arctangent
6	The amplitude of oscillation of the arctangent of the sample	Arctangent
7	The smaller of the two center frequencies of the I and Q channels	Frequency
8	The larger of the two center frequencies of the I and Q channels	Frequency

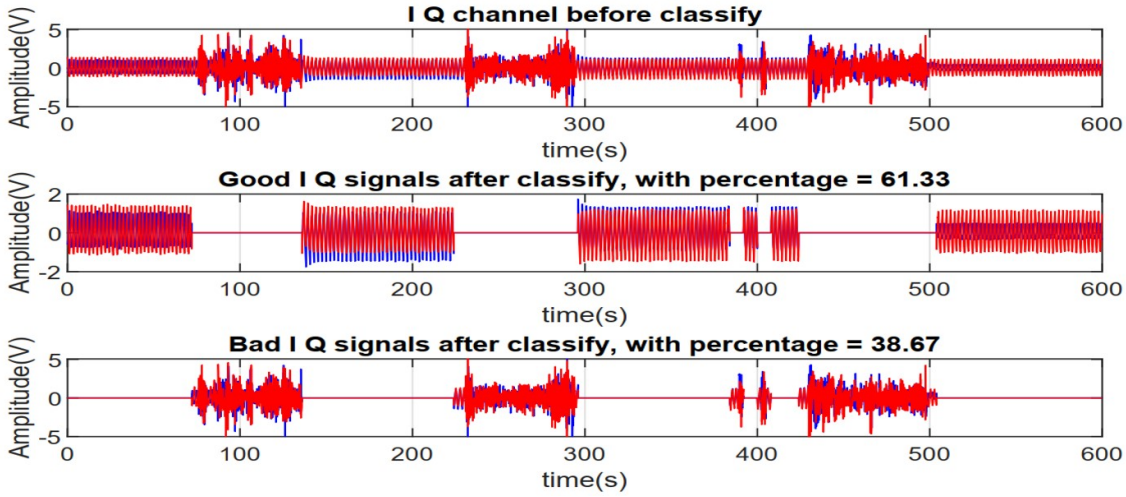

Figure 3.16: Signal quality classification result with plate movement signal

through a preprocessing block to extract 8 features (as shown in Figure 3.12), followed by training with the SVM machine learning algorithm. Once the training was completed, testing was conducted with a new data set of 10 minutes. Due to the simple and stable plate movement, the outputs indicate that it is possible to separate the signal with high accuracy, as shown in Figure 3.16.

c. Signal quality classification of healthy subjects

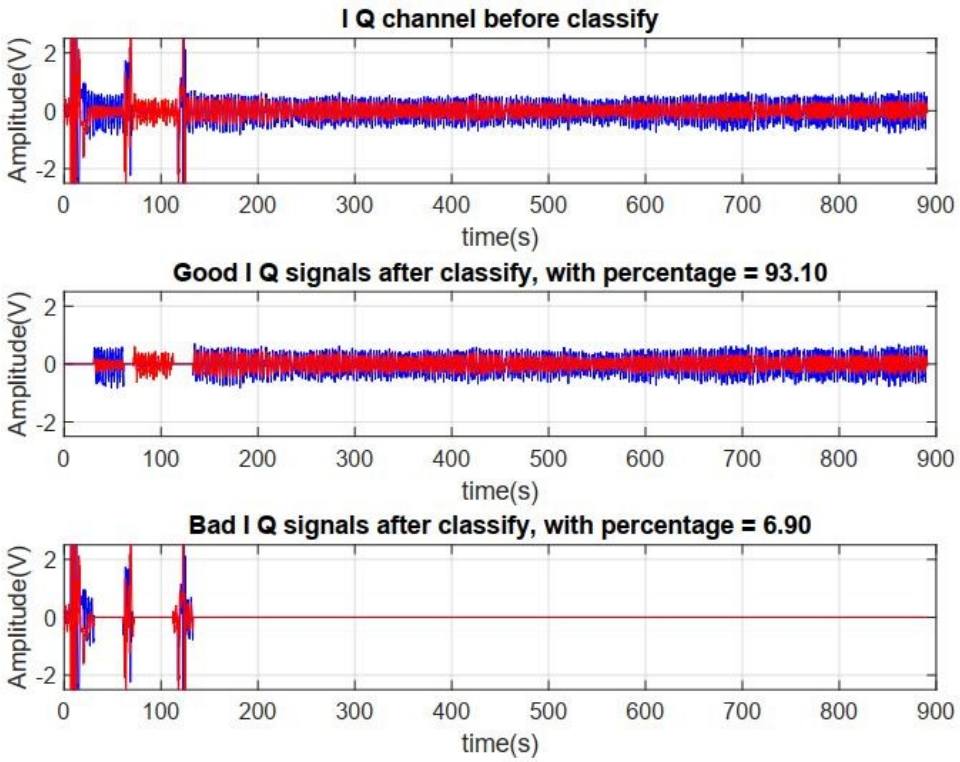

Figure 3.17: Signal quality assessment result on healthy subject measurement

To evaluate the performance of the method, the signal quality of healthy subjects was classified. Signal measurements were conducted on a group of 10 individuals, who were instructed to adjust their body position to align their chest with the radar located below while lying in bed. Low quality signals were recorded at regular intervals by the system during the initial phase when the subjects were still adjusting their position and were unsteady. However, good quality signals were obtained once they had stabilized their body and positioned themselves directly above the radar on their chest wall. To label the signal with or without random body movement, the laser which is a sensitive sensor was used to recognise the low quality sample.

During the study, two sets of signals were collected - one set of low quality signals and another set of high quality signals, each spanning 60 minutes. The length of each signal sample was 10240 milliseconds, and it was processed through the preprocessing block to extract 8 features. Subsequently, the SVM machine learning algorithm was

Table 3.2: Results of signal quality assessment on 10 healthy subjects

Subject	Number of samples	Reference		Proposed method		Number of error samples	Accuracy (%)
		Number of good samples	Number of bad samples	Number of good samples	Number of bad samples		
Subject 1	87	77	10	75	12	2	97.7
Subject 2	87	79	08	78	09	1	98.9
Subject 3	87	67	20	62	25	7	92
Subject 4	87	73	14	73	14	0	100
Subject 5	87	71	16	67	20	4	95.4
Subject 6	87	81	06	82	05	1	98.9
Subject 7	87	76	11	76	11	0	100
Subject 8	87	82	05	83	04	1	98.9
Subject 9	87	80	07	80	07	0	100
Subject 10	87	73	14	75	12	2	97.7

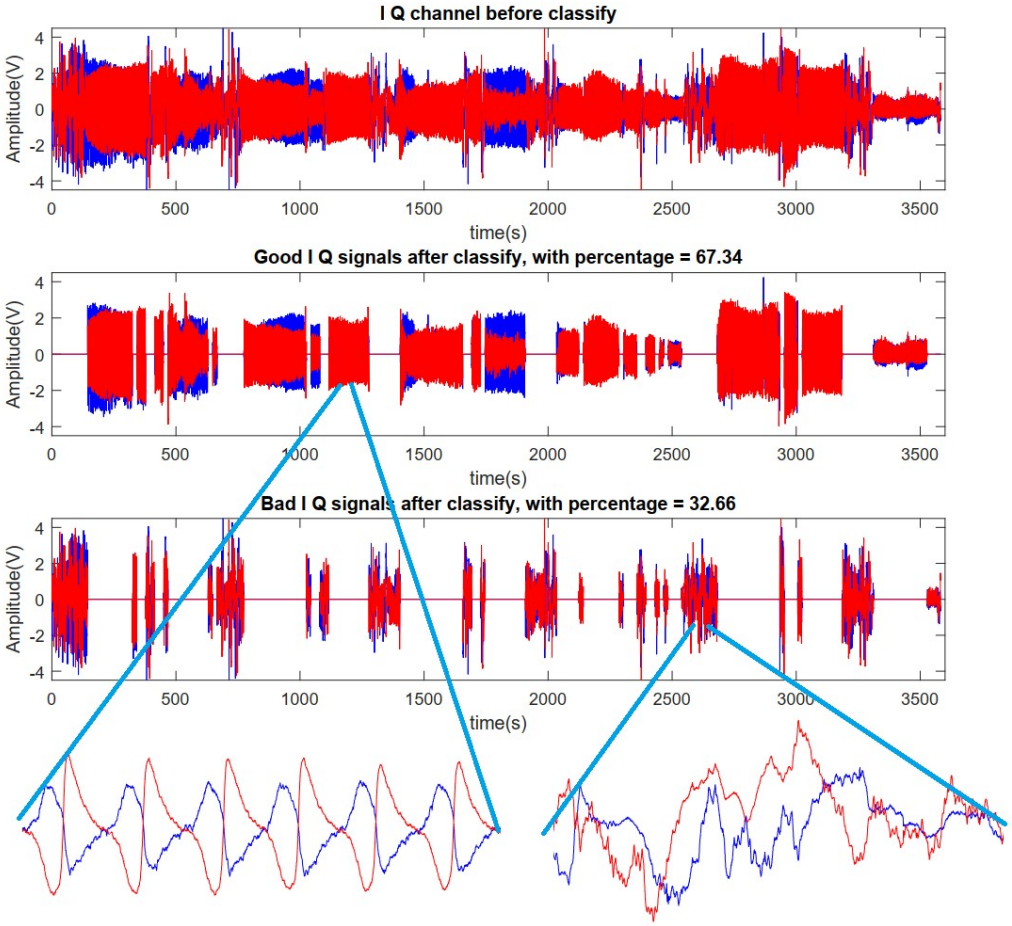

Figure 3.18: Signal quality assessment result on the elderly inpatient measurement

employed to train the model. The trained algorithm was then tested on a new dataset, which was 15 minutes long, and the outcomes indicated that the algorithm, using the extracted features, successfully identified and eliminated the low-quality signals. One

such instance is illustrated in Figure 3.17. Testing was also conducted with 10 healthy individuals, and the results are presented in Table 3.2.

d. Signal quality classification of clinical data

A data set containing measurements of elderly individual was received from the hospital and signal classification was carried out. To achieve this, 250 samples were labeled as good quality and 250 samples as bad quality, and a K-fold of 5 was used for training. The 500 signal samples were divided into 5 parts, with 400 used for training and 100 for testing. The process was repeated 5 times, each time using a different test set. The results indicate that the data was classified by the SVM training model with 99.1% accuracy. The results of a one-hour data test are depicted in Figure 3.18. The sleep quality of the elderly was evaluated through this signal quality classification, based on data collected during their nighttime sleep.

Chapter 4

SIGNAL PROCESSING ON VITAL SIGN DETECTION

4.1 Respiration Rate Detection

When measuring the vital sign without random body movements, the radar signal is the sum of the respiration rate, heart rate and noise components. In which, respiration rate has the largest amplitude. To find the respiration rate, two cases should be taken account: breathing displacement is larger than half the radar wavelength and breathing displacement is less than half the radar wavelength.

In case where breathing displacement is greater than half of the radar wavelength, one breath peak can produce more than one peak on the radar signal. Therefore, to calculate the RR, it is necessary to use both signal channels, calculate unwrap arctangent of two channels signal.

In case where breathing displacement is less than half the radar wavelength, a breath peak will produce a peak on the radar signal. Therefore, in this case, it is possible to use a signal channel that carries more information about the vital sign. For the selected signal channel, one of two methods can be used to find the RR: FFT for a signal channel and then find the maximum argument; use smoothing function such as envelope function and convolutional function.

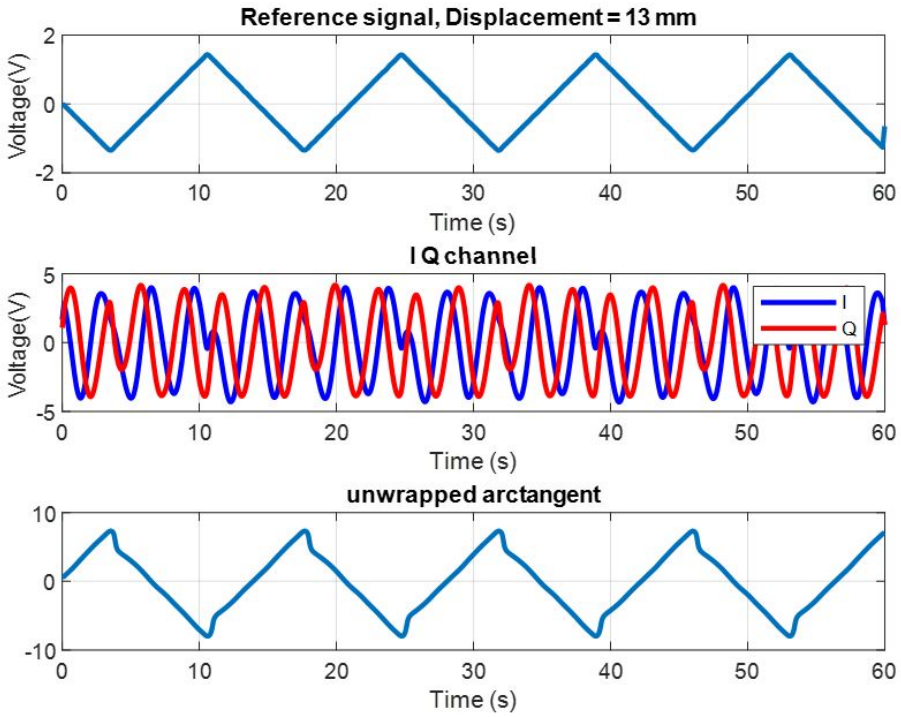

Figure 4.1: The description of plate movement with displacement of 13mm (a); two channel signals including I and Q signal of radar (b); unwrap arctangent signal of I and Q signal, this signal reflects accurately the motion of plate (c)

4.1.1 Respiration rate with displacement greater than half of radar wavelength

To clarify the frequency information on the two signal channels when the displacement is greater than half of the radar wavelength, the plate motion experiment is set with a displacement of 13mm, while the half wavelength of the radar is 6.2 mm.

The frequency analysis of I and Q signal channels is shown as in Figure 4.1. It can be seen that the actual plate motion is 0.07 Hz, however, since displacement is larger than $\lambda/2$, one peak of plate motion produces more than one peak on the I and Q signals. In this case it is necessary to use both I and Q channels. The unwrap arctangent function is used to find out the phase of the signal. The phase of the I, Q signals accurately reflects the number of beats as shown in Figure 4.1 and Figure 4.2.

From the experiment for the plate movement which can be accurately set the displace-

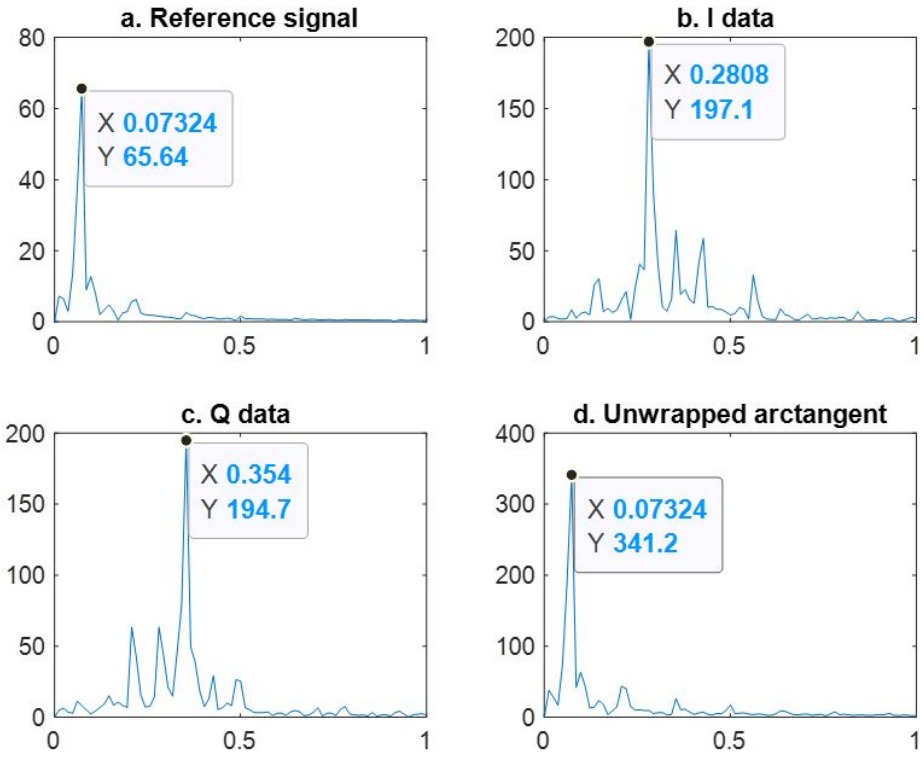

Figure 4.2: Frequency analysis of plate movement with displacement 13mm which is larger than a half of radar wavelength. (a) frequency analysis of reference signal which is from a laser; (b) frequency analysis of I channel signal of radar; (c) frequency analysis of Q channel signal of radar; (d) frequency analysis of unwrap arctangent from I and Q signals

ment from the computer, so that the experimental results can be analyzed to match the theoretical conclusions. To prove for the human signal, my research will perform radar signal analysis when measuring the breathing rate of the human body. The measured person is a 22-year-old boy, 1m70 tall, 60kg weight. The signal measurement was performed in a sitting position, the measured person inhaled and exhaled deeply, so that the displacement of the chest wall was greater than $\lambda/2$. The measured signal is shown in the Figure 4.3 and the frequency analysis as shown in Figure 4.4.

4.1.2 Respiration rate with displacement smaller than half of radar wavelength

a. Methodology

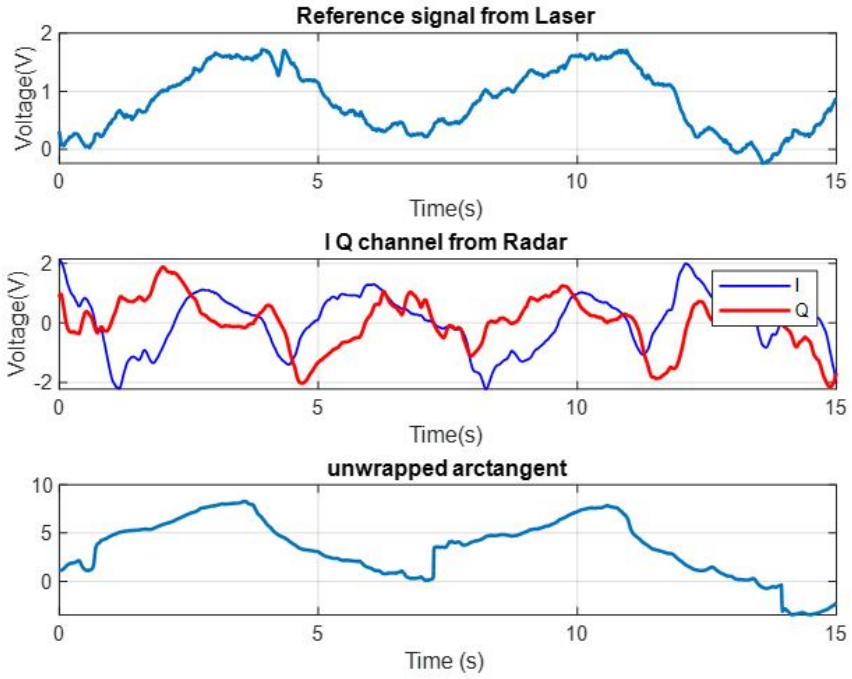

Figure 4.3: The description of chest movement measured on a healthy subject. (a) referenced signal; (b) two channel signals including I and Q signal of radar; (c) unwrap arctangent signal of I and Q signal, this signal reflects accurately the motion frequency of human chest

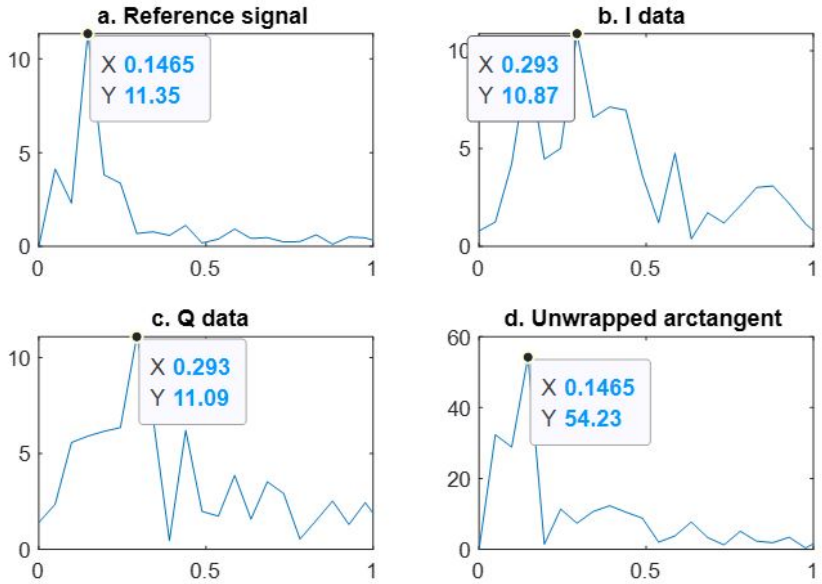

Figure 4.4: Frequency analysis of chest movement measured on a healthy subject. (a) frequency analysis of reference signal which is from a laser; (b) frequency analysis of I channel signal of radar; (c) frequency analysis of Q channel signal of radar; (d) frequency analysis of unwrap arctangent from I and Q signals

For motions with displacement less than half of radar wavelength ($\lambda/2$), one peak of radar signal corresponds to one beat of motion. Therefore, in this case, it is not required to use both signal channels but one channel that carries more information about the vital sign. Standard deviation is used to select signal channel. Signal channel selection is done on the software (MATLAB 2020a) as the steps shown below.

Algorithm 1 Channel selection base on standard deviation

1: Input: $\{I\}_n, \{Q\}_n$
2: Output: $\{OneCh\}_n$
3: $\{I\}_n \leftarrow$ I channel signal of radar
4: $\{Q\}_n \leftarrow$ Q channel signal of radar
5: $fs = 100 \leftarrow$ sampling rate
6: $\{OneCh\}_n \leftarrow$ one selected channel signal
7: $stdI = std\ \{I\}_n \leftarrow$ the standard deviation of I signal
8: $stdQ = std\ \{Q\}_n \leftarrow$ the standard deviation of Q signal
9: $\{OneCh\}_n = \{I\}_n\ if\ stdI \geq stdQ$
10: $\{OneCh\}_n = \{Q\}_n\ if\ stdQ > stdI$

Movement with displacement smaller than half of wavelength causes imbalance as shown in section 3.2. This small motion when represented on the unit circle, it is a circular arc. This arc projected onto the two axes I and Q can be seen as the unbalanced amplitude and phase when the object-to-radar distance is not on the bisector of the quadrants. There is an imbalance between the two signal channels. When the imbalance occurs, one channel of radar will carry more information about the vital sign, because it is more linear, as shown in the Figures 4.5

From Figure 4.6, it can be seen that, when imbalance occurs, one channel carries more information. In this case, considering the information of the RR, therefore, the channel which has a larger amplitude and larger standard deviation is the channel that should be selected to take to the next processing step. Figure 4.7 analyzes the frequency composition of the two signal channels of the radar. Compared with the reference signal, I channel includes a better respiratory frequency component. When choosing a channel with better

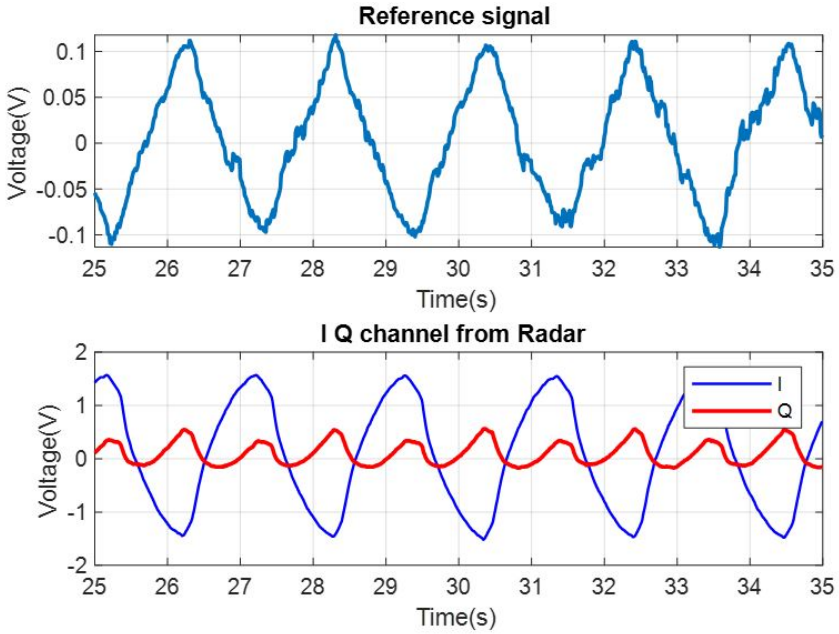

Figure 4.5: Radar signal of measuring the movement of the plate causes displacement that is less than half of the wavelength, I channel has bigger linearity

breathing information. The next step is to find the RR, which can be done using the FFT method, and then take the frequency component with the greatest power. This frequency is multiplied by 60, giving the result of RR. On the other hand, the breathing information signal can be found by smoothing function, which is the envelope and convolutional function. As shown in Figure 4.8, the envelope signal and convolutional function have

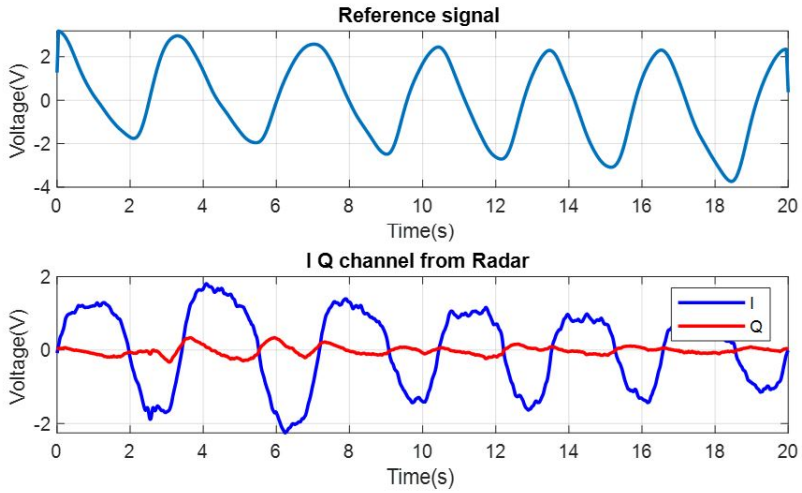

Figure 4.6: Radar signal of measuring chest movement with chest wall movement causes displacement that is less than half of wavelength

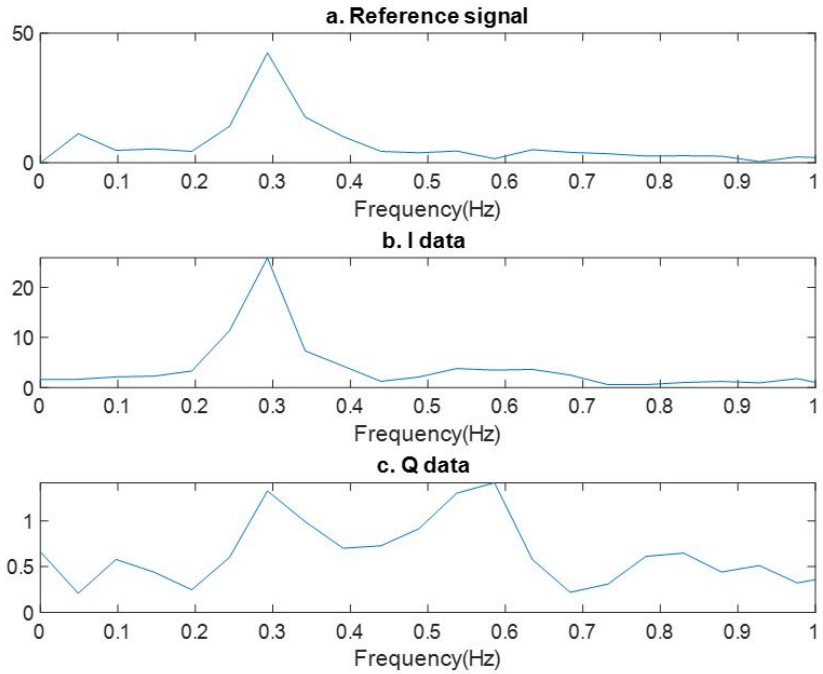

Figure 4.7: Radar signal of measuring chest movement with chest wall displacement smaller than half of wavelength; I channel with bigger standard deviation carries more vital signal information

the same peak and signal form as the reference signal.

b. The statistic results

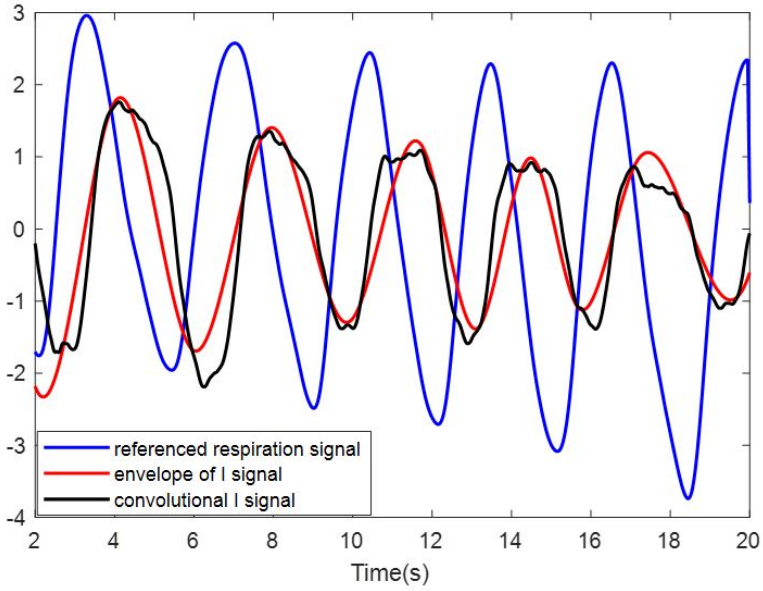

Figure 4.8: Envelope function and convolution function applied to selected channel of radar signal and reference signal, measurement from the back side of human

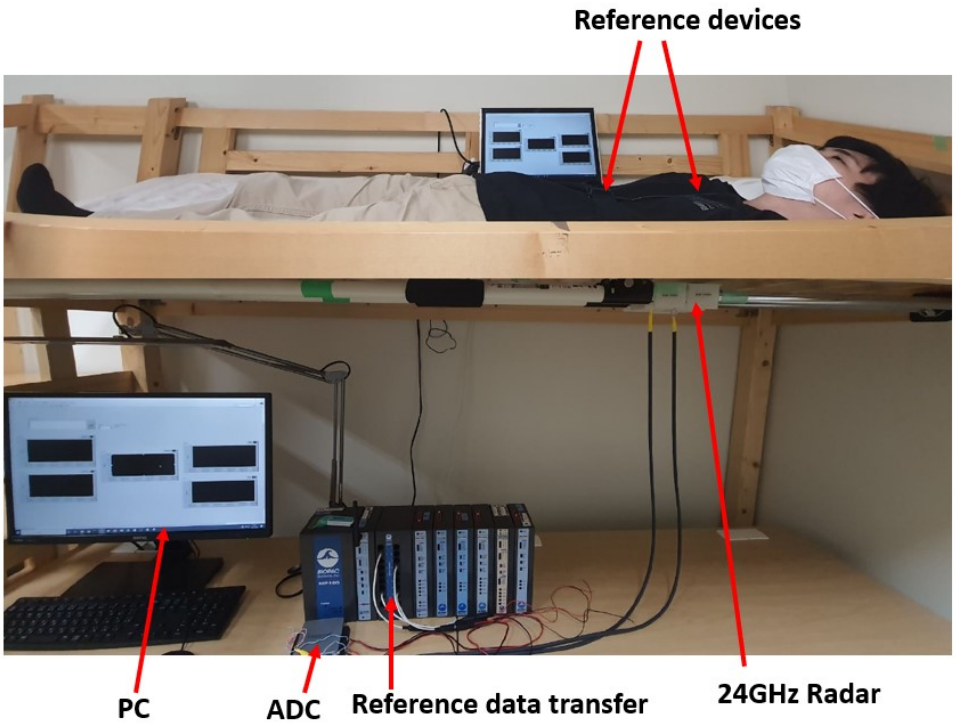

Figure 4.9: Arrangement to measure healthy subjects

In order to measure the vital signs of healthy individuals, one set of data was collected in our laboratory. The information from a total of 10 participants was gathered, with 7 male and 3 female subjects ranging in age from 19 to 32, and in height from 160 cm to 179 cm, and in weight from 53 kg to 75 kg. The measurement process involved having the participants lie down on a bed equipped with a radar system positioned 20 cm from the

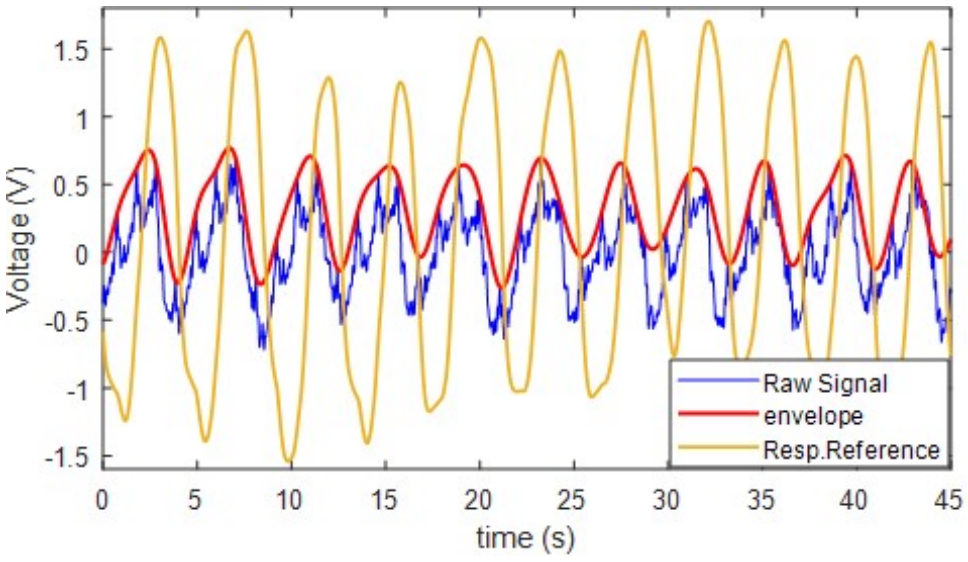

Figure 4.10: RR detection on radar signal based on proposed method and reference

bed surface. To evaluate the accuracy of method, participants wore ECG and respiration measurement devices (BIOPAC ECG100C and NIHON KOHDEN SR-601S, Japan) to obtain reference signals. Participants were initially asked to adjust their position until a high-quality signal was achieved, which took approximately 5 minutes due to initial movements from adjusting their posture. Once the signal quality was deemed acceptable, participants were asked to remain still for the remaining 5 minutes of the measurement period, which was captured in the arrangement shown in Figure 4.9.

The Ethics Committee of The University of Electro-Communications granted approval for this study. Additionally, all subjects provided written consent after being informed about this research.

Once the signals are categorized as high-quality, they are transmitted for vital signs extraction. It has been verified that the radar measurement produces a peak in the radar signal corresponding to the breathing rate. Consequently, the thesis employs the envelope function in MATLAB to identify the peaks of respiration, disregarding the impact of heart rate. To illustrate the outcome, an instance of the result is presented in Figure 4.10.

Table 4.1 displays the respiratory rate findings for ten healthy individuals over a period of five minutes. From Table 4.1 we can see that the difference in RR between reference and proposed method (subtraction of reference-RR to proposed-RR) extends from 0 to 3 beats per minute, only 1 minute out of the total 50 minutes is 3 bpm, the difference is primarily from 0 to 1 bpm (47 of 50 minutes of survey), as shown in Figure 4.11. As can be seen in Figure 4.11, the part of the variation error in respiration rate (RR) between the proposed method on radar signal and the reference is more to the positive side than to the negative side. This is because the RR detection algorithm still makes a mistake when there is a harmonic peak (harmonic peak is not the breath peak), while skipping the

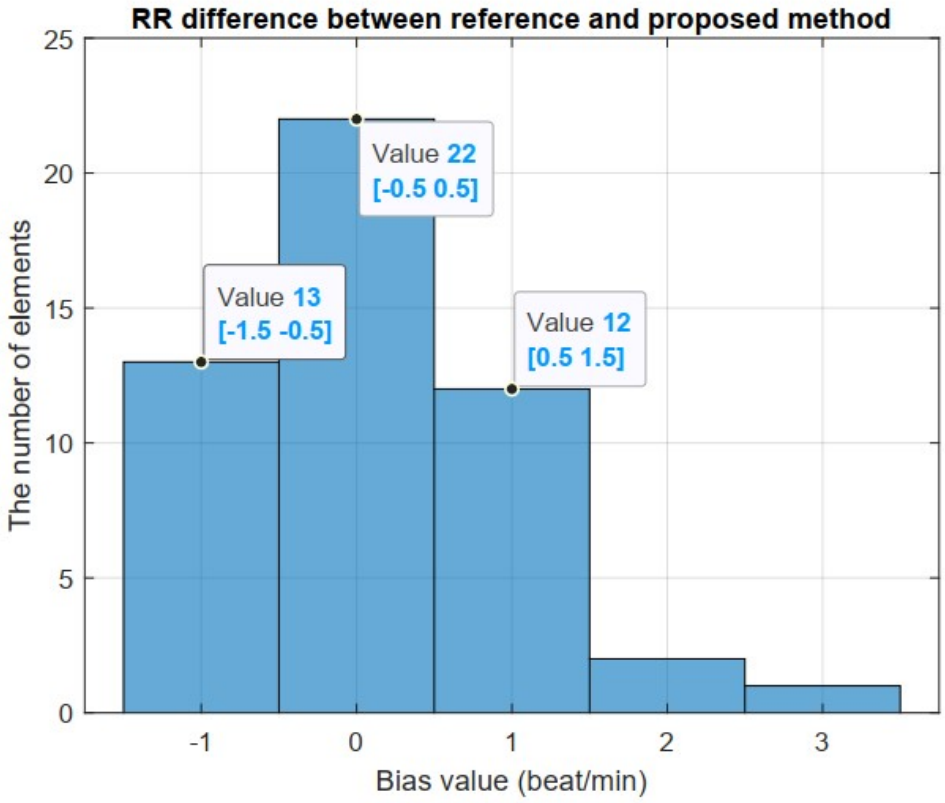

Figure 4.11: The histogram of the variation in RR between the proposed method on radar signal and the reference

breath peak is less occurrence.

4.2 Heart Rate Detection

4.2.1 Methodology: svd based heart peaks detection

By utilizing a 24GHz radar system, when the body wall movement due to vital signs is less than half of the radar wavelength, each respiratory peak aligns with one peak in the radar signal, which enables the extraction of respiratory peaks through enveloping the high-quality raw signal. To determine the heart rate, the following two-step process will be carried out. Firstly, a band-pass filter with a pass frequency range of 0.7 to 3 Hz will be applied to the signal. This range primarily contains the frequency component of the heart rate, although there may be some harmonic frequencies present. Next, singular

Table 4.1: Results of RR extraction on 10 healthy subjects

Subject	Reference/	Respiration Rate (bpm)				
	Radar	Minute 1	Minute 2	Minute 3	Minute 4	Minute 5
Subject 1	Resp (Reference)	15	16	15	18	15
	Radar (proposed)	15	16	15	17	16
Subject 2	Resp (Reference)	15	17	15	12	15
	Radar (proposed)	16	17	15	12	14
Subject 3	Resp (Reference)	18	15	15	14	15
	Radar (proposed)	15	16	14	14	15
Subject 4	Resp (Reference)	17	18	18	16	16
	Radar (proposed)	18	18	18	16	17
Subject 5	Resp (Reference)	16	15	16	14	16
	Radar (proposed)	15	15	15	15	15
Subject 6	Resp (Reference)	12	12	13	12	13
	Radar (proposed)	12	13	12	13	12
Subject 7	Resp (Reference)	17	18	18	18	17
	Radar (proposed)	18	18	18	18	18
Subject 8	Resp (Reference)	20	22	20	20	19
	Radar (proposed)	21	22	20	19	20
Subject 9	Resp (Reference)	15	15	15	16	15
	Radar (proposed)	15	15	15	15	13
Subject 10	Resp (Reference)	14	14	14	15	14
	Radar (proposed)	15	12	13	14	14

value decomposition (SVD) will be used to isolate the single frequency component contained in the signal [98]. By combining the vectors and singular values, the frequency components within the signal can be separated, allowing the heart rate to be determined without harmonic interference. Specifically, a 512-point window will be used to extract one sample. 512 sampling points are $[x(1), x(2), ..., x(512)]$, then they are spread in a matrix, as (4.1).

$$\mathbf{X} = \begin{bmatrix} x(1) & x(2) & ... & x(257) \\ x(2) & x(3) & ... & x(258) \\ ... & ... & ... & ... \\ x(256) & x(257) & ... & x(512) \end{bmatrix} \tag{4.1}$$

Implement SVD algorithm according to (4.2)

$$[\mathbf{U}, \mathbf{D}, \mathbf{V}] = svd(\mathbf{X}) \tag{4.2}$$

where the left orthonormal $\mathbf{U} = (u_1, u_2..., u_n)$ with u_j is the column vector and the right orthonormal $\mathbf{V} = (v_1, v_2..., v_n)$ with v_j is the column vector and σ_j is the singular value. So that, u_1 and u_2 are the first and second columns in matrix $\mathbf{U}$; v_1 andv_2 are the

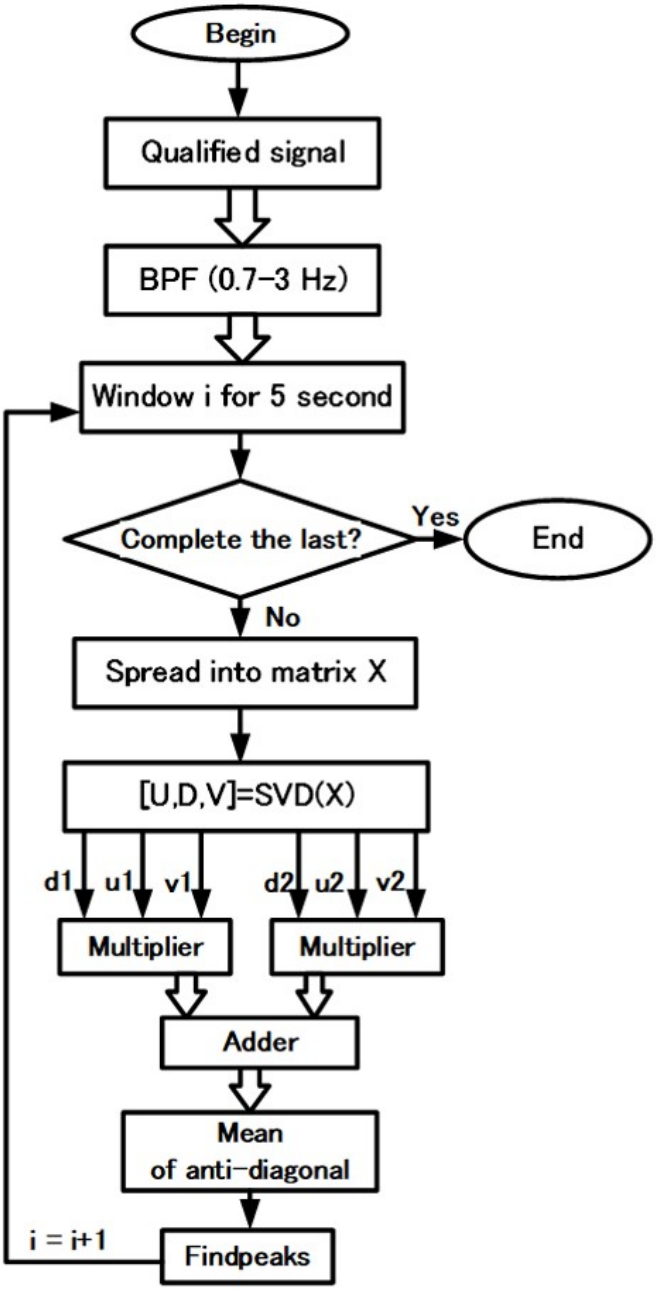

Figure 4.12: Diagram of the algorithm to determine heartbeat

first and second columns in matrix $\mathbf{V}$; σ_1 and σ_2 are the first and the second non-zero singular values. Calculate $\mathbf{H}_{12}$ as (4.3)

$$H_{12} = \sigma_1 u_1 v_1^T + \sigma_2 u_2 v_2^T \tag{4.3}$$

$\mathbf{H}_{12}$ has same size with $\mathbf{X}$. Performing averaging of each anti-diagonal of $\mathbf{H}_{12}$, a row vector $\mathbf{H}_1$ of size [1x512] that matches the length of the signal sample being considered is obtained. The next row vector is obtained by sliding the sample window to the next signal sample. This process is repeated until the end of the data is reached. The peaks corresponding to the R peak of the ECG are clearly shown by the signal when the results are redrawn. Figure 4.12 summarizes the vital signs extraction process.

4.2.2 Statistic results

Section 4.1 described the methodology used to measure the vital signs of 10 healthy individuals, utilizing data sets built in our laboratory. In order to obtain high-quality heartbeat signals, the signal segment is first classified and filtered with a pass frequency

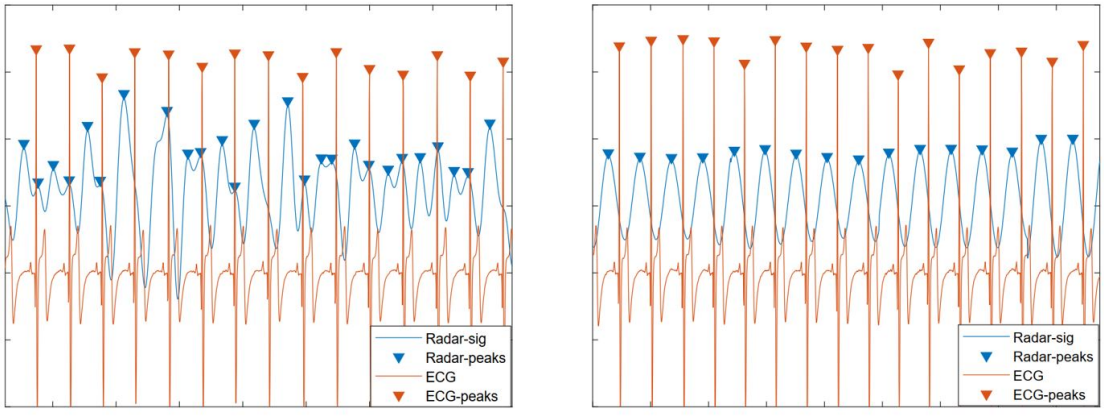

(a) Heart beat detection using conventional method

(b) Heart beat detection after using combined SVD

Figure 4.13: Heart beat detection using conventional method and combined SVD on radar signal

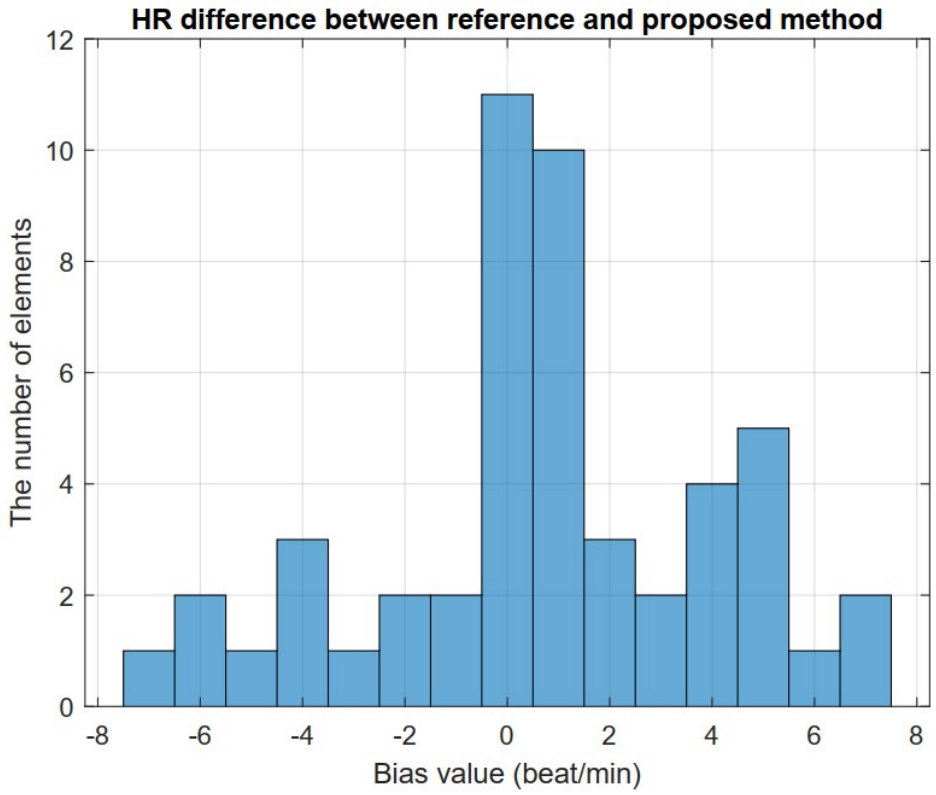

Figure 4.14: The histogram of the variation in HR between the proposed method on radar signal and the reference

range of 0.7-3Hz, and then sampled at intervals of 5120 ms. Each 5120 ms signal segment is then transformed into a matrix and inputted into the SVD algorithm to extract the 1st and 2nd order representing heartbeat. By combining these values, a matrix of the same size as the spread matrix of the signal is generated, and by averaging the anti-diagonal of this resulting matrix, a signal with clear heartbeat peaks is obtained. Figure 4.13 displays the results of applying the filter, which is the conventional method, and the combined SVD. Table 4.2 shows the heart rate of the 10 healthy subjects extracted from the 5-minute high-quality signal.

The range of difference in HR between the reference and proposed method, as shown in Table 4.2, is from 0 to 7 beats. Out of the total 50 minutes of the survey, only 2 minutes have a difference of 7 bpm. The difference is mainly from 0 to 4 bpm, which is observed for 38 of the 50 minutes. Figure 4.14 shows that the bias is mainly from 0 to 1 bpm,

Table 4.2: Results of HR extraction on 10 healthy subjects

		Heart Rate				
		Minute 1	Minute 2	Minute 3	Minute 4	Minute 5
Subject 1	ECG (Reference)	62	61	62	62	60
	Radar (proposed)	68	68	61	63	59
Subject 2	ECG (Reference)	57	57	58	56	58
	Radar (proposed)	56	57	58	55	57
Subject 3	ECG (Reference)	67	63	57	56	55
	Radar (proposed)	60	59	62	55	57
Subject 4	ECG (Reference)	62	63	63	62	63
	Radar (proposed)	62	63	59	58	60
Subject 5	ECG (Reference)	60	62	60	62	60
	Radar (proposed)	63	55	65	60	55
Subject 6	ECG (Reference)	60	64	61	62	63
	Radar (proposed)	58	61	65	62	61
Subject 7	ECG (Reference)	58	59	59	58	57
	Radar (proposed)	58	59	60	62	57
Subject 8	ECG (Reference)	58	60	58	61	59
	Radar (proposed)	58	55	54	67	64
Subject 9	ECG (Reference)	54	54	52	50	49
	Radar (proposed)	53	54	54	49	53
Subject 10	ECG (Reference)	82	83	82	87	82
	Radar (proposed)	76	77	81	86	82

which is observed for 22 of the 50 minutes.

4.3 Inter-beat Interval And Heart Rate Variability Detection

4.3.1 Methodology: time-frequency domain-based method for ibi and hrv detection

The raw radar signal received from the data acquisition (DAQ) includes two channel signals. The one-channel signal was then selected for the next processing. The selected channel signal was filtered by a low-pass filter using a finite impulse response (FIR) filter with a cutoff frequency of 3 Hz. This filter was used to cancel the high-frequency components of the heartbeat and noise while conserving the respiratory component. The filtered signal was then transmitted to a convolution filter to extract the respiration component.

The convolution filter removes the residual components of both the noise and heartbeat, resulting in a clean respirator. A signal containing both noise and heartbeat was obtained by subtracting the raw signal from the respiratory component. A high-pass filter with a cutoff frequency of 0.5 Hz is used to remove residual respiratory influence. The LPNR algorithm was then applied to extract the cardiac component without noise. A derivative function was applied to determine the peak with the highest slope. The sharpest peaks were identified as R peaks. A block diagram of the proposed method is shown in Figure 4.15. The details of each part of the diagram are presented in Subsections a to d in this

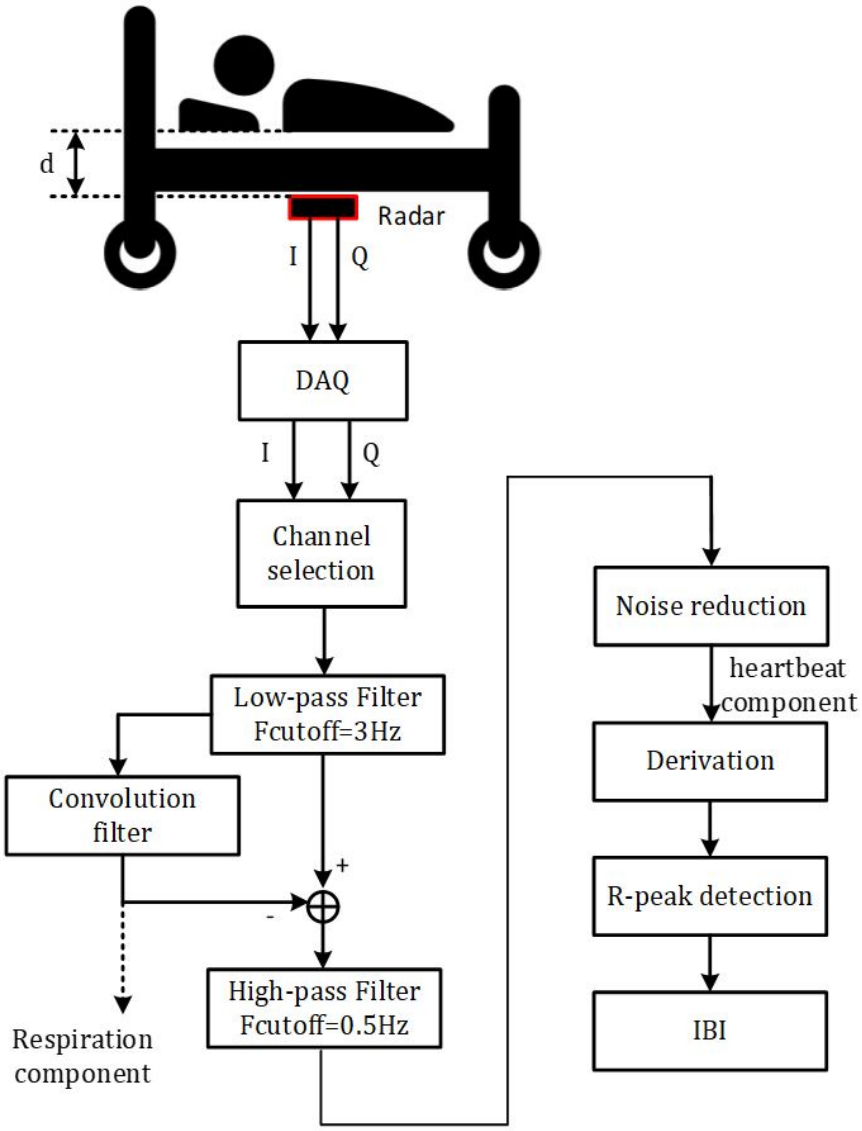

Figure 4.15: System of proposed method for IBI detection

part.

a. Channel selection of radar signal based on standard deviation

The output signal of 24 GHz radar includes two signal channels. When the displacement of measured object is smaller than half of wavelength, the distance from the radar to the measured object determines the balance of the output signal. When the measured object is at a distance d_b from the radar, as shown in Equation (4.4), the output signal is balanced [33].

$$d_b = \frac{\lambda}{16} + k\frac{\lambda}{8} - \frac{\lambda}{4\pi}\alpha_0,\ k \in \mathbf{Z} \tag{4.4}$$

where α_0 is $arctan(Q(t), I(t))$ at the distance $n.\lambda/2 (n \in Z)$ with the easiest visualization at $n = 0$.

However, distance d in Figure 4.15 is not always equal to d_b in Equation (4.4). Therefore, imbalances occur more often than balance. When an imbalance occurs, one of the two output channels of the radar carries more vital-sign information than the other. In this case, the channel with a higher standard deviation is selected for the processing block, as shown in Figure 4.16 and Equation (4.5).

$$Sd = \sqrt{\frac{1}{N_\Sigma}\sum_{i=1}^{N_\Sigma}(x_i - \mu)^2} \tag{4.5}$$

where N_Σ is the length of the signal and $\mu = \frac{1}{N_\Sigma}\sum_{i-1}^{N_\Sigma}(x_i)$

As shown in Figure 4.16, we can describe the movement of the chest wall, including the movement due to breathing, movement of the chest wall from A to B on the unit circle, and chest wall motion due to heartbeats between C and D on the blue arc. The CD arc describes the displacement caused by the heartbeat, and when projecting the arc on

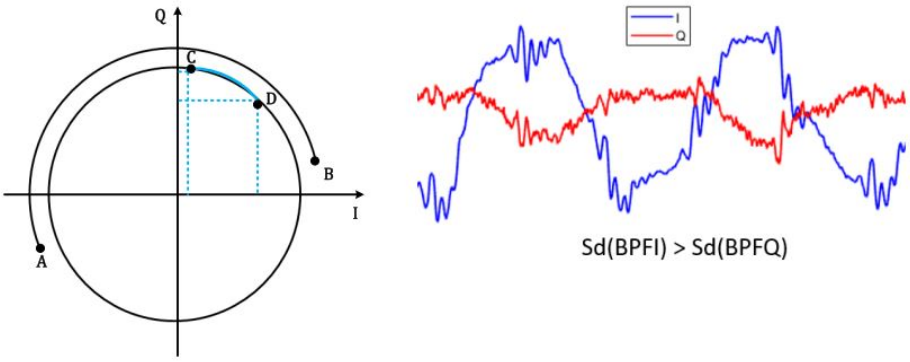

Figure 4.16: Imbalanced I and Q signals of radar

the two axes of the I-channel and Q-channel, we find that the information on the I-channel axis carries more weight than the information on the Q-channel axis.

Therefore, in this case, channel I was chosen to extract the heartbeat component information. To select the signal channel to extract the heart component information, the following steps were performed on the software (MATLAB 2020a) as algorithm of channel selection base on standard deviation.

b. Convolution filter of respiration component estimation

In this subsection, we estimate the components of respiration. As demonstrated in our previous paper [43], in the measurement of the vital sign signal from the back side, that is, lying in bed, the displacement is less than half of the wavelength; therefore, each peak

Algorithm 2 Channel selection base on standard deviation

Input: $\{I\}_n, \{Q\}_n$
Output: $\{OneCh\}_n$
$\{I\}_n \leftarrow$ I channel signal of radar
$\{Q\}_n \leftarrow$ Q channel signal of radar
$fs = 1000 \leftarrow$ sampling rate
$\{OneCh\}_n \leftarrow$ one selected channel signal
$bpfI = bandpass\ (\{I\}_n, [0.7\ 3], fs) \leftarrow$ perform BPF to I signal
$bpfQ = bandpass\ (\{Q\}_n, [0.7\ 3], fs) \leftarrow$ perform BPF to Q signal
$stdI = std\ (bpfI) \leftarrow$ the standard deviation of I signal
$stdQ = std\ (bpfQ) \leftarrow$ the standard deviation of Q signal
$\{OneCh\}_n = \{I\}_n\ if\ stdI \geq stdQ$
$\{OneCh\}_n = \{Q\}_n\ if\ stdQ > stdI$

of the envelope of the radar signal corresponds to one breathing. Based on this conclusion, a smoothing technique based on the convolution function was applied in this study. However, when applying the convolution function to find the respiration component, it is important to pay attention to the smoothing length ($Tconv$), as shown in Figure 4.17. If the $Tconv$ is too large, the respiration signal after calculation will include both the heart component and noise. After performing the subtraction step in Figure 4.15, the received signal loses its heartbeat information. If $Tconv$ is too small, the signal obtained after performing the subtraction step in Figure 4.15 will also contain information on respiration. Therefore, a suitable $Tconv$ size is required. In this study, $Tconv$ was calculated as an average heart rate cycle, and the respiration component was performed as shown in the steps below.

Algorithm 3 Respiration component estimation base on convolution filter

1: Input: $\{OneCh\}_n$,fs
2: Output: RR_n
3: $\{OneCh\}_n \leftarrow$ radar signal of one selected channel
4: $fs = 1000 \leftarrow$ sampling rate
5: $RR_n \leftarrow$ respiration component signal
6: $NFFT \leftarrow$ next power of 2 from data input length
7: $bpfSig = bandpass\ (RadarSig,\ [0.7\ 3],\ fs) \leftarrow$ perform BPF
8: $y = fft\ (bpfSig,\ NFFT) \leftarrow$ perform FFT
9: $fHR \leftarrow$ the heart frequency by argmax of FFT
10: $Tconv = fHR * 60 \leftarrow$ the average heart rate cycle
11: $tempVector = ones\ (1,\ Tconv) / Tconv \leftarrow$ create a vector *ones*
12: $RR_n = conv(\{OneCh\}_n, tempVector, 'same') \leftarrow$ the respiration component
13: End

c. Noise reduction based on locally projective noise reduction

The noise-reduction technique is based on LPNR [35,95,99,100] and embedding [101]. In-band noise reduction is achieved by using geometric projections in the delay space through the utilization of a nonlinear filtering technique. In summary, the LPNR technique was used to estimate the subspace of the noise-free time series in delay embedding

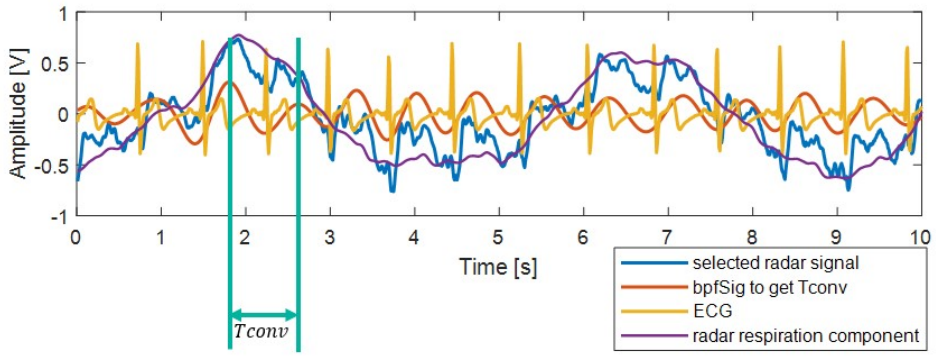

Figure 4.17: Radar respiration component extracted by convolution filter

using a local linear approximation and projecting the measured noisy delay vectors on this subspace. The algorithm can be summarized as follows.

Figure 4.18a illustrates the raw radar signal after choosing one channel and the ECG. Radars can reflect body wall displacement due to respiration and heartbeat. The respiration component can be extracted using a convolution filter, as shown in Figure 4.18b. By subtracting the raw radar signal in Figure 4.18a from the respiration component in Figure 4.18b, and then considering LPNR to remove the noise, we obtain Figure 4.18c.

From Figure 4.18, it can be observed that, in the case where the radar signal reflects the heartbeat, after applying noise reduction, the R-peak was seen with the largest slope peak rather than the neighboring peaks which are called undesired peaks. In the case of peak selection based on amplitude, the results may be incorrect, as shown in regions A and B. Region A has the largest peak located at first; however, in region B, the amplitude order changed. This implies that after applying the heartbeat component extraction algorithm, the peak shows the R-peak, even with a smaller amplitude than the undesired peaks. Therefore, to ensure that the R-peaks are indeed found, the next step in this study is to find peaks with steeper slopes performed by the derivative function, as shown in subsection d below.

d. Derivation for R-peak detection

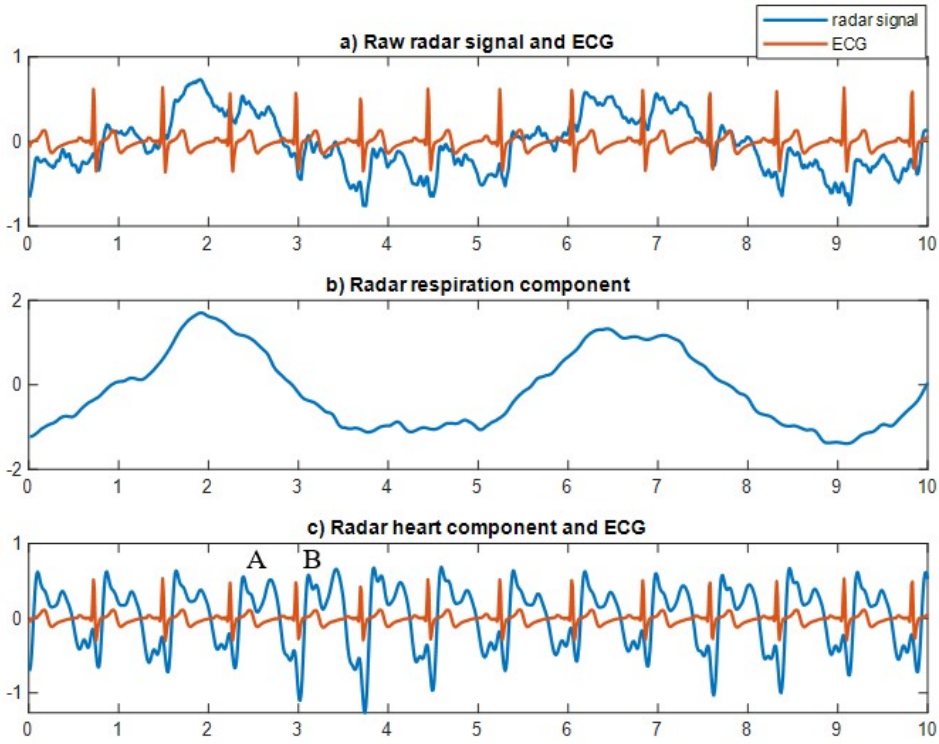

Figure 4.18: Raw radar signal (a), respiration component (b), and radar heart component after noise reduction (c) and ECG

After applying LPNR to extract the heart component information, the signal still includes noise peaks matching the real heart peaks. The process of derivation was performed to determine HRV. A derivative function, as shown in Equation (4.6), was applied to find the peak with the greatest slope among the peaks within one signal period. The derivative function used in this study was a five-point stencil. A previous study also used this function to find the QRS complex in the ECG signal [102]. In terms of cardiovascular physiology, it is believed that the R peak in the QRS complex is the sharpest. In the radar signal, the R peak has the largest slope peak in the signal. The electrical stimulus passing through the main portion of the ventricular walls is represented by the R-wave. The thick walls of the ventricles require more voltage due to the substantial amount of work they perform [103]. As a result, the R-wave is the sharpest wave generated during normal conduction. Based on this knowledge, in this study, we attempted to detect the

Algorithm 4 Noise reduction base on Locally Projective Noise Reduction algorithm

Input: x_n, m, k, q
Output: $\{\widetilde{x}\}_n$
$x_n \leftarrow$ heartbeat component with noise
$\{\widetilde{x}\}_n \leftarrow$ heartbeat component without noise
$n \leftarrow$ length of input data
$m = 50 \leftarrow$ dimension of delay vectors
$k = 60 \leftarrow$ minimum number of neigh-bour
$q = 49 \leftarrow$ dimension of null-space
$R \leftarrow$ the diagonal weight matrix
$e_g^{(n)} \leftarrow$ the smallest eigenvalues
$Q \leftarrow$ the number of orthonormal eigenvectors
$x_n \rightarrow \{x_1, ..., x_{m-1}, x_m\}, ..., \{x_{n-m+1}, ..., x_{n-1}, x_n\} \leftarrow$m-dimension delay vectors
for $l = 1$ to $(n-m+1)$ **do**
    $U_n \leftarrow$ find neighborhood with at least k points
    $\overline{x_n} = \frac{1}{|U_n|}\sum_{k(x_k \in U_n)} x_{k+i}, i = 0, 1, ..., m \leftarrow$ the average of neighborhood
    $C_{ij}^{(n)} = \frac{1}{|U_n|}\sum_{k(x_k \in U_n)} x_{k+i}x_{k+j} - \overline{x_i^{(n)}x_j^{(n)}} \leftarrow$ the covariance matrix
    $\Gamma_{ij}^{(n)} = R_i C_{ij}^{(n)} R_j \leftarrow$ the transformed matrix
    $Q_{ij}^{(n)} = \sum_{q=1}^{Q} e_{q,i}^{(n)} e_{q,j}^{(n)} \leftarrow$ projection on subspace
    $\theta_{n,i} = \frac{1}{R_i}\sum_{j=0}^{m} Q_{ij}^{(n)} R_j \left(\overline{x_j} - x_{n+j}\right) \leftarrow$ the component of correction
end for
$\{\theta\}_n = \left\{\overline{\theta_{n,i}}\right\} = \left\{\overline{\theta_1}, \overline{\theta_2}, ..., \overline{\theta_n}\right\} \leftarrow$ the average to each element of corrections
$\{\widetilde{x}\}_n = \{x\}_n + \{\theta\}_n \leftarrow$ the output of heartbeat component without noise
Exit

sharpest peaks in the HR period in radar signals.

The output of derivation filter in time domain:

$$y(n) = 0.2\left[-x(n-2) - 2x(n-1) + 2x(n+1) + x(n+2)\right] \tag{4.6}$$

where the input $x(n)$ is the heartbeat component.

The derivative results of the heartbeat component are shown in Figure 4.19a. After using the derivative function, the slope can be transmitted to the amplitude, and the R peaks can be easily determined as the largest amplitude peak in the window of one heartbeat cycle, as shown in Figure 4.19b. The bottom part of Figure 4.19c shows the result of R peak detection on radar signal and ECG signal.

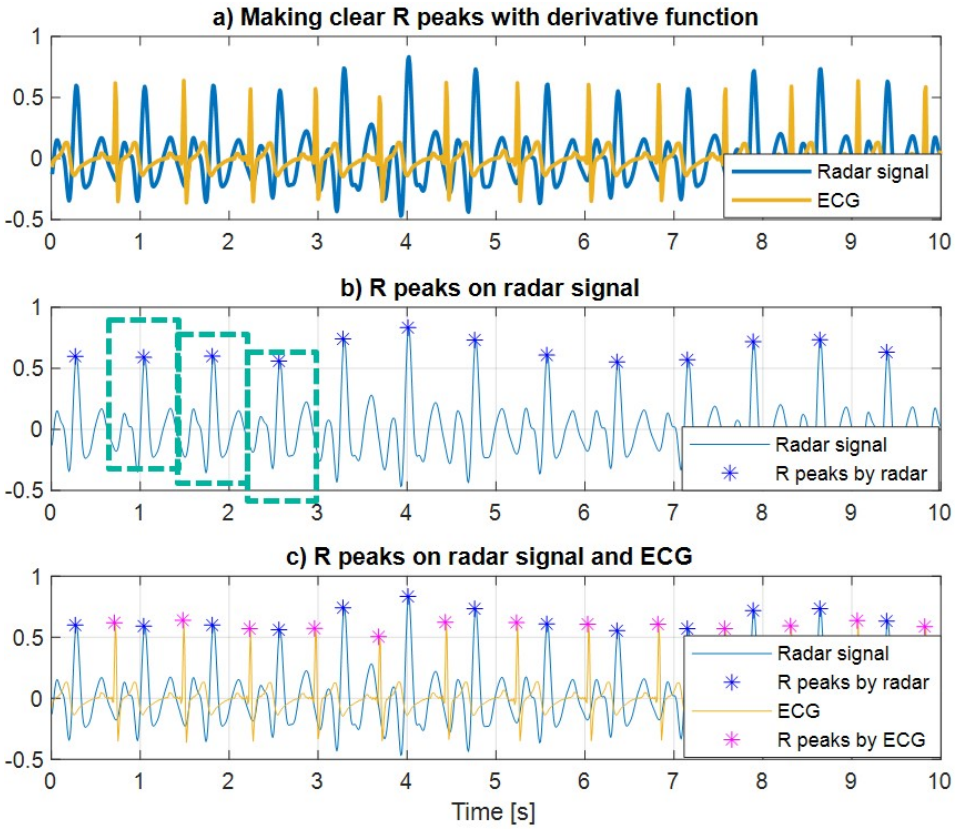

Figure 4.19: Radar signal after derivative function to make clear the R peaks (a), detected R peaks based on finding the biggest amplitude peak in one heartbeat cycle (b) and R peaks detection on radar signal and ECG (c)

4.3.2 Experiment design and data description

The IBI and HRV were calculated using radar and ECG signals to assess the proposed method. A signal from 10 healthy subjects was utilized, and their human signal was measured from the back while lying in bed. Healthy subjects were instructed to remain still while in bed, and the radar was affixed to the bottom of the bed, approximately 20 cm away from the bed surface. When measuring the signal, they wore a contact device, including an ECG device (BIOPAC ECG100C) and a respiration belt (NIHON KOHDEN, SR-601S, Japan), to obtain the reference signal, as shown in Figure 4.20. Each individual would be collected 2 min of data when the body was lying still in bed.

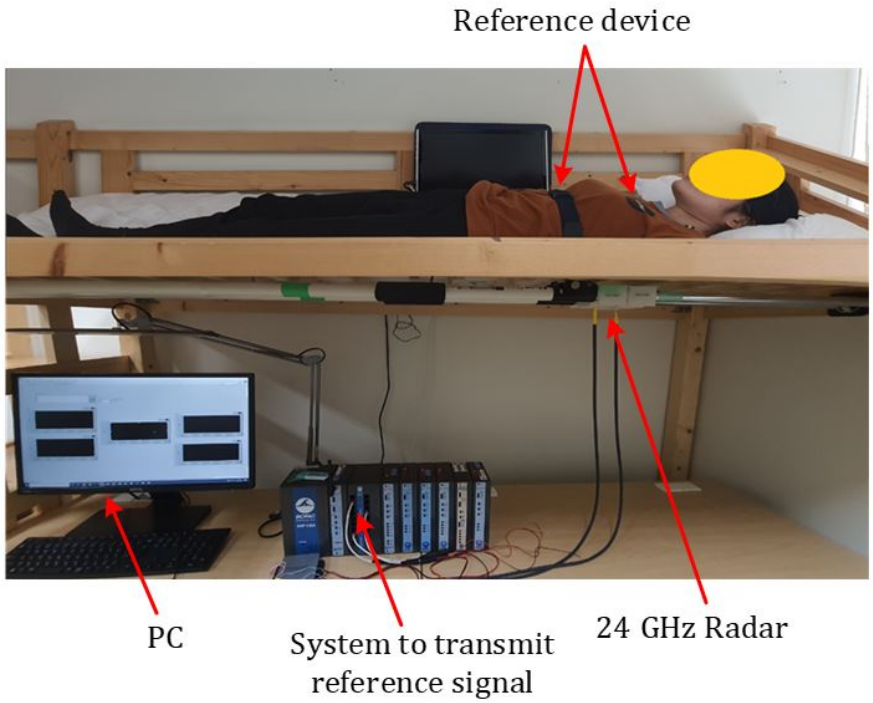

Figure 4.20: The arrangement of experiment to measure vital sign of healthy subjects

4.3.3 Result on healthy subjects

The data of 10 healthy subjects were measured, with a duration of 2 minutes for each subject. After the proposed method was applied, a comparison was made between the IBI obtained from the radar and the IBI obtained from the ECG for each individual. The calculation of HRV can be summarized in steps, as shown in Figure 4.21. After performing the calculation steps, as shown in subsection 4.3.1, we obtained the peak R peaks with the largest amplitude in a heartbeat cycle. These peaks are marked with their occurrence times, and consecutive periods of R-peak occurrence, called the IBI, are calculated. The timelines and IBIs are saved. Because the time intervals are not equal, resampling can be performed to obtain the HRV curve, as shown in Figure 4.21.

Four HRV features are extracted from the IBIs: standard deviation of IBIs (SDNN: ms), the root mean square of successive differences (RMSSD: ms), the low-frequency

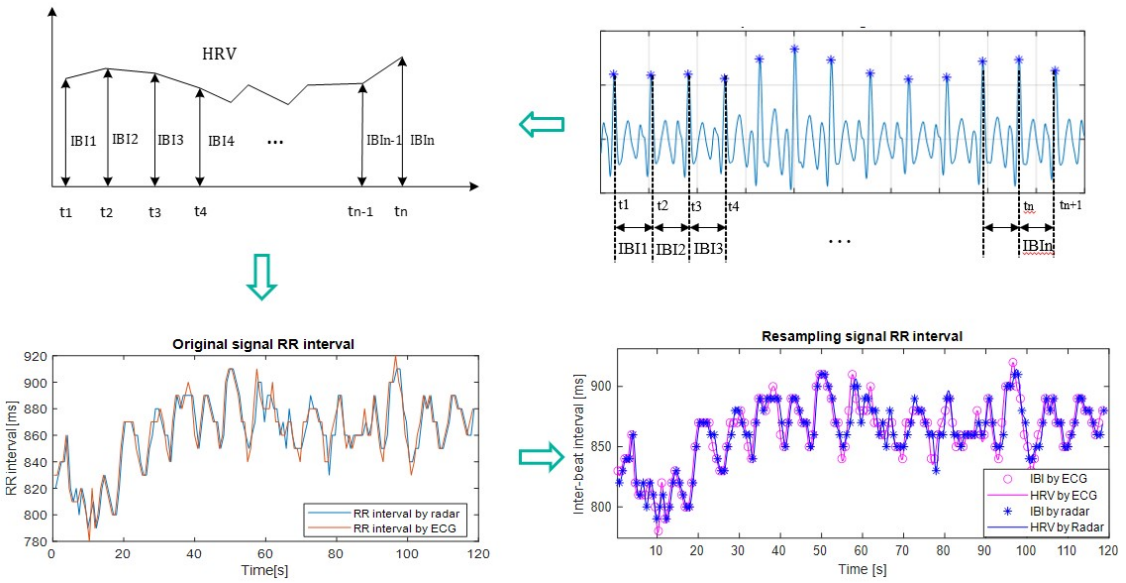

Figure 4.21: Steps to calculate HRV from radar signal after detecting R peaks with the highest amplitude in one heartbeat cycle

power (LF) is the absolute power of the low-frequency band (0.04–0.15Hz), in ms^2, and the high-frequency power (HF) is the absolute power of the high-frequency band (0.15–0.4Hz), in ms^2 [38]. The equations (4.7) and (4.8) provide the SDNN and RMSSD calculations.

$$SDNN = \sqrt{\frac{1}{N}\sum_{i=1}^{N}(IBI[i] - \overline{IBI})^2} \tag{4.7}$$

Table 4.3: Results of calculated heart rate variability features

Subject	SDNN (ms)		RMSSD (ms)		LF (ms^2)		HF (ms^2)	
	radar	ECG	radar	ECG	radar	ECG	radar	ECG
1	45.0	45.6	31.0	33.4	1894.5	1979.5	64.0	69.8
2	27.0	27.5	15.6	16.2	794.4	819.3	62.7	52.3
3	48.1	47.9	63.7	62.7	4834.6	4799.4	212.8	172.4
4	55.4	56.2	56.5	56.2	5824.9	5958.5	381.8	370.3
5	73.0	73.2	59.6	59.6	4395.5	4476.0	278.2	278.8
6	42.6	43.5	28.2	31.4	1566.6	1608.2	37.3	41.2
7	41.2	43.0	56.0	59.3	3866.3	4093.0	390.9	334.4
8	60.1	56.8	80.2	74.7	7763.1	7730.6	1183.0	1261.9
9	40.1	39.3	25.3	20.2	1408.1	1308.7	138.3	106.3
10	36.6	36.0	27.0	23.5	1161.3	1111.4	193.3	156.1

$$RMSSD = \sqrt{\frac{1}{N-1}\sum_{i=2}^{N}(IBI[i] - IBI[i-1])^2} \tag{4.8}$$

where N is the number of detected R-peaks and $\overline{IBI}$ is the mean value of all IBI.

Table 4.3 shows the results of the calculated heart rate variability features based on the IBIs extracted from the Doppler radar signals and from ECG signals, which are calculated as SDNN, RMSSD, LF and HF of HRV features based on FFT method. The difference between the calculated values of the radar signal and ECG signal was insignificant. Specifically, the difference in SDNN is from 0.2 to 3.3 ms (0.27% to 5.81%), in RMSSD it is from 0 to 5.5 ms (0% to 25.24%), in LF it is from 24.9 to 266.7 ms^2 (0.42% to 7.59%), and in HF it is from 0.6 to 78.9 ms^2 (0.21% to 30.1%).

The evaluation based on the correlation and Bland-Altman, root-mean-squared error (RMSE), and mean relative error (MRE) are listed in Table 4.4, with the RMSE and MRE defined as equations (4.9) and (4.10), respectively.

$$RMSE = \sqrt{\frac{1}{N}\sum_{i=1}^{N}(IBI_{radar}[i] - IBI_{ECG}[i])^2} \tag{4.9}$$

Table 4.4: Evaluation based on the correlation, Bland-Altman, and error estimation

Subject	IBI average (ms)		RMSE (ms)	MRE (%)	Correlation (%)	Bland-Altman (ms)	
	radar	ECG				Bias	(1.96*SD)
1	1060.4	1060.2	8.16	0.54	98.37	0.1802	16.07
2	861.38	861.45	6.99	0.52	96.7	-0.073	13.75
3	1081.48	1081.30	14.53	1.04	95.38	0.19	28.61
4	1099.63	1099.63	11.02	0.78	98.04	0.01	21.71
5	1040.62	1040.62	8.92	0.66	99.25	0.01	17.57
6	1063.33	1063.05	8.11	0.53	98.24	0.29	15.95
7	1020.61	1020.61	7.58	0.48	98.46	-0.02	14.91
8	911.78	911.71	27.58	1.75	90.75	0.08	54.26
9	723.50	723.56	11.21	1.04	96.01	-0.06	22.05
10	855.14	855.29	11.86	0.99	94.65	-0.14	23.32

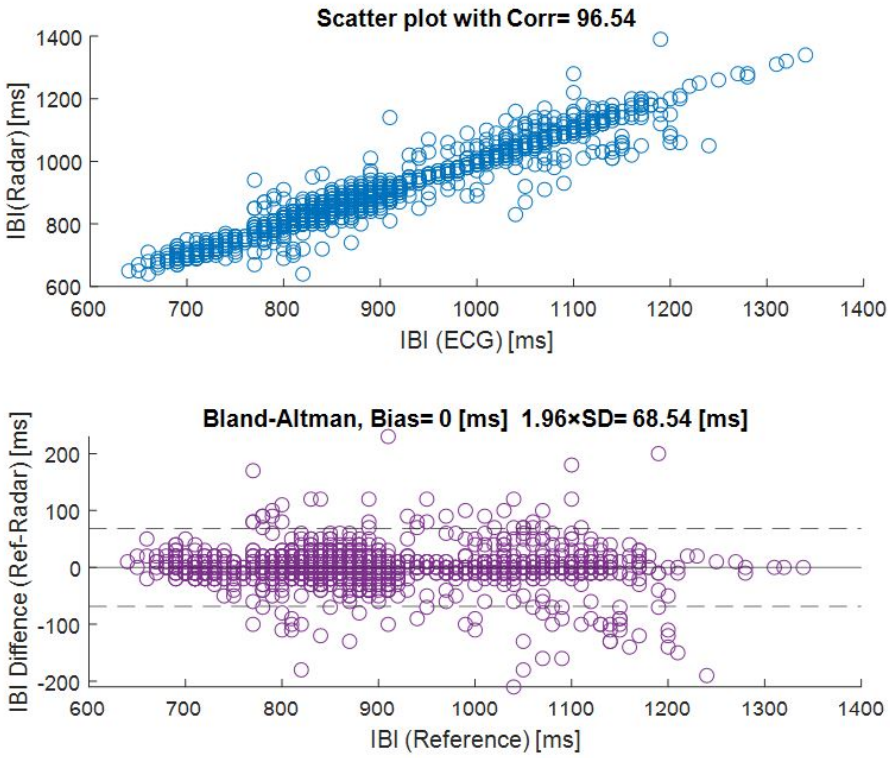

Figure 4.22: Scatter plot (upper) and Bland-Altman plot (lower) for the result of IBI detection using proposed method to radar signal and ECG

$$MRE = \frac{1}{N}\sum_{i=1}^{N}\frac{|IBI_{radar}[i] - IBI_{ECG}[i]|}{IBI_{ECG}[i]} \tag{4.10}$$

The results show that the proposed method on the radar signal yields results close to those obtained from the ECG. Specifically, RMSE from 6.99 to 27.58 ms, MRE from 0.48 to 1.75%, while correlation from 90.75% to 99.25%, and Bland-Altman (1.96*SD:1.96*standard deviation) from 13.75 to 54.26 ms.

To summarize, Figure 4.22 shows the correlation and Bland-Altman results for all 10 subjects. The calculation results show that the IBI calculated with the ECG signal is in the range of 723.56–1099.6 ms. The IBI calculated with the radar signal reaches between 723.5 and 1099.6 ms. The Figure shows that the proposed method has a high performance with a scatter plot showing a correlation of 96.54%, whereas Bland-Atman shows a bias

of 0 ms and a 95% limit of agreement of 68.54 ms.

To further clarify the contribution achieved, a list of results compared to previous work is provided in Table 4.5. It can be observed that the proposed method was tested on more individuals, achieving better accuracy with an average RMSE of 12.97 ms and an average MRE of 1.02%.

From Table 4.5, the better result should be low value of RMSE, MRE and standard mean deviation (SMD). Our study can achieve such result. Low values of MSD indicate that the HRV indices were clustered more closely around the mean; so that lower SMD shows higher reliable, with SMD is calculated as below.

The denominator is simply the square root of the average variance.

$$s = \sqrt{\frac{s_1^2 + s_2^2}{2}} \tag{4.11}$$

where s_1^2 and s_2^2 are the variance of values by radar and ECG, respectively.

The SMD (Cohen's SMD) is then calculated as the following.

$$s = \sqrt{\frac{s_1^2 + s_2^2}{2}} \tag{4.12}$$

where $\overline{x_1}$ and $\overline{x_2}$ are the mean of values by radar and ECG, respectively.

Table 4.5: Results of HRV based on proposed method compare to previous work

Research	Radar Frequency (GHz)	Type of radar	Number of subjects	Measured time per subject (s)	Average RMSE (ms)	Average MRE (%)	SMD of LF	SMD of HF
[31]	24	CW	10	120	47.5	-	-	-
[32]	24	CW	10	180	16.7	1.54	-0.167	0.018
[34]	8.7	UWB	15	480	-	-	0.771	0.739
[41]	79	UWB	3	300	26.7	-	-	-
This research	24	CW	10	120	12.97	1.02	-0.016	0.02

Chapter 5

DISCUSSION AND CONCLUSION

5.1 Discussion About Real Application Design

5.1.1 Real-time performance on labview

A LabVIEW-designed system for monitoring vital signs is presented in Figure 5.1. The system involves data acquisition through a USB port, which connects to an analog-to-digital converter (ADC). A 10-second signal segment is then extracted to identify five features, which are sent to a quadratic SVM classifier. If the SVM output indicates a "low-quality signal" the vital sign detection is circumvented and the LED turns off, displaying "0" for both the RR and HR parameters. This signifies that the patient is making random body movements. In contrast, if the SVM output shows a "high-quality signal", it indicates that the signal sample does not contain random body movements, and the sample is then sent to the vital sign detection process to extract the RR and HR parameters. At this point, the LED turns "green on" indicating that the patient is lying still without

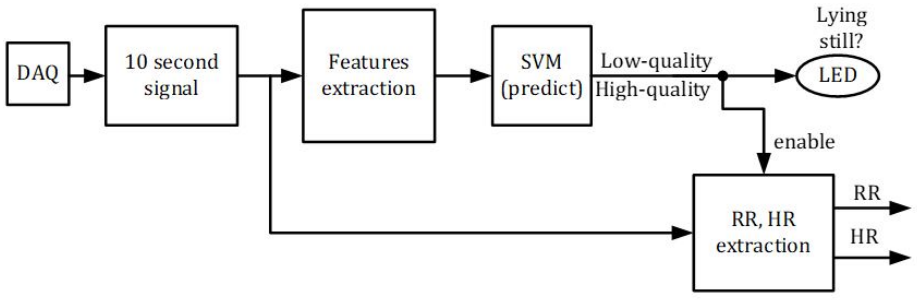

Figure 5.1: The system of vital sign monitoring on LabVIEW

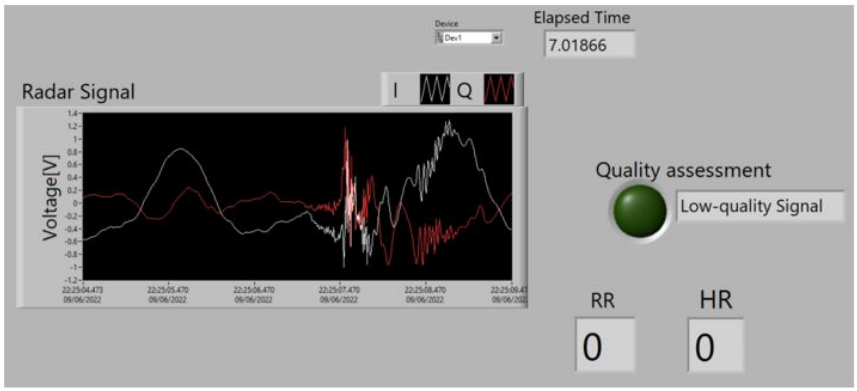

(a) Monitoring screen when patient makes random body movements

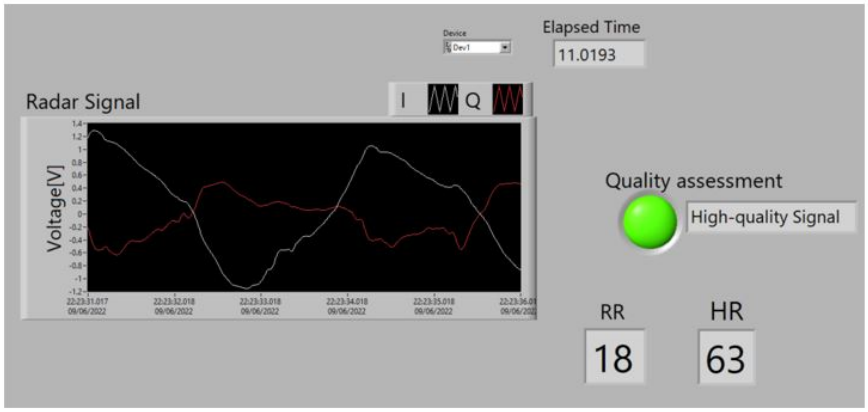

(b) Monitoring screen when patient is without random body movements

Figure 5.2: Real-time vital signs monitoring screen designed on LabVIEW

any random body movements. The system uses a 10-second signal segmentation window with a 9-second overlap, allowing for signal quality assessment and vital sign separation to be performed every 1 second.

The LabVIEW-designed patient monitoring system's user interface is depicted in Figure 5.2. Through this interface, medical professionals can view essential indicators such as RR and HR as well as the patient's condition, which may include remaining stationary or exhibiting sporadic physical movements.

Evaluation

To gauge the random physical movements and determine RR and HR in healthy subjects, a model that was tested in laboratory conditions was employed. The real-time ex-

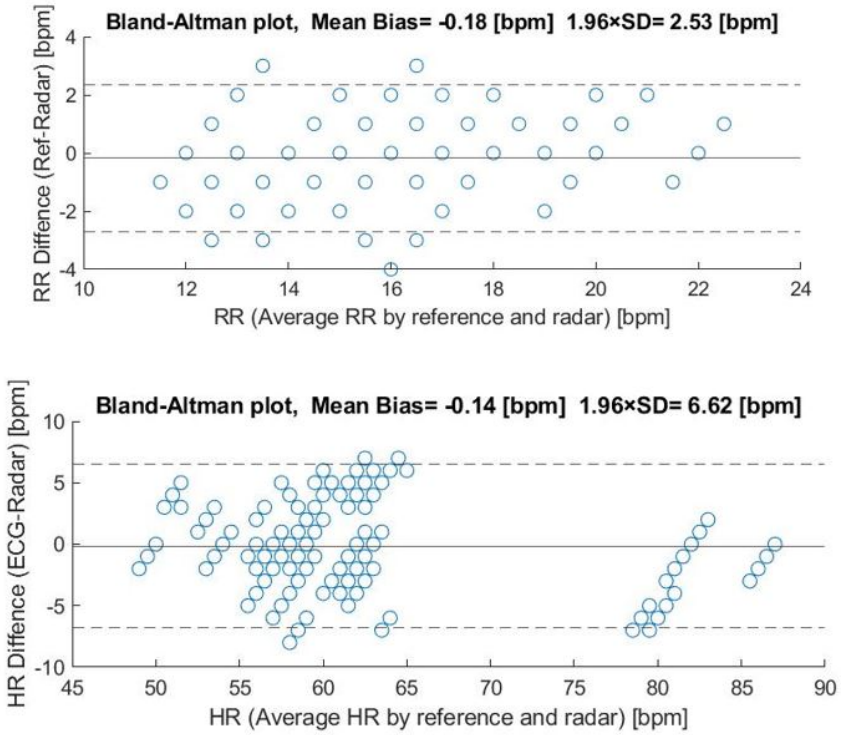

Figure 5.3: Bland-Atman plot of RR and HR present the agreement between radar measurement and contact-type

periments on five subjects were conducted, each healthy subject was asked to perform the test for five minutes. During the initial two minutes, the participants were required to execute three random movements, whereas they were asked to remain stationary for the last three minutes. The results showed that the real-time system correctly identified random movements in 13 out of 15 instances. Furthermore, the RR and HR readings obtained by the radar-based measurement system closely matched those obtained by the contact-type sensors (BIOPAC ECG100C for HR and NIHON KOHDEN, SR-601S for RR), with a mean bias value of -0.14 bpm and -0.18 bpm, respectively. The Bland-Atman plot of RR and HR, presented in Figure 5.3, showed good agreement between the two measurement methods. The 1.96×SD (95% limits of agreement) values of RR and HR were 2.53 bpm and 6.62 bpm, respectively.

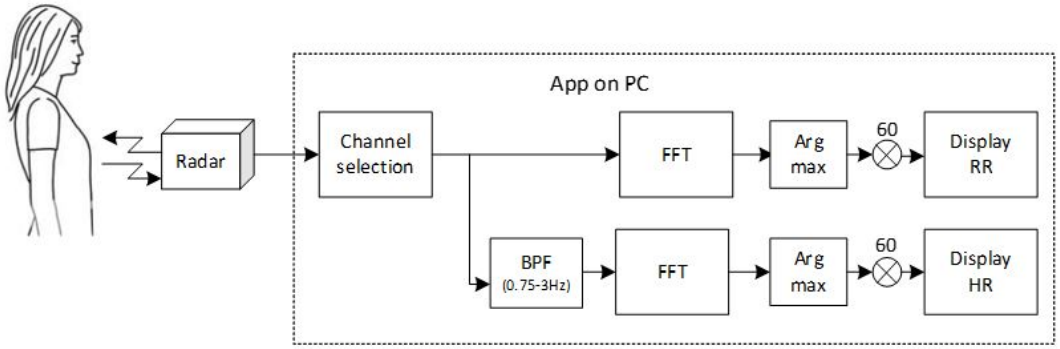

Figure 5.4: Diagram of the system processing

5.1.2 The health check-up system using radar

In the diagram depicted in Figure 5.4, the RR and HR system process is illustrated. The system incorporates a radar that senses the movement of the chest surface caused by breathing and heart rate. The received radar signal is then transmitted to a personal computer (PC) for further analysis. The PC is equipped with a channel selection block that considers the balance of the two signal channels. The channel with better linearity is selected and then directed towards the Band-Pass Filter (BPF) and fast Fourier transform (FFT) block. The BPF and FFT block are used to isolate the frequency range associated with breathing and pulse rates. Afterwards, the most significant point is chosen, and the components indicating respiration and heartbeat are exhibited on the monitor.

In actual usage, the design of the system is depicted in Figure 5.5. The radar is housed in a small enclosure and positioned on a stand that can be adjusted to reach the height of the human chest. The signal received is transmitted to the computer by means of the USB port. The whole process of analyzing and exhibiting the outcomes is executed on a MATLAB-based PC application.

Figure 5.6 illustrates the application's user interface. To initiate the measurement, the START button is pressed, which displays the I and Q signal channels. Afterward, by

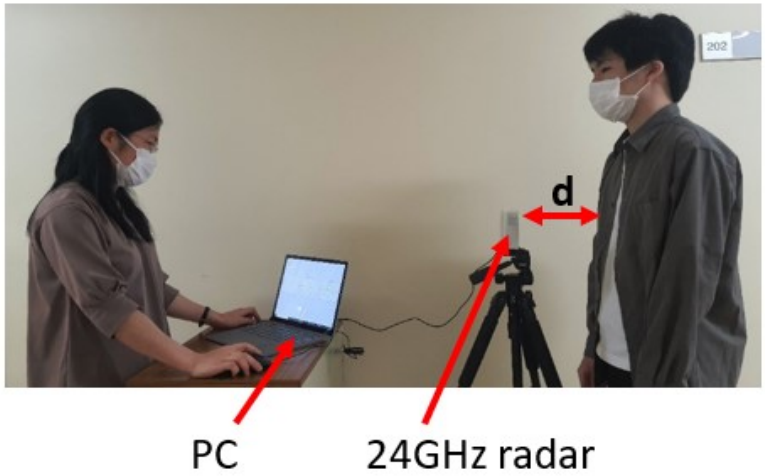

Figure 5.5: Measurement system in real applications

pressing the RR and HR buttons, the system selects the more linear channel to calculate the RR and HR. For the measurement shown in Figure 5.6, the Q channel was chosen for the calculation of RR and HR.

To test the system's accuracy, 6 healthy individuals between the ages of 19 and 32 years old were tested in our laboratory. Each person was tested 5 times. The results show that the RR and HR deviation are acceptable compared to the contact device, ranging from 0 to 2 and 0 to 4 beats per minute, respectively.

5.1.3 Hardware implementation on fpga

With the aim of developing an independent measuring device, this study utilized an FPGA (field-programmable gate array) kit to embed signal processing onto the circuit.

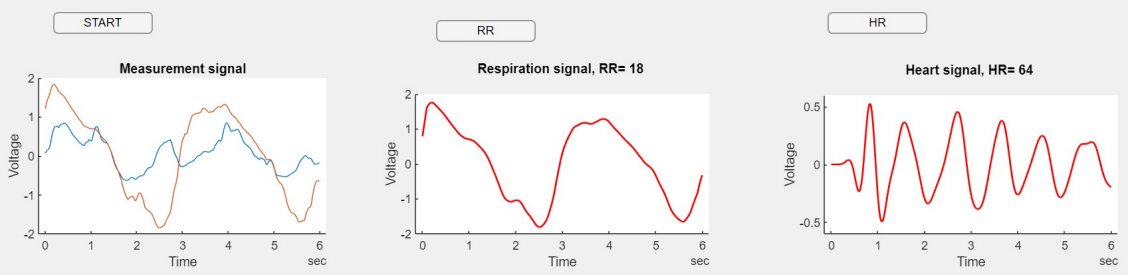

Figure 5.6: The interface for monitoring respiratory and cardiac rates

Figure 5.7: Vital sign detection system implemented on FPGA myRIO kit

The circuit can operate independently from the computer after the code has been embedded. The system of device on the myRIO board [104] is shown in Figure 5.7 below. With a compact radar chip placed inside a plastic box, the radar will measure the movement of the chest when the body is completely still or sitting still. DAQ will collect signals I and Q, and the processing part will evaluate whether the signal obtained is in a still state or not. If the body is in a motionless state, the respiratory and heart rates will be extracted. The results of the respiratory and heart rates will be displayed on the liquid-crystal display (LCD) as shown in Figure 5.7.

5.1.4 Monitoring the subjects with high heart rate

The subjects surveyed in this study are students at UEC, in good health, so their resting heart rate is within a not wide range. To make clear about whether radar can monitor high frequency of heart rate, I would like to measure the subjects with factors that increase heart rate such as doing exercise, drinking caffeinated water. The raw signal measured by radar show that, after doing exercise the heart rate of student is so high, it is about more than 100 bpm. Then heart rate decreased by time of rest. To show the potential for measuring the heart rate in high bpm, the results based on the proposed method was figured out. The heart rate results by radar using proposed method based

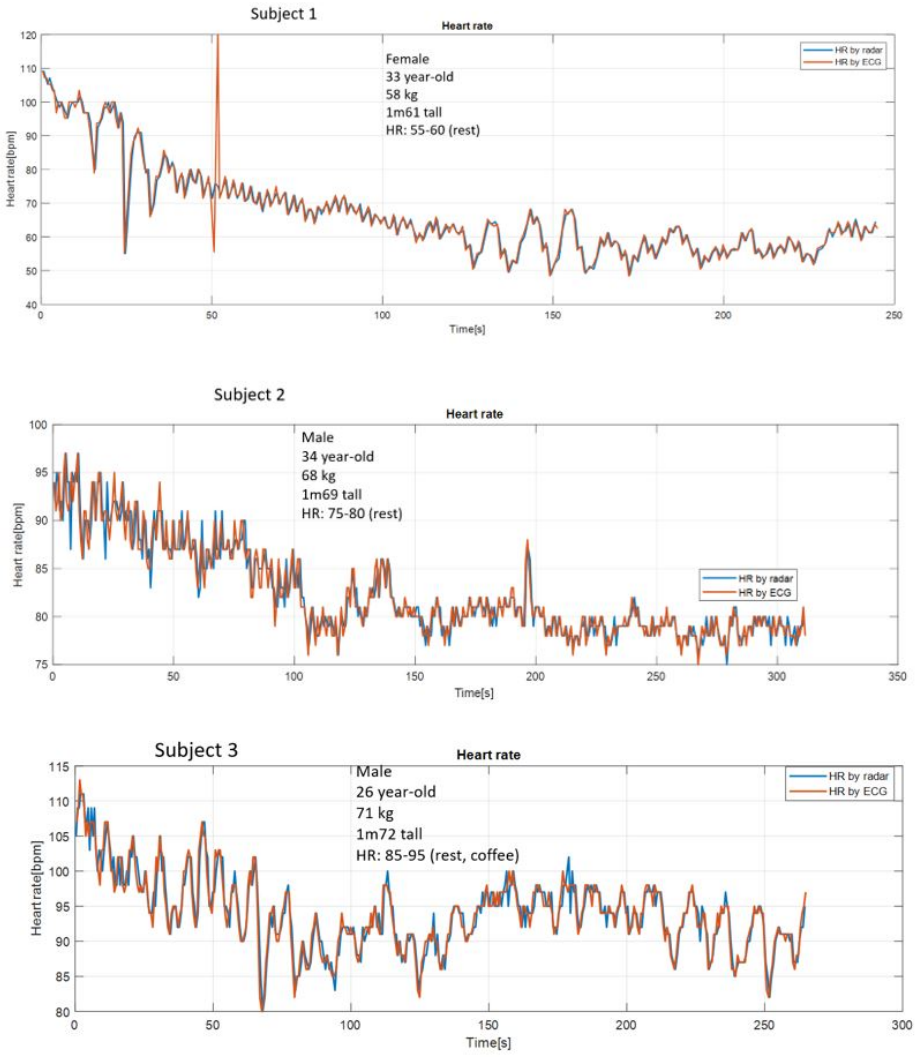

Figure 5.8: The heart rate results by radar using proposed method based on three healthy subjects with some factor making heart rate increases

on Locally Projective Noise Reduction and derivative function and by ECG as shown in Figure 5.8

5.2 Potential In Health Care Setting

This subsection demonstrates the proposed system's use in clinical settings by performing signal quality classification on a dataset obtained from a hospital. The dataset comprises measurements of elderly patients. With an anxious expression on patient's face, physical examination revealed that she was 150 cm tall, 30.1 kg weight , body tem-

perature 37.1°C, blood pressure 94/65 mmHg, average heart rate 60-70 bpm with ECG features of normal sinus rhythm, respiration rate 20 bpm and oxygen saturation 94%. Data set includes 250 samples of both good and bad quality were selected from the measurement files, which contained 2 hours of data and had 1024 sampling points per sample. The training was carried out using K-fold cross-validation, where the 500 signal samples were divided into 400 training samples and 100 testing samples, and this process was repeated five times with varying test sets. The classification results indicate that the data was accurately classified with a validation accuracy of 99.1% for the training model using SVM, without including the training data in the testing data. The training dataset was also trained with other machine learning algorithms, such as Tree Decision, Logistic Regression, and Fine KNN (k-nearest neighbors), which yielded results of 98.2%, 94.5%, and 95.5%, respectively. These findings suggest that the extracted features are better suited for the SVM model.

After undergoing training, the model was put into practice by evaluating the signals of two patients, each of whom had 24 data files per day for 7 consecutive days. To assess the quality of the signals, a classification analysis on the data collected during their nighttime sleep hours was performed, with a specific focus on evaluating the sleep quality of elderly patients. It's important to note that our inferences about sleep quality were based on the ratio of low-quality signal to the total signal length, and were only made when the signals were not impacted by external factors such as doctor or nurse visits. The results of the one-hour data test for Patient 1 can be seen in Figure 5.9.

After being categorized as high-quality signals, the RR and HR data were extracted and subjected to detailed analysis, with a specific focus on analyzing the RR and HR of two patients during a particular time period. The risk of Cheyne-Stokes respiration

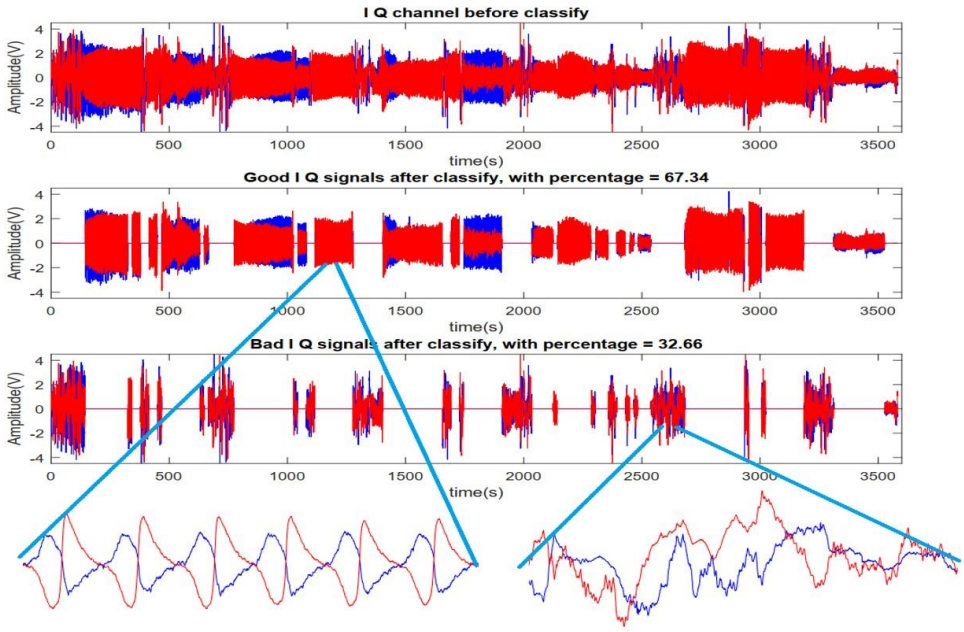

Figure 5.9: An example of the classification results for signal quality based on a one-hour measurement of an inpatient at Yokohama Hospital in Japan

(CSR) and sleep apnea was evaluated with particular emphasis. Any abnormalities in the RR and HR data for Patient 1 were assessed in the analysis from January 5 to January 11, 2017, and Patient 2 from January 17 to January 23, 2020, over the course of 7 days.

Throughout each day, the RR and HR were calculated 24 times (over the course of 24 hours) using high-quality radar signals for both patients. A box chart showing the RR and HR for each day can be found in Figure 5.10. For Patient 1, it is clear that from January 5 to January 8, both the RR and HR exhibited a linear increase, with the mean HR reaching its peak on January 8. After detecting this abnormality, a decision was made to closely examine the raw signal before and after this date. It was discovered that on January 8, there was a significant change in the respiratory amplitude, leading to a diagnosis of CSR for the patient. Prior to the onset of CSR, the raw signal exhibited a consistent amplitude, as can be seen in Figure 5.11. It's important to note that the distinctive raw signal on January 8 served as an alert to the presence of CSR.

An abnormal increase in both the mean HR and absolute HR on January 19 was

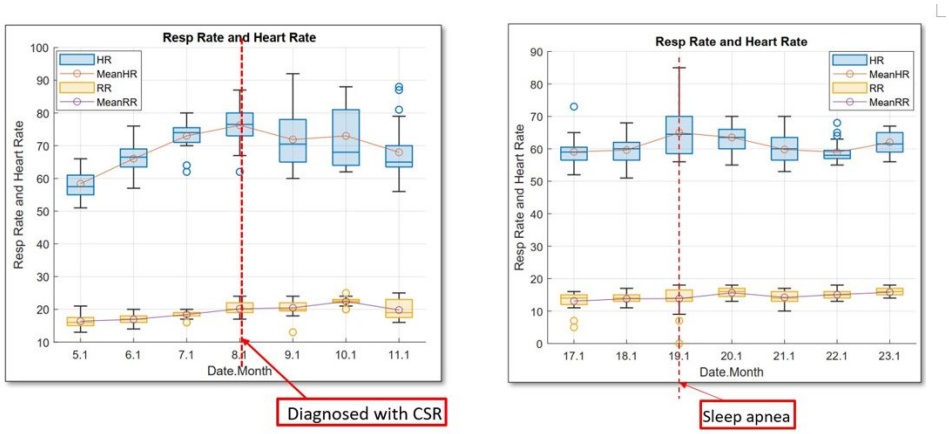

(a) (b)

Figure 5.10: The 24-hour respiratory rate and heart rate patterns in two patients suffering from central sleep apnea (a) and obstructive sleep apnea (b)

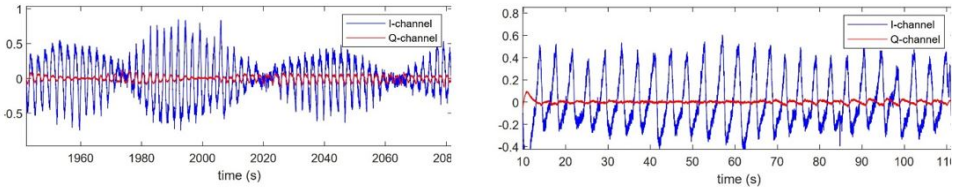

(a) (b)

Figure 5.11: The respiratory amplitude exhibited by Patient 1 during central sleep apnea (a) and prior to the onset of central sleep apnea (b)

observed in the case of Patient 2. At 11 am on that day, the heart rate suddenly spiked to 85 bpm, whereas an average HR of approximately 60 bpm was noted for the patient.

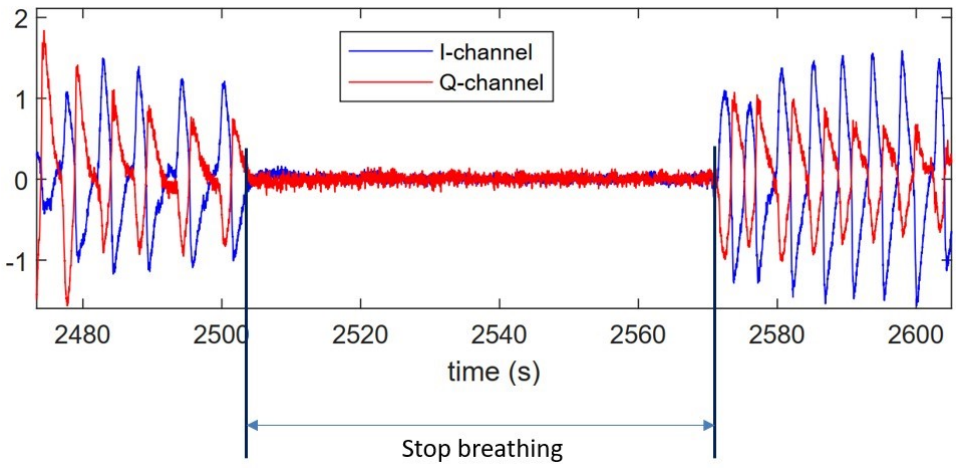

Figure 5.12: A portion of the signal indicating sleep apnea from the Patient 2

Upon further investigation of the raw data, it was discovered that 15 instances of stopped breathing per hour were experienced by the patient, with the longest period of apnea lasting for 66 seconds (from 2505 s to 2571 s), as depicted in Figure 5.12. It was found that an increase in heart rate occurred when sleep apnea occurred. The patient was made aware of their apnea, and their breathing rate increased, leading to the need for medical intervention in the following days to manage their condition. It is known that sleep apnea can result in a drop in heart rate and oxygen deprivation, with involuntary reflexes leading to sudden awakening and a rapid acceleration in heart rate and blood pressure [105, 106].

The hospital nurses also recorded the heart rate and temperature of the patients three times a day, every day. The records indicated an abnormal increase in heart rate on January 7 and 8, 2017, for patients diagnosed with CSR, and on January 19, 2020, for patients with sleep apnea syndrome, which is consistent with this study results.

5.3 Limitation Of The Dissertation

Firstly, the dataset measured on healthy subjects is limited in age, the proposed method should be demonstrated in more subjects with a wider age range, because people of different ages have different physiology, therefore, vital sign is different.

Secondly, this paper does not present a signal quality classification that show signal containing random body movement. For signals containing small random body movement, an algorithm to perform vital sign compensation is required. This content will be further developed by the authors for future research.

Thirdly, this study performed real-time computation for RR and HR. However, to compute HRV, the method based on LPNR is a computationally intensive algorithm that is difficult to implement in real-time, and so far, the real-time computation of HRV is a

goal for the next phase of this study.

Finally, the trend for practical applications is a computer-independent system that can transmit parameters over a distance, forming an IoT network in healthcare. This requires integration with the field of communication to create a telemedicine system. This study has not achieved this, and it will be the goal for the next phase of the study.

5.4 Future Work Toward Real Application

From our survey and research, it can conclude that if we can accurately estimate the duration of the R peak of the heart at two measurement points, we can find the Pulse Wave Velocity (PWV) and from that we can deduce the blood pressure. Although there is a delay between the ECG and the radar signal, however the delay is constant. Therefore, the rules for inferring blood pressure from radar are the same as from the ECG.

The next study is set to develop an IoT system for hospital use, utilizing radar technology. The application aims to monitor the vital signs including respiration rate, heart rate, heart rate variability and blood pressure of inpatients who are lying in bed for extended

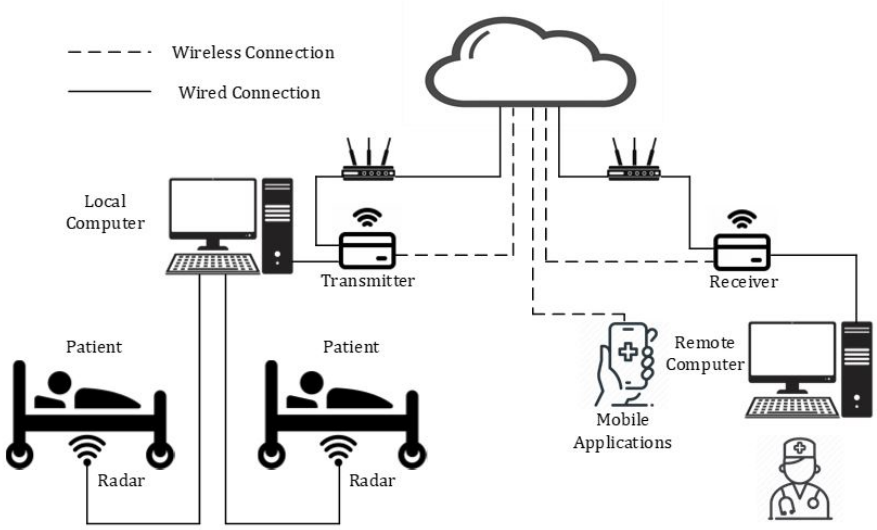

Figure 5.13: An outline of the design for a real-time monitoring system in the future plan

periods. Figure 5.13 illustrates that vital sign measurements are taken from the patient's back. A radar device is mounted beneath the bed to detect small body movements caused by RR, HR and BP. The signals received are then sent to a computer for processing, and the results are transmitted through the internet and displayed on a screen at the destination. The displayed results indicate the patient's status, whether they are making random body motions or lying still. In the case of random body motions other than RR, HR and BP, the signal is classified as "random motion", resulting in low-quality signal and displayed as "0." However, if the patient is lying still, resulting in only harmonic movements of RR, HR and BP, the signal is classified as "Lying still", indicating a high-quality signal. In this case, vital signs (RR, HR and BP) are calculated and displayed on the screen.

5.5 Conclusion

Vital signs refer to a set of medical indicators, including RR, HR, BP and BT. These measurements are useful in assessing physical and psychological stress levels. Compared to BP and BT, changes in RR and HR are more pronounced in both healthy individuals and those at risk of cardiopulmonary arrest, and can assist in the diagnosis of cardiovascular and lung diseases. However, traditional vital sign monitoring methods involve attaching multiple electrodes or terminals to the patient's body, which can be uncomfortable and unsuitable for long-term monitoring or individuals with skin abrasions. To address these issues, a non-contact method utilizing radar to monitor changes in cardiac volume has the potential to meet these requirements.

When visiting the patient's situation in Hospital, it can be recognized that monitoring the patient's vital signs is very important. However, the patients have to be placed many sensors on the body. When the patient is the elder and infants, this is a real disadvantage.

The aim of the research is to assist doctors in determining the patient's vital sign including respiration rate, heart rate and heart rate variability based on the output signal of a radar which is a non-invasive monitoring device. To do this, it requires to design a system to automatically classify radar output signal and a processing block after classification. The system automatically recognizes signals based on machine learning algorithms, which can classify signals into two groups: signals with random body movement and signals without random body movement. For groups of signals without random body movement, the next processing is do algorithm to find the vital signs.

This study is the first to demonstrate the operating principle of CW radar in measuring vital signs. To understand radar signals, and to achieve high accuracy in signal analysis and processing, the first requirement is to understand the operating principle of radar in measuring vital signs, from which the essence of the signal and the change in signal shape during measurement can be understood. Based on an understanding of the radar output signal, appropriate signal processing and algorithm selection can improve the accuracy of measurements.

The study reveals differences in radar signals when measuring from the front and back of the body. The essence of this difference is displacement compared to the wavelength. Experimental results demonstrate that measuring vital signs from the back of the body results in displacement that is always less than half the wavelength of the radar, enabling the detection of breathing rate by taking the envelope of the radar signal.

Heart rate is separated using an SVD algorithm with clear peaks, no longer exhibiting harmonic peaks. As a result, the corresponding heartbeats on the screen are very clear, corresponding to the ECG heartbeat.

This thesis is the first to use the theory of finding the peak with the highest slope in

the radar output signal, corresponding to the R peak in the ECG signal. Prior to this, an LPNR algorithm was used to remove unwanted peak noise and retain desired peaks without time shift. Therefore, the results of IBI and HRV are highly accurate. However, this study still has some limitations, such as a narrow age range of healthy subjects, and a lack of diversity in medical characteristics of the measured group. The HRV algorithm has not been implemented in real-time, and transmitting results to remote patients and doctors has not yet been achieved. These limitations will be addressed in future research.

BIBLIOGRAPHY

1. Coca, Aitor, Raymond J. Roberge, W. Jon Williams, Douglas P. Landsittel, Jeffrey B. Powell, and Andrew Palmiero. "Physiological monitoring in firefighter ensembles: Wearable plethysmographic sensor vest versus standard equipment." Journal of occupational and environmental hygiene 7, no. 2 (2009): 109-114.

2. Paradiso, Rita, Tommaso Faetti, and S. Werner. "Wearable monitoring systems for psychological and physiological state assessment in a naturalistic environment." In 2011 Annual International Conference of the IEEE Engineering in Medicine and Biology Society, pp. 2250-2253. IEEE, 2011.

3. Laupland, Kevin B. "Fever in the critically ill medical patient." Critical care medicine 37.7 (2009): S273-S278.

4. Öner, Can, Mehmet Avcı, and Ekrem Orbay. "A Night In The Sea: A Hypothermia Case." The Anatolian Journal of Family Medicine 1.1 (2018): 21-23.

5. Kelly GS. Body temperature variability (Part 2): masking influences of body temperature variability and a review of body temperature variability in disease. Alternative medicine review. 2007 Mar 1;12(1).

6. Pickering, Dianne, and Sue Stevens. "How to measure and record blood pressure." Community Eye Health 26.84 (2013): 76.

7. Rai, Pallavi. "Heart Rate." In Encyclopedia of Evolutionary Psychological Science, pp. 3649-3655. Cham: Springer International Publishing, 2021.

8. Park, David S., and Glenn I. Fishman. "The cardiac conduction system." Circulation 123.8 (2011): 904-915.

9. Cretikos, Michelle A., et al. "Respiratory rate: the neglected vital sign." Medical Journal of Australia 188.11 (2008): 657-659. 10. Subbe, CP1, et al. "Effect of introducing the Modified Early Warning score on clinical outcomes, cardio-pulmonary arrests and intensive care utilisation in acute medical admissions." Anaesthesia 58.8 (2003): 797-802.

11. Hill, Barry, and Sarah H. Annesley. "Monitoring respiratory rate in adults." British Journal of Nursing 29.1 (2020): 12-16.

12. Poh, M. Z., McDuff, D. J., Picard, R. W. (2010). Advancements in noncontact, multiparameter physiological measurements using a webcam. IEEE transactions on biomedical engineering, 58(1), 7-11.

13. Allen, John. "Photoplethysmography and its application in clinical physiological measurement." Physiological measurement 28.3 (2007): R1.

14. Allen, J., and A. Murray. "Effects of filtering on multisite photoplethysmography pulse waveform characteristics." Computers in Cardiology, 2004. IEEE, 2004.

15. Greene, Keith R. "8 The ECG waveform." Baillière's Clinical Obstetrics and Gynaecology 1.1 (1987): 131-155.

16. Gregg, Richard E., et al. "What is inside the electrocardiograph?." Journal of electrocardiology 41.1 (2008): 8-14.

17. Mehta, S. S., Lingayat, N. S. (2008, October). Detection of P and T-waves in Electrocardiogram. In Proceedings of the world congress on Engineering and computer science (pp. 22-24).

18. Cromwell, Leslie, et al. "Biomedical instrumentation and measurements (Book- Biomedical instrumentation and measurements.)." Englewood Cliffs, N. J., Prentice-Hall, Inc., 1973. 457 p (1973).

19. AL-Khalidi, Farah Q., Reza Saatchi, Derek Burke, H. Elphick, and Stephen Tan. "Respiration rate monitoring methods: A review." Pediatric pulmonology 46, no. 6 (2011): 523-529.

20. Shneerson, John M. Sleep medicine: a guide to sleep and its disorders. John Wiley Sons, 2009.

21. Newell, Alejandro, et al. "Stacked hourglass networks for human pose estimation." European conference on computer vision. Springer, Cham, 2016.

22. Nibali, Aiden, et al. "3d human pose estimation with 2d marginal heatmaps." 2019 IEEE Winter Conference on Applications of Computer Vision (WACV). IEEE, 2019.

23. Liu, Jun, et al. "Feature boosting network for 3D pose estimation." IEEE transactions on pattern analysis and machine intelligence 42.2 (2019): 494-501.

24. Poh, Ming-Zher, et al. "Advancements in noncontact, multiparameter physiological measurements using a webcam." IEEE transactions on biomedical engineering 58.1 (2010): 7-11.

25. Negishi, Toshiaki, et al. "Contactless vital signs measurement system using RGB-thermal image sensors and its clinical screening test on patients with seasonal influenza." Sensors 20.8 (2020): 2171.

26. Sun, Guanghao, et al. "Non-contact monitoring of heart rate variability using medical radar for the evaluation of dynamic changes in autonomic nervous activity during a head-up tilt test." Journal of Medical Engineering Technology 43.7 (2019): 411-417.

27. Shi, Kilin, et al. "Contactless analysis of heart rate variability during cold pressor test using radar interferometry and bidirectional LSTM networks." Scientific

reports 11.1 (2021): 1-13.

28. Nosrati, Mehrdad, and Negar Tavassolian. "High-accuracy heart rate variability monitoring using Doppler radar based on Gaussian pulse train modeling and FTPR algorithm." IEEE Transactions on Microwave Theory and Techniques 66.1 (2017): 556-567.

29. Tu, Jianxuan, and Jenshan Lin. "Fast acquisition of heart rate in noncontact vital sign radar measurement using time-window-variation technique." IEEE Transactions on Instrumentation and Measurement 65, no. 1 (2015): 112-122.

30. Li, Meiyu, and Jenshan Lin. "Wavelet-transform-based data-length-variation technique for fast heart rate detection using 5.8-GHz CW Doppler radar." IEEE Transactions on Microwave Theory and Techniques 66, no. 1 (2017): 568-576.

31. Yamamoto, Kohei, Kentaroh Toyoda, and Tomoaki Ohtsuki. "Spectrogram-based non-contact RRI estimation by accurate peak detection algorithm." IEEE Access 6 (2018): 60369-60379.

32. Petrović, Vladimir L., et al. "High-accuracy real-time monitoring of heart rate variability using 24 GHz continuous-wave Doppler radar." IEEE Access 7 (2019): 74721-74733.

33. Yen, Hoang Thi, Masaki Kurosawa, Tetsuo Kirimoto, Yukiya Hakozaki, Takemi Matsui, and Guanghao Sun. "A medical radar system for non-contact vital sign monitoring and clinical performance evaluation in hospitalized older patients." Biomedical Signal Processing and Control 75 (2022): 103597.

34. Ahmed, Sarfaraz, Yonggu Lee, Young-Hyo Lim, Seok-Hyun Cho, Hyun-Kyung Park, and Sung Ho Cho. "Noncontact assessment for fatigue based on heart rate variability using IR-UWB radar." Scientific Reports 12, no. 1 (2022): 1-10.

35. Y. Yao, et al., "Model-Based Verification of a Non-Linear Separation Scheme for Ballistocardiography," in IEEE Journal of Biomedical and Health Informatics, vol. 18, no. 1, pp. 174-182, 2013.

36. Inan, Omer T. "Recent advances in cardiovascular monitoring using ballistocardiography." 2012 Annual International Conference of the IEEE Engineering in Medicine and Biology Society. IEEE, 2012.

37. Cimr, Dalibor, and Filip Studnička. "Automatic detection of breathing disorder from ballistocardiography signals." Knowledge-Based Systems 188 (2020): 104973.

38. Ishizaka, Shuzo, Kohei Yamamoto, and Tomoaki Ohtsuki. "Non-contact blood pressure measurement using doppler radar based on waveform analysis by LSTM." ICC 2021-IEEE International Conference on Communications. IEEE, 2021.

39. Jung, Marie, Michael Caris, and Stephan Stanko. "Non-contact Blood Pressure Estimation Using a 300 GHz Continuous Wave Radar and Machine Learning Models." 2021 IEEE International Symposium on Medical Measurements and Applications (MeMeA). IEEE, 2021.

40. M. Alizadeh, G. Shaker and S. Safavi-Naeini, "Remote Heart Rate Sensing with mm-wave Radar," 2018 18th International Symposium on Antenna Technology and Applied Electromagnetics (ANTEM), 2018, pp. 1-2, doi: 10.1109/ANTEM.2018.8572982.

41. Sakamoto, Takuya, Sohei Mitani, and Toru Sato. "Noncontact monitoring of heartbeat and movements during sleep using a pair of millimeter-wave ultra-wideband radar systems." IEICE Transactions on Communications 104, no. 4 (2021): 463-471.

42. Sun, Guanghao, et al. "Non-contact monitoring of heart rate variability using medical radar for the evaluation of dynamic changes in autonomic nervous activity.

43. Yen, Hoang Thi, et al. "Proof-of-principle Experiment on 24 GHz Medical Radar for Non-contact Vital Signs Measurement." 2021 43rd Annual International Conference of the IEEE Engineering in Medicine Biology Society (EMBC). IEEE, 2021.

44. S. Kang, Y. Lee, Y.-H. Lim, H.-K. Park, S. H. Cho, and S. H. Cho, "Validation of noncontact cardiorespiratory monitoring using impulse-radio ultra-wideband radar against nocturnal polysomnography," Sleep and Breathing, vol. 24, no. 3, pp. 841–848, 2020.

45. Kebe, Mamady, et al. "Human vital signs detection methods and potential using radars: A review." Sensors 20.5 (2020): 1454.

46. Zakrzewski, Mari, et al. "Comparison of center estimation algorithms for heart and respiration monitoring with microwave Doppler radar." IEEE Sensors Journal 12, no. 3 (2011): 627-634.

47. Li, Changzhi, et al. "A review on recent advances in Doppler radar sensors for noncontact healthcare monitoring." IEEE Transactions on microwave theory and techniques 61.5 (2013): 2046-2060.

48. Shen, Hongming, et al. "Respiration and heartbeat rates measurement based on autocorrelation using IR-UWB radar." IEEE transactions on circuits and systems II: express briefs 65, no. 10 (2018): 1470-1474.

49. Fang, Guan-Wei, Ching-Yao Huang, and Chin-Lung Yang. "Switch-based low intermediate frequency system of a vital sign radar for simultaneous multitarget and multidirectional detection." IEEE Journal of Electromagnetics, RF and Microwaves

in Medicine and Biology 4, no. 4 (2020): 265-272.

50. Pal, Surendra. "FMCW–Radar Design: by M. Jankiraman, London, ARTECH HOUSE, 2018, 415 pp., 179 (hardback), ISBN-13: 978-1-63081-567-7." (2019): 576-577.

51. Lazaro, Antonio, David Girbau, and Ramon Villarino. "Analysis of vital signs monitoring using an IR-UWB radar." Progress In Electromagnetics Research 100 (2010): 265-284.

52. Lu, Guofeng, Predrag Spasojevic, and Larry Greenstein. "Antenna and pulse designs for meeting UWB spectrum density requirements." In IEEE Conference on Ultra Wideband Systems and Technologies, 2003, pp. 162-166. IEEE, 2003.

53. J.-Y. Kim, J.-H. Park, S.-Y. Jang, and J.-R. Yang, “Peak detection algorithm for vital sign detection using doppler radar sensors,” Sensors, vol. 19, no. 7, p. 1575, 2019.

54. N. Malesevi ˇ c, V. Petrovi ´ c, M. Beli ´ c, C. Antfolk, V. Mihajlovi ´ c, ´ and M. Jankovic, “Contactless real-time heartbeat detection via 24 ´ ghz continuous-wave doppler radar using artificial neural networks,”Sensors, vol. 20, no. 8, p. 2351, 2020.

55. W.-K. Liu, H.-P. Fu, and Z.-K. Yang, “A doppler radar vital sign detection system using concurrent dual-band hybrid down conversion architecture,” IEICE Electronics Express, pp. 16–20 190 665, 2019.

56. G. Sun, Y. Hakozaki, S. Abe, O. Takei, and T. Matsui, “A neural network-based infection screening system that uses vital signs and percutaneous oxygen saturation for rapid screening of patients with influenza,” Health, vol. 2013, 2013.

57. A. Lazaro, D. Girbau, and R. Villarino, “Analysis of vital signs monitoring us-

ing an ir-uwb radar," Progress In Electromagnetics Research, vol. 100, pp. 265–284, 2010.

58. M. Leib, W. Menzel, B. Schleicher, and H. Schumacher, "Vital signs monitoring with a uwb radar based on a correlation receiver," in Proceedings of the Fourth European Conference on Antennas and Propagation. IEEE, 2010, pp. 1–5.

59. Z. Yu, D. Zhao, and Z. Zhang, "Doppler radar vital signs detection method based on higher order cyclostationary," Sensors, vol. 18, no. 1, p. 47, 2018.

60. S. Wu, T. Sakamoto, K. Oishi, T. Sato, K. Inoue, T. Fukuda, K. Mizutani, and H. Sakai, "Person-specific heart rate estimation with ultra-wideband radar using convolutional neural networks," IEEE Access, vol. 7, pp. 168 484–168 494, 2019.

61. Ø. Aardal, Y. Paichard, S. Brovoll, T. Berger, T. S. Lande, and S.- E. Hamran, "Physical working principles of medical radar," IEEE Transactions on Biomedical Engineering, vol. 60, no. 4, pp. 1142– 1149, 2012.

62. A. De Groote, M. Wantier, G. Chéron, M. Estenne, and M. Paiva, "Chest wall motion during tidal breathing," Journal of Applied Physiology, vol. 83, no. 5, pp. 1531–1537, 1997.

63. O. Boric-Lubecke, V. M. Lubecke, A. D. Droitcour, B.-K. Park, and A. Singh, Doppler radar physiological sensing. Wiley Online Library, 2016.

64. Kooman, Jeroen P., Fokko Pieter Wieringa, Maggie Han, Sheetal Chaudhuri, Frank M. van der Sande, Len A. Usvyat, and Peter Kotanko. "Wearable health devices and personal area networks: can they improve outcomes in haemodialysis patients?." Nephrology Dialysis Transplantation 35, no. Supplement.2 (2020): ii43-ii50.

65. J. Y. Lee and J. C. Lin, "A microcprocessor-based noninvasive arterial pulse

wave analyzer," IEEE transactions on biomedical engineering, no. 6, pp. 451–455, 1985.

66. G. Sun, S. Gotoh, Z. Zhao, S. Kim, S. Suzuki, N. Imamoglu, W. Yu, and T. Matsui, "Vital-cube: A non-contact vital sign monitoring system using medical radar for ubiquitous home healthcare," Journal of Medical Imaging and Health Informatics, vol. 4, no. 6, pp. 863–867, 2014.

67. G. Sun, T. Matsui, Y. Watai, S. Kim, T. Kirimoto, S. Suzuki, and Y. Hakozaki, "Vital-scope: design and evaluation of a smart vital sign monitor for simultaneous measurement of pulse rate, respiratory rate, and body temperature for patient monitoring," Journal of Sensors, vol. 2018, 2018.

68. S. Kang, Y. Lee, Y.-H. Lim, H.-K. Park, S. H. Cho, and S. H. Cho, "Validation of noncontact cardiorespiratory monitoring using impulse-radio ultra-wideband radar against nocturnal polysomnography," Sleep and eathing, vol. 24, no. 3, pp. 841–848, 2020.

69. Kumar, D., P. Carvalho, M. Antunes, R. P. Paiva, and J. Henriques. "Noise detection during heart sound recording using periodicity signatures." Physiological measurement 32, no. 5 (2011): 599.

70. H. Tang, M. Wang, Y. Hu, B. Guo, and T. Li, "Automated signal quality assessment for heart sound signal by novel features and evaluation in open public datasets," BioMed Research International, vol. 2021, 2021.

71. K. Shi, S. Schellenberger, F. Michler, T. Steigleder, A. Malessa, F. Lurz, C. Ostgathe, R. Weigel, and A. Koelpin, "Automatic signal quality index determination of radar-recorded heart sound signals using ensemble classification," IEEE transactions on biomedical engineering, vol. 67, no. 3, pp. 773–785, 2019.

72. Y. Lee, J. W. Choi, and S. H. Cho, “Vital sign quality assessment based on ir-uwb radar sensor,” in 2017 International Conference on Information and Communication Technology Convergence (ICTC). IEEE, 2017, pp. 896–900.

73. J.-Y. Kim, J.-H. Park, S.-Y. Jang, and J.-R. Yang, “Peak detection algorithm for vital sign detection using doppler radar sensors,” Sensors, vol. 19, no. 7, p. 1575, 2019.

74. N. Malešević, V. Petrović, M. Belić, C. Antfolk, V. Mihajlović, and M. Janković, “Contactless real-time heartbeat detection via 24 ghz continuous-wave doppler radar using artificial neural networks,” Sensors, vol. 20, no. 8, p. 2351, 2020.

75. W.-K. Liu, H.-P. Fu, and Z.-K. Yang, “A doppler radar vital sign detection system using concurrent dual-band hybrid down conversion architecture,” IEICE Electronics Express, pp. 16–20 190 665, 2019.

76. Y. Xu, Q. Li, and Z. Tang, “Accurate and contactless vital sign detection in short time window with 24 ghz doppler radar,” Journal of Sensors, vol. 2021, 2021.

77. G. Sun, M. Okada, R. Nakamura, T. Matsuo, T. Kirimoto, Y. Hakozaki, and T. Matsui, “Twenty-four-hour continuous and remote monitoring of respiratory rate using a medical radar system for the early detection of pneumonia in symptomatic elderly bedridden hospitalized patients,” Clinical case reports, vol. 7, no. 1, p. 83, 2019.

78. Edanami, Keisuke, et al. "Design and Evaluation of Digital Filters for Non-Contact Measuring of HRV using Medical Radar and Its Application in Bedside Patient Monitoring System." 2021 43rd Annual International Conference of the IEEE Engineering in Medicine Biology Society (EMBC). IEEE, 2021.

79. Singh N, Moneghetti KJ, Christle JW, Hadley D, Plews D, Froelicher V.

Heart Rate Variability: An Old Metric with New Meaning in the Era of using mHealth Technologies for Health and Exercise Training Guidance. Part One: Physiology and Methods. Arrhythm Electrophysiol Rev. 2018 Aug;7(3):193-198. doi: 10.15420/aer.2018.27.2. PMID: 30416733; PMCID: PMC6141929.

80. Edla, Shwetha, et al. "Is heart rate variability better than routine vital signs for prehospital identification of major hemorrhage?" The American journal of emergency medicine 33.2 (2015): 254-261.

81. Sessa, Francesco, et al. "Heart rate variability as predictive factor for sudden cardiac death." Aging (Albany NY) 10.2 (2018): 166.

82. Shekha K, Ghosh J, Thekkoott D, Greenberg Y. Risk stratification for sudden cardiac death in patients with non-ischemic dilated cardiomyopathy. Indian Pacing Electrophysiol J. 2005; 5:122–38.

83. Sessa F, Anna V, Messina G, Cibelli G, Monda V, Marsala G, Ruberto M, Biondi A, Cascio O, Bertozzi G, Pisanelli D, Maglietta F, Messina A, Mollica MP, Salerno M. Heart rate variability as predictive factor for sudden cardiac death. Aging (Albany NY). 2018 Feb 23;10(2):166-177. doi: 10.18632/aging.101386. PMID: 29476045; PMCID: PMC5842851.

84. L.C. Cancio, A.I. Batchinsky, W.L. Baker, C. Necsoiu, J. Salinas, A.L. Goldberger, et al. Combat casualties undergoing lifesaving interventions have decreased heart rate complexity at multiple time scales J Crit Care, 28 (2013), pp. 1093-1098

85. A.Y. Mejaddam, O.A. Birkhan, A.C. Sideris, G.M. Van der Wilden, A.M. Imam, J.O. Hwabejire, et al. Real-time heart rate entropy predicts the need for lifesaving interventions in trauma activation patients J Trauma Acute Care Surg, 75 (2013), pp. 607-612

86. M.L. Ryan, C.M. Thorson, C.A. Otero, T. Vu, K.G. Proctor Clinical applications of heart rate variability in the triage and assessment of traumatically injured patients Anesthesiol Res Pract, 2011 (2011), pp. 416590-416597

87. M. Alizadeh, G. Shaker and S. Safavi-Naeini, "Remote Heart Rate Sensing with mm-wave Radar," 2018 18th International Symposium on Antenna Technology and Applied Electromagnetics (ANTEM), 2018, pp. 1-2, doi: 10.1109/ANTEM.2018.8572982.

88. Sun, Guanghao, et al. "Non-contact monitoring of heart rate variability using medical radar for the evaluation of dynamic changes in autonomic nervous activity during a head-up tilt test." Journal of Medical Engineering Technology 43.7 (2019): 411-417.

89. Nosrati, Mehrdad, and Negar Tavassolian. "High-accuracy heart rate variability monitoring using Doppler radar based on Gaussian pulse train modeling and FTPR algorithm." IEEE Transactions on Microwave Theory and Techniques 66.1 (2017): 556-567.

90. J. Tu and J. Lin, “Fast acquisition of heart rate in noncontact vital sign radar measurement using time-window-variation technique,” IEEE Trans. Instrum. Meas., vol. 65, no. 1, pp. 112–122, Jan. 2016.

91. M. Li and J. Lin, “Wavelet-transform-based data-length-variation technique for fast heart rate detection using 5.8-GHz CW Doppler radar,” IEEE Trans. Microw. Theory Techn., vol. 66, no. 1, pp. 568–576, Jan. 2018

92. K. Yamamoto, K. Toyoda, and T. Ohtsuki, “Spectrogram-based noncontact RRI estimation by accurate peak detection algorithm,” IEEE Access, vol. 6, pp. 60369–60379, Oct. 2018

93. Petrović, Vladimir L., et al. "High-accuracy real-time monitoring of heart rate variability using 24 GHz continuous-wave Doppler radar." IEEE Access 7 (2019): 74721-74733.

94. Otake, Yusuke, et al. "Non-contact heart rate variability monitoring using Doppler radars located beneath bed mattress: a case report." European Heart Journal-Case Reports 5.8 (2021): ytab273.

95. Y. Yao, et al., "Extracting Cardiac Information from Medical Radar Using Locally Projective Adaptive Signal Separation," Frontiers in Physiology, vol. 10, Article 568, 2019.

96. D. A. Pisner and D. M. Schnyer, "Support vector machine," in Machine Learning. Elsevier, 2020, pp. 101–121.

97. W. S. Noble, "What is a support vector machine?" Nature biotechnology, vol. 24, no. 12, pp. 1565–1567, 2006.

98. X. Zhao and B. Ye, "Separation of single frequency component using singular value decomposition," Circuits, Systems, and Signal Processing, vol. 38, no. 1, pp. 191–217, 2019.

99. P. Grassberger, et al., On noise reduction methods for chaotic data, Chaos 3 (1993) 127–141, doi:10.1063/1.165979.

100. Kantz, Holger, et al. "Nonlinear noise reduction: A case study on experimental data." Physical Review E 48.2 (1993): 1529.

101. T. Sauer, J. A. Yorke, and M. Casdagli, "Embedology," J. Stat. Phys., vol. 65, no. 3–4, pp. 579–616, 1991.

102. Pan, Jiapu, and Willis J. Tompkins. "A real-time QRS detection algorithm." IEEE transactions on biomedical engineering 3 (1985): 230-236.

103. Pérez-Riera, Andrés Ricardo, et al. "R-peak time: An electrocardiographic parameter with multiple clinical applications." Annals of Noninvasive Electrocardiology 21.1 (2016): 10-19.

104. Guide, User, and N. I. Specifications. "myRIO-1900." National Instruments, August (2013).

105. S. M. Series, “Obstructive sleep apnea and heart disease,” Am J Respir Crit Care Med, vol. 188, pp. P1–P2, 2013.

106. N. Vitulano, A. Di Marco Berardino, A. Re, G. Riccioni, F. Perna, F. Mormile, S. Valente, and F. Bellocci, “Obstructive sleep apnea and heart disease: the biomarkers point of view.” Frontiers in bioscience (Scholar edition), vol. 5, pp. 588–599, 2013.

Appendix A

Related Publication

A.1 Journal

[1] **Hoang Thi Yen**, Masaki Kurosawa, Tetsuo Kirimoto, Yukiya Hakozaki, Takemi Matsui, and Guanghao Sun. "A medical radar system for non-contact vital sign monitoring and clinical performance evaluation in hospitalized older patients," in *Biomedical Signal Processing and Control*, vol. 75 (2022): 103597.

[2] **Hoang Thi Yen**, Masaki Kurosawa, Tetsuo Kirimoto, Yukiya Hakozaki, Takemi Matsui, and Guanghao Sun. "Non-contact estimation of cardiac inter-beat interval and heart rate variability using time-frequency domain analysis for CW radar," in *IEEE Journal of Electromagnetics, RF and Microwaves in Medicine and Biology*, (Under Review).

A.2 Conference

[1] **Hoang Thi Yen**, M. Kurosawa, T. Kirimoto, K. Edanami and G. Sun, "Proof-of-principle Experiment on 24 GHz Medical Radar for Non-contact Vital Signs Measurement," in *43rd Annual International Conference of the IEEE Engineering in Medicine Biology Society (EMBC 2021)*, 2021, pp. 6884-6884, doi: 10.1109/EMBC46164.2021.9630735, Mexico.

[2] **Hoang Thi Yen**, Van-Phuc Hoang, Nguyen Huu Son, Quang Kien Trinh, Xuan Nam

Tran, Koichiro Ishibashi, and Guanghao Sun. "Real-Time Medical Radar-based Vital Sign Monitoring System Implemented with Signal Quality Classification Algorithm," in *2022 International Conference on Advanced Technologies for Communications (ATC 2022)*, pp. 356-359. IEEE, 2022.

[3] **Hoang Thi Yen**, Masaki Kurosawa, Tetsuo Kirimoto, Satoshi Suzuki, and Guanghao Sun. "I/Q Channel Selection for 24 GHz CW Radar to Non-Contact Vital Signs Detection for Health Check System," in *IEEE 11th Global Conference on Consumer Electronics (GCCE 2022)*, 18 - 21, October, 2022 Osaka, Japan.

[4] **Hoang Thi Yen**, Van-Phuc Hoang, Quang-Kien Trinh, Van Sang Doan, Guanghao Sun. "Sleep Apnea Patient Monitoring Using Continuous-wave Radar". In *22nd IEEE Statistical Signal Processing (SSP)*, IEEE, 2023.

Appendix B

Full Publication List

B.1 Journal

[1] **Hoang Thi Yen**, Masaki Kurosawa, Tetsuo Kirimoto, Yukiya Hakozaki, Takemi Matsui, and Guanghao Sun. "A medical radar system for non-contact vital sign monitoring and clinical performance evaluation in hospitalized older patients, in *Biomedical Signal Processing and Control 75*, (2022): 103597.

[2] Edanami Keisuke, Masaki Kurosawa, **Hoang Thi Yen**, Takeru Kanazawa, Yoshifusa Abe, Tetsuo Kirimoto, Yu Yao, Takemi Matsui, and Guanghao Sun. "Remote sensing of vital signs by medical radar time-series signal using cardiac peak extraction and adaptive peak detection algorithm: Performance validation on healthy adults and application to neonatal monitoring at an NICU," in *Computer Methods and Programs in Biomedicine* 226 (2022): 107163.

[3] **Hoang Thi Yen**, Masaki Kurosawa, Tetsuo Kirimoto, Yukiya Hakozaki, Takemi Matsui, and Guanghao Sun. “Non-contact estimation of cardiac inter-beat interval and heart rate variability using time-frequency domain analysis for 24 GHz CW radar,” in *IEEE Journal of Electromagnetics, RF and Microwaves in Medicine and Biology*, (2023) (Under Review).

B.2 Conference

[1] **Hoang Thi Yen**, Van-Phuc Hoang, Quang-Kien Trinh, Van Sang Doan, Guanghao Sun. “Sleep Apnea Patient Monitoring Using Continuous-wave Radar”. In *22nd IEEE Statistical Signal Processing (SSP)*, IEEE, 2023

[2] **Hoang Thi Yen**, Masaki Kurosawa, Tetsuo Kirimoto, Satoshi Suzuki, and Guanghao Sun. “I/Q Channel Selection for 24 GHz CW Radar to Non-Contact Vital Signs Detection for Health Check System”, in *2022 IEEE 11th Global Conference on Consumer Electronics (GCCE 2022)*, IEEE, October 2022.

[3] **Hoang Thi Yen**, Van-Phuc Hoang, Nguyen Huu Son, Quang Kien Trinh, Xuan Nam Tran, Koichiro Ishibashi, and Guanghao Sun. "Real-Time Medical Radar-based Vital Sign Monitoring System Implemented with Signal Quality Classification Algorithm." in *2022 International Conference on Advanced Technologies for Communications (ATC)*, pp. 356-359. IEEE, 2022.

[4] Son Nguyen Huu, **Hoang Thi Yen**,Guanghao Sun, and Koichiro Ishibashi. "High-Accuracy Heart Rate Estimation By Half/Double BBI Moving Average and Data Recovery Algorithm of 24GHz CW-Doppler Radar." In: *2022 International Conference on Advanced Technologies for Communications (ATC)*, pp. 360-363. IEEE, 2022.

[5] **Hoang Thi Yen**, M. Kurosawa, T. Kirimoto, K. Edanami and G. Sun, "Proof-of-principle Experiment on 24 GHz Medical Radar for Non-contact Vital Signs Measurement," in *2021 43rd Annual International Conference of the IEEE Engineering in Medicine Biology Society (EMBC)*, 2021, pp. 6884-6884, doi: 10.1109/EMBC46164.2021.9630735.

[6] Keisuke Edanami, Yu Yao, **Hoang Thi Yen**, Masaki Kurosawa, Tetsuo Kirimoto, Yukiya Hakozaki, Takemi Matsui, Guanghao Sun, "Design and Evaluation of Digital

Filters for Non-Contact Measuring of HRV using Medical Radar and Its Application in Bedside Patient Monitoring System," In: *2021 43rd Annual International Conference of the IEEE Engineering in Medicine Biology Society (EMBC),* 2021, pp. 6962-6965, doi: 10.1109/EMBC46164.2021.9629643.

[7] Vu Hoang-Gia, **Hoang Thi Yen**. "Prefix-Based Multi-Pattern Matching on FPGA." In: *2020 International Conference on Green and Human Information Technology (ICGHIT),* pp. 68-69. IEEE, 2020.

[8] **Hoang Thi Yen**, Van-Thanh Ta, Han Le Duc, Duong Quang Manh, and Van-Phuc Hoang. "Background calibration of multiple channel mismatches in time-interleaved ADCs," in *2019 3rd International Conference on Recent Advances in Signal Processing, Telecommunications Computing (SigTelCom),* pp. 43-47. IEEE, 2019.

[9] **Hoang Thi Yen**, Van-Thanh Ta, Le Duc Han, Trinh Xuan Minh, Van-Phuc Hoang, Do Ngoc Tuan, “Analysis of adaptive algorithms for timing mismatch calibration in Time-Interleaved ADC,” in *21st National Conference on Electronics, Communications and Information Technology (REV-ECIT 2018),*, pp.78-82, Vietnam.

[10] Ta Van-Thanh, **Hoang Thi Yen**, Han Le Duc, and Van-Phuc Hoang. "Fully digital background calibration technique for channel mismatches in TIADCs. "In *2018 5th NAFOSTED conference on information and computer science (NICS),* pp. 270-275. IEEE, 2018.

[11] Xuan Minh Trinh, Nghia Pham Minh, **Hoang Thi Yen**, and Thanh Nguyen Trung. "Modified Three-stage algorithm for forest height estimation using Polarimetric SAR Interferometry Image." In *2018 International Conference on Advanced Technologies for Communications (ATC)*, pp. 37-41. IEEE, 2018.

This page intentionally left blank

Author Biography

Hoang Thi Yen received B.Cs. degree in Biomedical Electronics Engineering and the M.S. degree in Electronics Engineering from Le Quy Don Technical University, Hanoi, Vietnam, in 2013 and 2019, respectively. She is currently pursuing the Ph.D. degree in Biomedical Engineering with the University of Electro-Communications (UEC), Tokyo, Japan. She is also researcher and lecturer with Le Quy Don Technical University, Hanoi, Vietnam.

THE END